FACULTY OF ELECTRICAL ENGINEERING AND COMMUNICATION

Department of Electrical and Electronic Technology

25th ABAF

BRNO 2024

Advanced Batteries, Accumulators and Fuel Cells

INTERNATIONAL CONFERENCE

August 25th - August 28th 2024

Organised by:

Department of Electrical and Electronic Technology,
Faculty of Electrical Engineering and Communication,
Brno University of Technology

Organizing committee:
Marie Sedlaříková
Tomáš Kazda

Honourary Scientific Committee:

- Petr Vanýsek, *Northern Illinois University, DeKalb, Illinois, USA*
- Arnaldo Visintin, *INIFTA, La Plata, Argentina*
- Günter Fafilek, *TU Wien, Vienna, Austria*
- Elena Shembel, *USCTU, Dnipro, Ukraine*
- Vito Di Noto, *University of Padova, Padova, Italy*
- Harry Hoster, *Universität Duisburg-Essen, Duisburg, Germany*
- Boris Markovsky, *Bar-Ilan University, Tel Aviv, Israel*
- Philipp Adelhelm, *Friedrich Schiller University, Jena, Germany*
- Laurence Hardwick, *University of Liverpool, Liverpool, UK*
- Renata Oriňáková, *UPJŠ, Košice, Slovakia*
- Andrea Fedorková-Straková, *UPJŠ, Košice, Slovakia*
- Grzegorz Lota, *Poznan University of Technology, Poznan, Poland*
- Mariusz Walkowiak, *Institute of Non-Ferrous Metals, Poznan, Poland*

Organisation Committee:

- Marie Sedlaříková, *FEEC BUT, Brno, Czech Republic*
- Tomáš Kazda, *FEEC BUT, Brno, Czech Republic*
- František Klein, Brno, *Czech Republic*
- Vítězslav Novák, *FEEC BUT, Brno, Czech Republic*
- Miroslav Zatloukal, *FEEC BUT, Brno, Czech Republic*
- Jiří Libich, *FEEC BUT, Brno, Czech Republic*
- Tomáš Binar, *FEEC BUT, Brno, Czech Republic*
- Jiří Švarc, *University of Defence, Brno, Czech Republic*
- Pavlína Sedlaříková, *Brno, Czech Republic*

Program Committee:

- Marie Sedlaříková, *FEEC BUT, Brno, Czech Republic*
- Arnaldo Visintin, *INIFTA, La Plata, Argentina*
- Mariela Ortiz, *INIFTA, La Plata, Argentina*
- Petr Vanýsek, *Northern Illinois University, DeKalb, Illinois, USA*
- Günter Fafilek, *TU Wien, Vienna, Austria*
- Boris Markovsky, *Bar-Ilan University, Tel Aviv, Israel*
- Harry Hoster, *Universität Duisburg-Essen, Duisburg, Germany*
- Grzegorz Lota, Poznan *University of Technology, Poznan, Poland*
- Mariusz Walkowiak, *Institute of Non-Ferrous Metals, Poznan, Poland*
- Ondřej Čech, *FEEC BUT, Brno, Czech Republic*
- Jiří Vaněk, *FEEC BUT, Brno, Czech Republic*
- Vítězslav Novák, *FEEC BUT, Brno, Czech Republic*
- Petr Bača, *FEEC BUT, Brno, Czech Republic*
- Tomáš Kazda, *FEEC BUT, Brno, Czech Republic*
- Helena Polsterová, *FEEC BUT, Brno, Czech Republic*
- Miroslav Zatloukal, *FEEC BUT, Brno, Czech Republic*
- Kristýna Jandová, *FEEC BUT, Brno, Czech Republic*
- Andrea Fedorková-Straková, *UPJŠ, Košice, Slovakia*
- Jiří Libich, *FEEC BUT, Brno, Czech Republic*
- Tomáš Binar, *FEEC BUT, Brno, Czech Republic*

ISBN 978-80-214-6257-1

Main Sponsors:

Other Sponsors:

Co-Sponsored by

We would like to express our thanks to the Brno University of Technology, Faculty of Electrical Engineering and Communication for support and help with organising 25th ABAF conference

Contents

Lithium Batteries and Related Systems

J. Červenka, G. Abbas, M. Šilhavík, A. El Guerraf, K. Knížek, M. Cieslar, J. Houdková, P. Jiříček, Z. Vlčková, O. Frank
Engineering of Nanostructured High-Capacity Anode Materials for Lithium-Ion Batteries 8

K. Fröhlich, P. P. Sahoo, A. Güneren, B. Hudec
Performance of the ZnO Coated Silicon/Graphite Anode in Electrolyte with the Fluoroethylene Carbonate Additive 9

Gregor Glanz, Markus Koller, Katja Fröhlich, Alexander Bergmann
State Estimation of a Lithium-Ion Battery Pack Using Piezoelectric Transducers 12

S. Keles, G. Glanz, K. Fröhlich, A. Petz
State Estimation of Lithium-Ion-Batteries using Strain Gages 15

Krum Banov, Ulf Breddemann, Miriam Khodeir, and Petr Novák
Impact of Transition Metal Contaminants in the Electrolyte on the Electrochemistry of Oxides in Lithium-Ion Batteries 19

Xu Liu, Cheng Xu, Stefano Passerini
Locally Concentrated Ionic Liquid Electrolytes for High-Energy Batteries 20

Prangya P. Sahoo, Boris Hudec, Miroslav Mikolášek, Magdaléna Precnerová, Matej Mičušík, Peter Nádaždy, Peter Siffalovi, Karol Fröhlich
Atomic Layer Deposition of Alumina for Enhanced Electrochemical Performance of $LiFePO_4$ Cathodes 22

Jiří Báňa, Antonín Šimek, Tomáš Kazda
Innovative approaches to recycling graphite from lithium-ion batteries by enhancing capacity with silicon from PV panels 25

H. Hálová, L. Preisler, L. Chladil
Spray drying Synthesis and Electrostatic Precipitation in Li-ion Battery Cathode Material Production 28

K. Jaššo, D. Biolek
Electrochemical Impedance Spectroscopy for Lithium-ion Batteries 31

J. Kasper, P. Hrzina, L. Černá, T. Finsterle, and V. Knap
Kinetic Model for Improved Dynamic Current Response in Lithium-ion Battery Electrical Circuit Models 35

O. Klvač, D. Trochta, T. Kazda
Preparation of Battery Cross-sections Using Broad Ion Beam Polishing 38

O. L. Riabokin, K. D. Pershina, T. V. Lysnicha
Non-Faradaic Capacitance of Porous Manganese Dioxide Nanoparticles 41

M. Šedina and T. Kazda
Exploring the Influence of Temperature on Li-ion Batteries 44

M. Vuksanovic, B. Boz, K. Fröhlich, E. K. Ehmoser
Shellac - Application of a Sustainable Biopolymer as a Binder for Si/Gr-Anodes in Li-Ion Batteries 47

Bernd Eschelmüller, Katja Fröhlich
Advancing Sustainability in Lithium-Ion Battery Production through Innovations from the BatWoMan Project.....49

K. Vavilon, V. Zinin, Yu. Polishchuk, O. Potapenko
Synthesis of Graphene by Controlled Gas Detonation Method for Batteries Application.....50

Y. Pustovalov, E. Shembel, D. Kaszuba, K Sukhy, V. Redko, T. Pastushkin, A. Markevich, Y. Sknar, N. Zaderey, V. Khandetskyy, A.Redko
Innovative Anode based on Nanographite and Silicon Powder Without Binder for High Energy Batteries.....54

Yu. V. Shmatok, N. I. Globa, V. A. Sirosh, I. V. Romanova
Ni and La Doping Effect on Characteristics of $LiMn_2O_4$ as Cathode Material for Lithium-Ion Batteries with Aprotic and Aqueous Electrolytes.....57

Supercapacitors

N. I. Globa, Yu. V. Shmatok, O. B. Pushyk, O. I. Milovanova, M. I. Gorobets, V. A. Sirosh, S. A. Kirillov
Specific Conductivities of Tetraalkylammonium Bis(oxalato)borates in Acetonitrile, Dimethyl Sulfoxide, and Propylene Carbonate.....60

O. Zima, A. Stranovsky, P. Ondrejka, M. Sojkova and M. Mikolasek
Integration of Nickel-Ammonium Complex Precipitation, Reduction and Electrochemical Activation for Superior Nickel Hydroxide Supercapacitor Electrodes.....63

Fuel Cells

M. O. Danilov, G. I. Dovbeshko, I. A. Rusetskyi, O. P. Gnatyuk, S.S. Fomanyuk, G. Ya. Kolbasov
Graphitic carbon nitride - nitride partially unzipped carbon nanotubes nanocomposite: synthesis, properties and application for oxygen electrodes of alkaline fuel cells.....66

M. K. Sukhyi, V. G. Nefedov, Yu. V. Polishchuk
Analysis of the Electrochemical Method of Producing Environmentally Friendly Hydrogen Energy Carrier According to the Evans Diagram.....69

Michael Georg Stadt, Michael Nelhiebel, Silvia Larisegger, Günter Fafilek
High-Temperature Electrochemistry for the Investigation of Redox Reactions on Metal Surfaces.....72

Da Xing, Leander Kucklick, Ioannis Spanos, Blaz Toplak, Doris Segets and Harry Hoster
On The Stability of Perowskit Oxygen Evolution Electrocatalysts in alkaline Solutions.....73

Aqueous Batteries

Marek Baraniak, Radosław Płowens, Katarzyna Lota, Marek Bajsert, Grzegorz Lota
Novel Carbon Material with Potential Application in Lead-Acid Battery Technology.....74

J. Charvát, J. Pocedič, J. Vrána
Progress in redox flow battery development.....77

P. Mazúr, P. Richtr, D. Graf, M. Bureš, J. Hnat, M. Paidar, J. Charvat, J. Pocedic
Optimization of performance and stability of zinc-air flow battery.....79

M. Nádherná, T. Chvojka, R. Pfeifer, G. Abbas,c, Z. A. Zafar, J. Červenka
Design of "water-in-salt" electrolytes for dual-ion batteries – influence of salt concentration and additives.....80

K. Tokarek, J. Wojciechowski, F. Walkiewicz, M. Baraniak, M. Pająk, K. Hubkowska, D. Monikowska, A. Czerwiński, G. Lota
Ionic Liquid and Palladium Nanoparticle Modifications for Nickel-Metal Hydride Negative Electrode.....81

Yitao He, Jiří Červenka
Suspension electrolyte for zinc metal dual-ion batteries.....85

Petr Křivík
Temperature Changes in a Lead-Acid Battery During Cycling.....86

New Systems of Batteries

J.R. Buchheim, F. Beutler
Aerosol-based processes to produce battery materials.....89

M. Zukalová, O. Porodko, M. Fabián, B. Pitňa Lásková, L. Kavan
Novel lithiated high-entropy spinel type oxychloride and oxyfluoride and its electrochemical performance in Li-ion batteries.....91

P. Čudek, K. Jaššo
Preparation and analysis of biological derived carbon for lithium-sulfur batteries.....92

M. Spurný, J. Žitka, P. Mazúr
Solid-state composite materials for redox-mediated flow batteries.....96

A. Šimek, T. Kazda and O. Čech
Use of Raman spectroscopy to examine the suitability of carbonaceous materials for Li-ion vs. Na-ion anodes.....99

M. Tahertalari, SA Ahad, D. Capkova, H. Geaney and D. Thompson
Silicon/Graphite Composite as Lithiophilic Lithium Metal Anode.....102

P. Ondrejka, A. Petrík, M. Kemény, P. Novák, M. Sojková, M. Mikolášek
Enhancing Supercapacitor Performance: Molybdenum Oxide Substrate for Molybdenum Sulfide Electrodes.....105

Photovoltaics

S. V. Chivikov
Development of the Reversible photoelectrochemical cell.....108

T. Finsterle, J. Kasper, P. Hrzina, L. Černá
The Effect of Backsheet Repairs on Insulation Resistance in Photovoltaic Modules.....111

J. Vanek, and J. Pekarek
Comparison of the use of a virtual battery in a photovoltaic system.....115

Corrosion, Applications and Simulations

X. Li, L. Trnkova
Advanced Exploration of the Electrode-electrolyte Interface using Elimination Voltammetry with Linear Scan.....118

Miroslav Mikolášek, Lukáš Gardian, Martin Brázda, Boris Bajla, Martin Kemény, and Matej Novak
Advanced approaches for state-of-charge (SOC) and state-of-health (SOH) estimation of Li-ion batteries 121

B. Rajagopalan, G. Thorat, L. Pavlovec, N. Fernando, K. G. Kalligowdan, S. Khankeshizadeh, N. Levy, J. Reiter
R&D Development Path of Inobat´s Cell Chemistry 124

M. Sedlařík, T. Kazda, D. Capkova, P. Vyroubal
Comparison of machine learning techniques for estimating battery health 126

L. Trnkova, X. Li
Elimination Voltammetry with Linear Scan: Theory and Applications 129

S. Bátorová, M. Zatloukal, G. Fafilek
Influence of Scan Rate on Potentodynamic Polarisation Measurement of Sintered Materials 132

M. Kemény, P. Ondrejka, D. Šišmišová, M. Mikolášek
Distribution of Relaxation Times (DRT) for Determination of Internal Temperature of EV Battery Modules 135

M. Novák, M. Kemény, M. Mikolášek
A Current Pulse Response as an Alternative to EIS Measurements for Accurate Internal Temperature Estimation of Lithium-Ion Battery Cells 138

Mitchell Rae, Michela Ottaviani, Dominika Capkova, Tomáš Kazda, Luigi Jacopo Santa Maria, Kevin M. Ryan, Stefano Passerini, Mehakpreet Singh
Development of Machine Learning Methods for State of Charge Estimation of Li-ion Batteries: A Comparative Study 141

D. Trochta, O. Klvač, T. Kazda, L. Novák
Advanced in-situ SEM Analysis of Electrode Structural Changes in Li-ion Coin Cell During Cycling 144

P. Vyroubal, T. Kazda
HPPC Data Preparation for Reduced Order Model of Li-Ion Battery 148

Petra Slotová, Marie Sedlařiková, Pavel Čudek
Corrosion of Fe-Mg Material in 0.9 % NaCl Solution 151

M. Ceylan
Development and Parameterization of a Realtime Thermal Model as an Extra Safety Layer for Battery Management Systems 154

M. Budáč, V. Miloš, M. Carda, M. Paidar, K. Bouzek
Simulation of Properties of Composite Electrodes Using Monte Carlo 3D Equivalent Electronic Circuit Networks 155

Engineering of Nanostructured High-Capacity Anode Materials for Lithium-Ion Batteries

J. Červenka[a], G. Abbas[a,b], M. Šilhavík[a], A. El Guerraf[c], K. Knížek[a], M. Cieslar[d], J. Houdková[a], P. Jiříček[a], Z. Vlčková[c], O. Frank[c]

[a] Institute of Physics of the Czech Academy of Sciences, 162 00 Prague 6, Czechia

[b] Department of Chemical Engineering and Waterloo Institute of Nanotechnology,

University of Waterloo, Waterloo, Ontario N2L, 3G1, Canada

[c] Department of Electrochemical Materials, J. Heyrovsky Institute of Physical Chemistry of the Czech Academy of Sciences, 183 23 Prague 8, Czechia

[d] Faculty of Mathematics and Physics, Charles University, 12116 Prague 2, Czech Republic

This study demonstrates a nanoengineering approach for designing stable, reversible, and high-capacity nanostructured Si and MoS_2 anode materials for Li-ion batteries. It is shown that the nanostructuring of the active anode materials on a nanometer scale and the encapsulation in highly conductive carbon structures provides an effective strategy for relieving the stress and improving the cyclic stability of the high-capacity Si and MoS_2 based anodes. The electrochemical characterization of nanoparticle-based Si and MoS_2 anode materials embedded in carbon matrix deliver discharge capacity above 800 mAh/g for more than 500 cycles. The embedded carbon structure not only enhances the mechanical integrity of the hybrid anode materials but also provides effective charge transfer channels during the lithium storage process. This approach allows for excellent improvement in the performance and the cyclic stability of the studied anode materials, paving the way toward stress-tolerable high-capacity anode materials for the next generation of Li-ion batteries.

Performance of the ZnO Coated Silicon/Graphite Anode in Electrolyte with the Fluoroethylene Carbonate Additive

K. Fröhlich[1,2*], P. P. Sahoo[1], A. Güneren[1,3], B. Hudec[2]

[1] Centre for Advanced Materials Application, Slovak Academy of Sciences, Bratislava, Slovakia

[2] Institute of Electrical Engineering, Slovak Academy of Sciences, Bratislava, Slovakia

[3] Institute of Inorganic Chemistry, Slovak Academy of Sciences, Bratislava, Slovakia

Performance of the silicon/graphite anode coated by ZnO ultrathin film prepared by atomic layer deposition (ALD) is presented. ZnO coated anode exhibit improved rate capability, in particular at the c-rate of 2. ZnO coated anode shows enhanced capacity retention in the electrolyte with fluoroethylene carbonate (FEC) additive. Combination of the ZnO ALD protection layer together with the FEC additive is shown to be promising way to increase the silicon/graphite anode performance.

Introduction

Silicon is a promising anode material for Li-ion batteries due to its high theoretical capacity (4200 mA h g^{-1}) and abundant presence in the earth's crust. However, significant volume expansion of silicon during lithiation and formation of an unstable solid electrolyte interphase result in a decrease of the Si-based anode performance.

It was already shown that the operation of the silicon-based anode can be improved by surface modification using atomic layer deposition (ALD) (1). Thin oxide films can be used for this modification as this technique allows for growth of ultrathin conformal films of excellent quality on complex surfaces at low temperatures. An alternative way to enhance performance of the silicon/graphite anode is the addition of the fluoroethylene carbonate (FEC) in the electrolyte (2). In our contribution we compare both alternatives for increasing the silicon/graphite anode performance. We show that ZnO coating combined with FEC additive results in enhanced performance, in particular in improved capacity retention of the silicon/graphite anode.

Preparation and characterization

Silicon/graphite anode was fabricated by mixing 80 wt% of ball milled silicon/graphite as active material, 10 wt% of carbon black as the conductive agent, and 10 wt% of S-alginate as the binder. The slurry was then cast onto a copper foil using doctor blade technique. Resulting porosity of the fabricated anode was about 70%.

ZnO films were deposited by ALD at 100 °C using diethyl zinc (DEZn) and deionized water as a precursor and reactant, respectively. 5-40 ALD cycles of ZnO deposition was performed to obtain different thickness of the oxide films. A modified deposition parameters of the ALD process were used for porous substrates, which involved longer precursor doses and increased purging times. Growth on the silicon control wafer in the same deposition run revealed growth per cycle of 0.17 nm per cycle. Fabricated silicon/graphite anodes were analyzed by scanning electron microscopy, X-ray photoelectron spectroscopy (XPS) and electrochemical measurements.

Electrochemical measurements were performed in coin-cell design in a half-cell configuration using silicon/graphite as a working electrode and Li-metal as the counter electrode. 1 M $LiPF_6$ in EC/DMC (ethylene carbonate/diethyl carbonate) was used as an electrolyte. 10 vol% of the fluoroethylene carbonate was added to the electrolyte in some experiments. Electrochemical tests were performed in the voltage range of 0.01−1.5 V vs Li/Li+. Initially, a formation cycle was applied to all cells using a C-rate of 0.05.

Results and discussion

Charging/discharging measurements are displayed in the Figure 1. The measurements revealed improved rate capability (higher discharge capacity) for the ALD coated electrodes compared to pristine silicon/graphite samples. The anode was coated by 20 ALD cycles of ZnO, which corresponds approximately to 3 nm thickness. Similarly, addition of the FEC to the electrolyte resulted in improved rate capability of the batteries. At the charging/discharging rate of 2 C (fully charging in ½ hour) the discharge capacity of the ZnO coated was more than 2 times higher than the uncoated pristine anode.

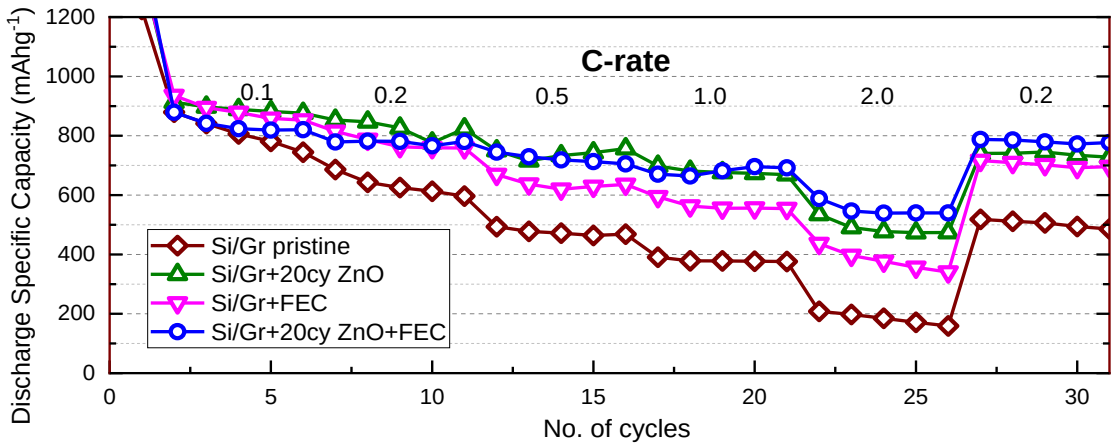

Figure 1. *Charging/discharging at different c-rates of the pristine and 20 ALD cycles ZnO coated silicon/graphite anodes in the electrolyte without and with the FEC additive.*

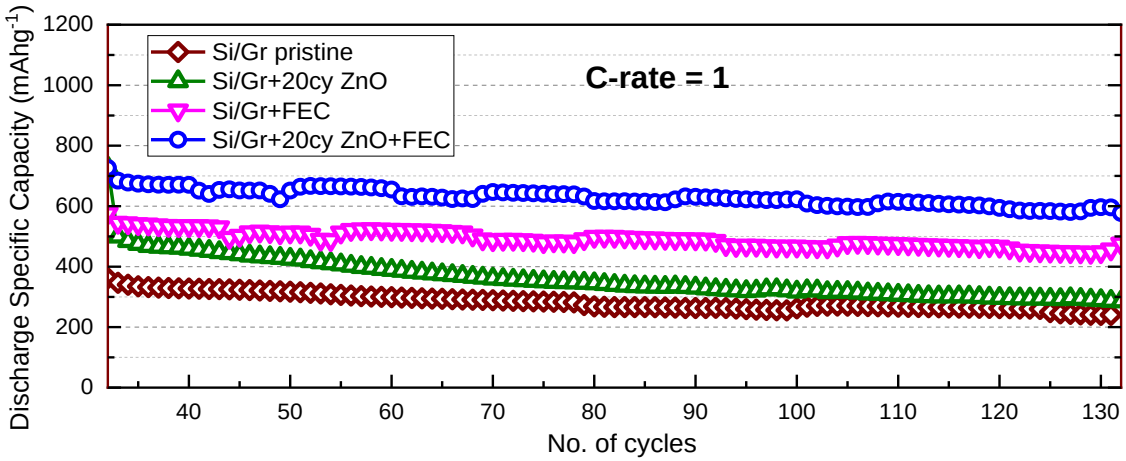

Figure 2. *100 charging/discharging cycles at the c-rate 1 of the pristine and 20 ALD cycles ZnO coated silicon/graphite anodes in the electrolyte without and with the FEC additive.*

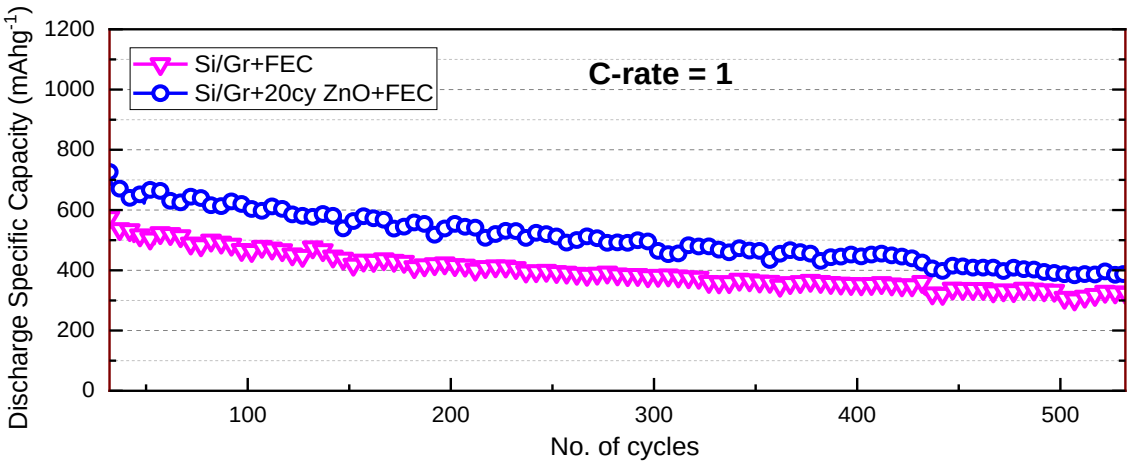

Figure 3. *500 charging/discharging cycles at the c-rate 1 of the pristine and 20 ALD cycles ZnO coated silicon/graphite anodes in the electrolyte without and with the FEC additive.*

During 100 charging/discharging cycles at c-rate 1 differential capacity analysis detected degradation of the silicon part of the anode, while ZnO coating remained more stable. This resulted in the capacity decrease of the pristine anode, while ZnO protected anode retained higher capacity, Figure 2. Anodes in electrolyte with the FEC additive showed very good long-term stability. Long-term cycling during 500 charging/discharging cycles at c-rate 1 of the anodes in electrolyte with the FEC additive revealed excellent capacity retention up to 500 cycles. Impedance spectroscopy unveiled lower solid electrolyte interphase layer and charge transfer resistances for ZnO coated samples. The XPS analysis of the pristine and 20 ALD cycles of ZnO on silicon/graphite anode showed an increase of Li_2CO_3 in the pristine sample after cycling. The ZnO protected silicon/graphite electrode minimized the amount of the carbonate formation during cell cycling. It has been well established in the literature that Li_2CO_3 is a product of electrolyte reduction.

The protection of the anode surface by ALD ZnO layer in combination with FEC additive seems to be an effective way for stabilizing the electrode/electrolyte interphase to achieve better performace and long term charging/discharging stability.

Acknowledgments

The authors acknowledge the support from VEGA 2/0162/22 and APVV−19−0461 projects.

References

1. P. P. Sahoo et al., ACS Appl. Nano Mater. 2024, https://doi.org/10.1021/acsanm.3c05066.
2. T. Jaumann et al. Energy Storage Mater., **6** 26 (2017).

State Estimation of a Lithium-Ion Battery Pack Using Piezoelectric Transducers

Gregor Glanz[a,b], Markus Koller[a], Katja Fröhlich[a], Alexander Bergmann[b]

[a] AIT Austrian Institute of Technology GmbH, Center for Low-Emission Transport, Giefinggasse 2, 1210 Vienna

[b] Graz University of Technology, Institute of Electrical Measurement and Sensor Systems, Inffeldgasse 10/2, 8010 Graz, Austria

Lithium-ions intercalate and deintercalate into the active materials of the electrodes during charging and discharging of lithium-ion batteries (LIBs), which results in an overall change in the mechanical properties of the battery. These changes can be monitored with the help of piezoelectric transducers by exciting and observing a propagating mechanical wave through the LIB. This can provide important information about the current battery state (SOX). This method is applied in a realistic approach by connecting four commercial 60Ah pouch cells in series, depicting a small battery pack. The measurements and the resulting interplay between different current rates and temperatures, which represent an operation close to reality, is discussed in this work.

Motivation

In electric vehicles (EVs), the condition monitoring of the LIB is done by a battery management system (BMS). This system continuously monitors key parameters, including voltage, current and temperature of the cells. Essential metrics such as the state of charge (SOC) and the state of health are calculated. Additionally, it ensures that the battery operates safely within its safe operation limits. In this work, a novel and realistic approach to determine the actual state of the LIB is presented that is not based on the electric two pole behavior of the cell.

Introduction

This work introduces a novel method to determine the characteristics and state of a battery pack by utilizing piezoelectric transducers. Two transducers are mounted on a pouch cell, on the same surface and at a certain distance between each other, where one of the transducers acts as emitter and the other one as a receiver. By exciting the emitter, a so-called Lamb wave propagates through the LIB which will subsequently be detected by the receiver [1]. Due to the mechanical property changes caused during charging and discharging in the LIB, the characteristics of the propagating wave change and can be directly linked to the battery's state (SOX). Over the battery's lifetime, additional mechanical changes occur due to degradation processes such as the growth of the solid electrolyte interface (SEI), particle cracking, and lithium plating. Measuring these degradation processes based solely on the electrical behavior of LIBs is highly challenging. By utilizing piezoelectric transducers, not only can the state of charge (SOC) be determined more accurately, but these degradation processes can also be tracked. This comprehensive approach allows for precise estimation of the state of health (SOH) of the LIB, enhancing the monitoring and management of the battery's condition throughout its lifespan.

Measurement Setup

In this study, an experimental setup, close to realistic conditions, was developed which includes a battery pack composed of four 60Ah pouch cells connected in series. This setup integrates the developed ultrasonic battery management system (UBMS) [2], a cell balancer, and piezoelectric transducers attached to two of the pouch cells. To measure the pressure variations resulting from the mechanical property changes during cycling, two load cells were incorporated. The entire arrangement is housed within a climatic chamber to simulate various environmental conditions, ensuring accurate and controlled testing. This comprehensive setup, shown inf Figure 1 a), enables the precise monitoring and analysis of the battery pack's performance under realistic operating conditions.

Results and Outlook

To produce this realistic use cases, the shown battery pack was cycled at different temperatures and various current rates (C-rates). The developed UBMS continuously processes the collected data to calculate the group velocity of the propagating wave and its amplitude, two key metrics for assessing state changes (SOX) in the battery cells.

In addition to these advanced ultrasonic measurements, the UBMS also tracks standard parameters such as cell voltage, current, and temperature of the LIBs. The interplay between these variables—cell voltage, applied current, wave propagation, temperature, and pressure changes—is illustrated in Figure 1 b). Measurements at different C-rates and temperatures were conducted and the changes and correlations between these values and the group velocity and amplitude will be discussed. With the help of ultrasonic measurements, safety critical events like a rise in pressure or temperature or certain chemical events e.g., lithium plating, can be, compared to a regular BMS, immediately detected and necessary steps to avoid safety risks can be implemented. An outlook on these topics based on the measurement results for future research will be given.

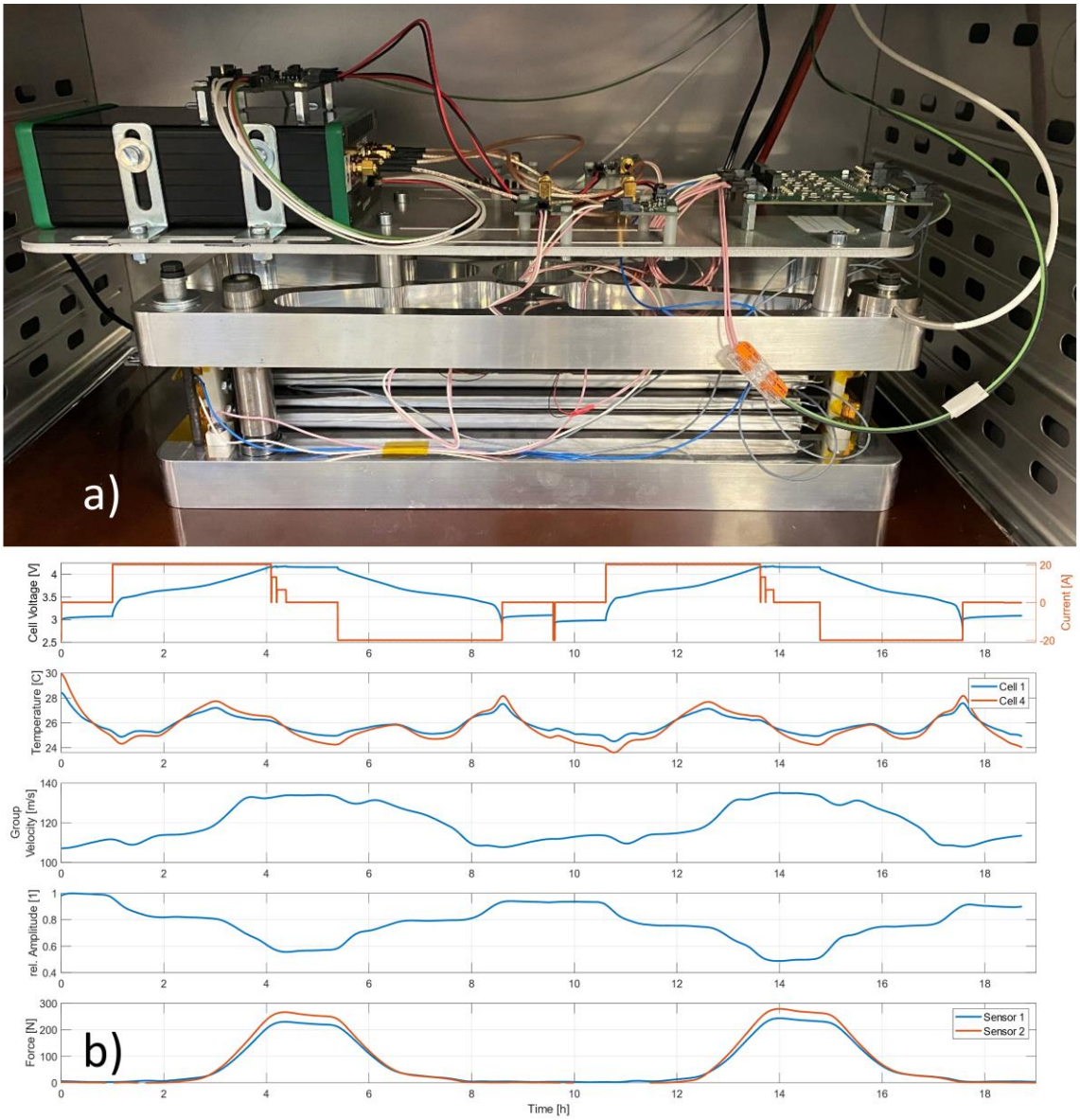

Figure 1. *a) Demonstrator of a Lithium-Ion battery pack consisting of four 60Ah pouch cells connected in series inside a climatic chamber. Equipped with an ultrasonic battery management system, cell balancer, temperature sensors, load cells and piezoelectric transducers. b) Measurement results during cycling the battery pack with 0.3C at room temperature (25°C).*

References

1. M. Koller, G. Glanz, A. Bergmann, und H. Popp, „Determination of Lamb Wave Modes on Lithium-Ion Batteries Using Piezoelectric Transducers“, *Sensors*, Bd. 22, Nr. 13, Art. Nr. 13, Jan. 2022, doi: 10.3390/s22134748.
2. M. Koller, G. Glanz, R. Jaber, und A. Bergmann, „Ultrasonic Battery Management System for Lamb wave mode tracking on Lithium-ion pouch cells“, *J. Energy Storage*, Bd. 74, S. 109347, Dez. 2023, doi: 10.1016/j.est.2023.109347.

State Estimation of Lithium-Ion-Batteries using Strain Gages

S. Keles[a, b], G. Glanz[a], K. Fröhlich[a], A. Petz[b]

[a] Austrian Institute of Technology (AIT), Center for Low Emission Transport, Battery Technologies, Vienna, Austria

[b] UAS Campus Vienna, Department of Engineering, Vienna, Austria

During lithiation and delithiation of a lithium-ion battery (LIB), the anode can undergo a volume change of approximately 10%. This effect can be measured with strain gages. In this work, multiple cylindrical cell types have been equipped with strain gages. The strain of cylindrical cells, measured during charging and discharging cycles, exhibits a strong correlation with the lithiation state, indicated by a coefficient of 0.97. This information can be further utilized for State of Charge (SOC) estimation.

Introduction

As electric vehicles play a significant role in the climate crisis, battery technologies undergo a rapid development. For a reliable and safe application of LIBs, a precise state estimation is necessary. Currently, the State of X (SOX) of LIBs are determined based on voltage, current and temperature. The application of multiple sensor types enables more precise estimations, for not only first-life applications but also second-life integration of LIBs. In this study, strain gages have been applied to cylindrical cells to disclose the correlation between strain and SOC.

Experimental Setup

In this study, linear strain gages from Hottinger Brüel & Kjaer GmbH (HBM) have been selected to measure the strain on cylindrical cells. The strain gages have a measuring grid of 6 mm x 2.7 mm with a resistance of 120 Ohm. To achieve reproducible results, a contraption has been designed, as shown in Figure 1, that ensures consistent application of the strain gages in terms of location, orientation, and application force. Prior to the application of the strain gages, the cylindrical cells were discharged to 0% SOC and rested for 12 hours. The strain measurements were conducted with the cells standing freely and vertically. This ensures a free expansion in all directions. To supply and measure the strain gage signal, an amplifier from HBM was used. The strain gage was connected in a quarter-bridge configuration with a supply voltage of 2.5 mV.

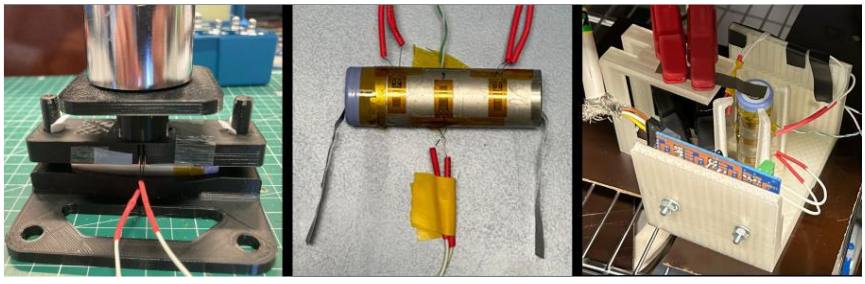

Figure 1. *Experimental Setup*

Measurements and results

The first measurements were done with Samsung INR18650 29E cylindrical cells. The cells, based on lithium nickel manganese cobalt oxides (NMC), have a nominal capacity of 2.85 Ah. For the measurements, the strain gage was applied with the previously described contraption on the center of the cell. Measurements on this cell type revealed an inverse strain behavior in the majority of the measurements, as shown in Figure 2(a). During charging, the strain decreased, and during discharging, the strain increased, which is contrary to what is reported in the literature[1,2]. This behavior was observed at three different positions along the axis and circumference of the cell. Only when the strain gage covered the anode tab did the strain increase during charging and vice versa during discharging, as shown in Figure 2(b).

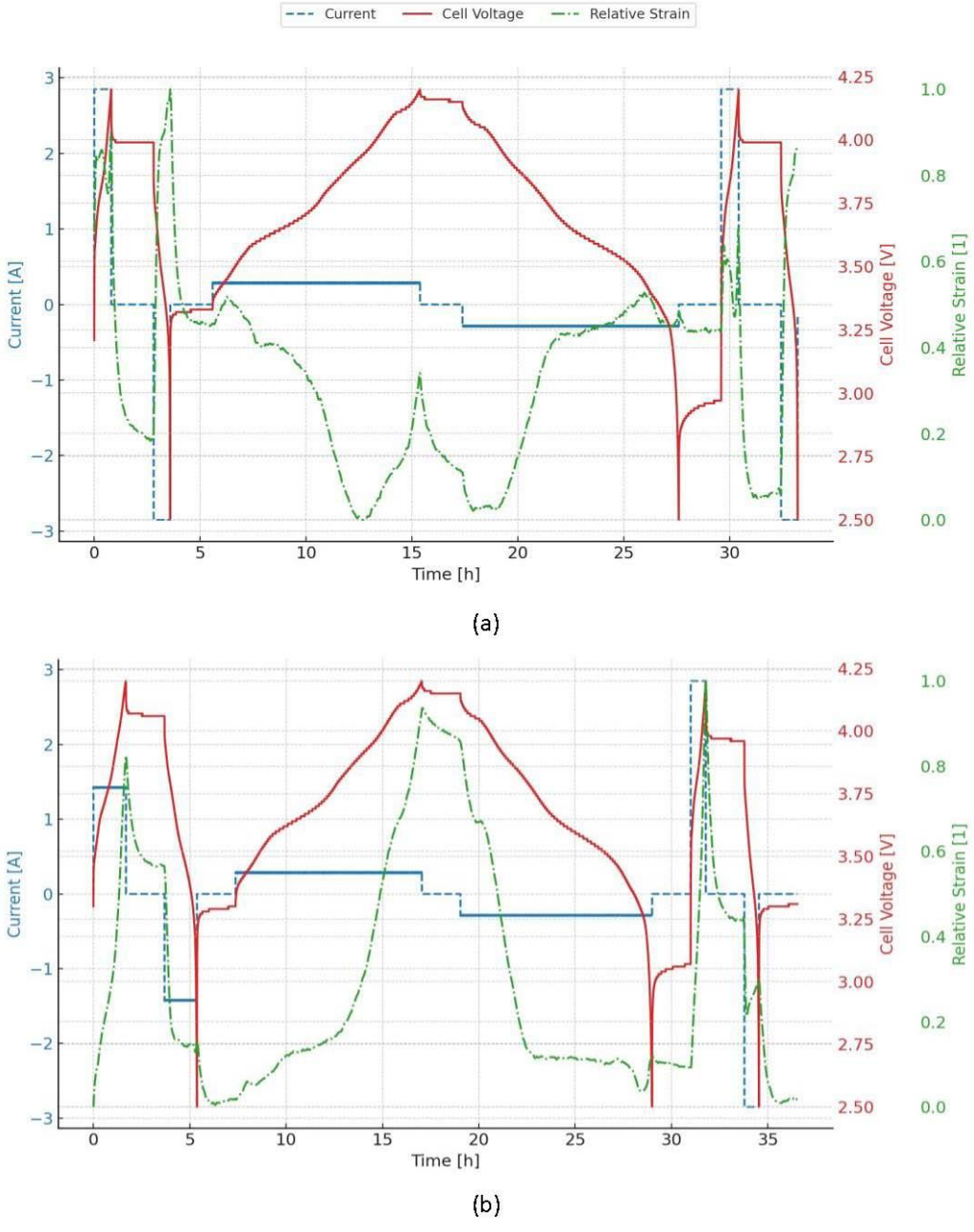

Figure 2. *Strain Measurement Samsung 29E. (a) Inverse Strain and (b) Position on Anode Tab*

The same procedure was repeated with Samsung INR18650 35E NMC cells, which have a nominal capacity of 3.5 Ah. This cell displayed the behavior observed in other studies. The results are shown in Figure 3. For this cell model, multiple positions were examined, all exhibiting similar characteristics. This indicates that the strain measurement of Samsung 35E cells is independent of the strain gage position. To avoid edge effects, strain gages for further measurements were applied at the middle position.

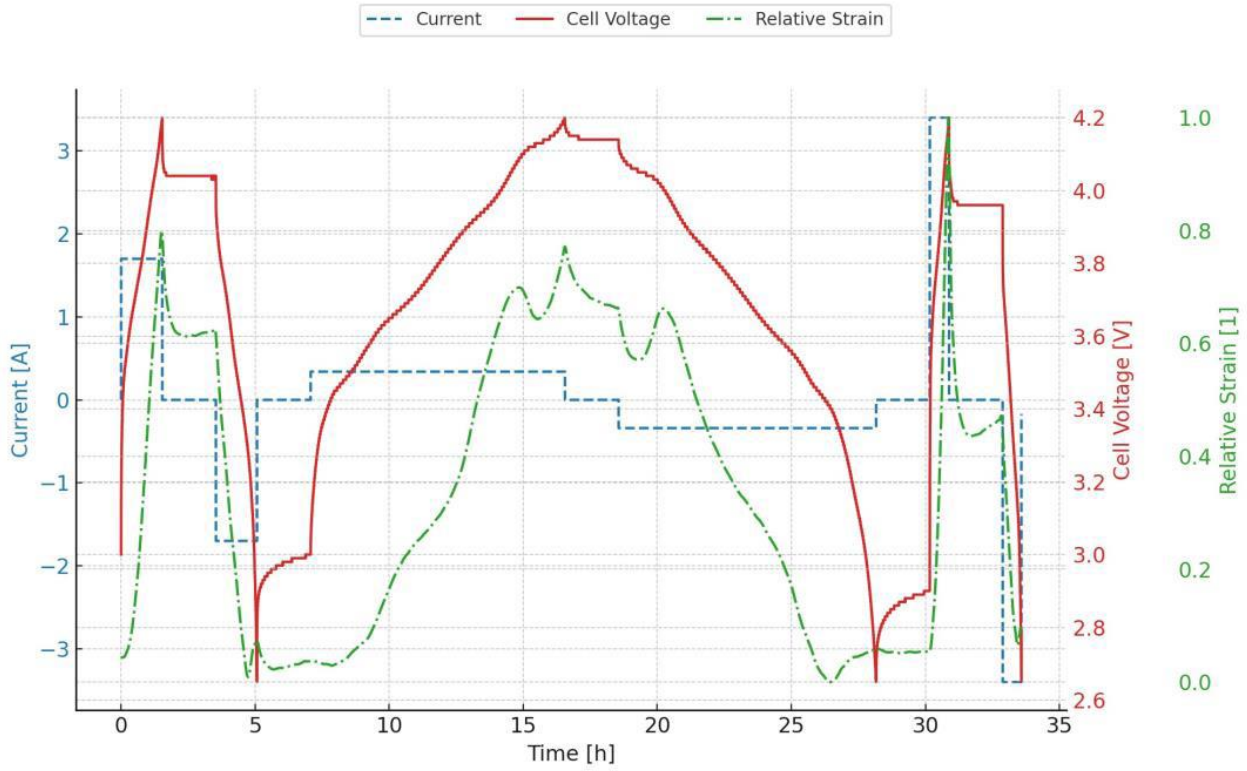

Figure 3. *Strain Measurement Samsung 35E*

To determine the cause of the difference between the cells, a post-mortem analysis was conducted. Both cells shared an identical design, with a positive tab along the entire length and a negative tab covering only the bottom half. As the cell designs were identical, they would not offer an explanation for the different strain curves. Therefore, the anode materials were investigated further. In fact, the Samsung 35E cell had an anode containing silicon, which explains the higher amplitudes and homogeneous strain throughout the cell. In contrast, no silicon was detected in the anode of the Samsung 29E cell, explaining its inhomogeneous behavior. This is due to silicon's much higher expansion rate, up to 300%, compared to graphite's expansion rate of up to 10%.

Conclusions and Outlook

This study has successfully proven, that strain values measured during charge and discharge on a cylindrical cell are closely linked to the SOC. Reproducible results were achieved only with anodes containing silicon. Cells with silicon displayed much higher amplitudes and a more homogeneous strain along the entire cell. In contrast, cells without silicon showed inhomogeneous and non-reproducible expansion. Additionally, strain values can be used to determine the state of health of a cell. It is also expected that strain values can identify safety-critical conditions, such as overcharging and overheating.

Acknowledgements

This project has received funding from the European Union's Horizon research and innovation programme under Grant Agreement No. 101137615.

References

1. L. K. Willenberg, P. Dechent, G. Fuchs, D. U. Sauer, and E. Figgemeier, *Sustainability*, **12**, 557 (2020).
2. W. Ren et al., *J. Mater. Sci.*, **57**, 13560–13569 (2022).

Impact of Transition Metal Contaminants in the Electrolyte on the Electrochemistry of Oxides in Lithium-Ion Batteries

Krum Banov[1], Ulf Breddemann[1], Miriam Khodeir[1], and Petr Novák[1,2]

[1]Technische Universität Braunschweig, Institute of Energy and Process Systems Engineering, Braunschweig, Germany

[2]Technische Universität Braunschweig, Battery LabFactory, Braunschweig, Germany
Email: p.novak@tu-braunschweig.de,

website: https://www.tu-braunschweig.de/en/ines

Recycling old battery cells is a green way to reuse materials by cleaning them and using them in new cells. However, this process can be complicated and might leave behind impurities like transition metal carbonates and sulfates. These impurities can get into the electrolyte and affect the performance of the battery over time.

To understand these effects, we conducted a series of electrochemical tests. We intentionally added impurities like Mn, Ni, and Co in the form of carbonates, sulfates, and acetates to the electrolyte. Then, we tested how these impurities affected the performance of NMC811 and NCA oxides in model lithium-ion batteries. The tests were done using both, half cells (versus lithium) and symmetrical Li||Li cells to isolate the impact on the cathodes. We used various techniques like constant current constant voltage (CCCV) cycling, electrochemical impedance spectroscopy (EIS), and rate capability tests to analyze the electrochemical characteristics of the industry-relevant cathodes NMC811 and NCA when exposed to electrolytes with artificially reduced purity levels.

The findings showed that transition metals (Ni, Co, and Mn) in the electrolyte, regardless of their form, significantly impact the performance of the oxide electrodes. This contamination changes the cathode-electrolyte interphase (CEI), increasing interfacial resistance and affecting the battery's performance. However, these effects on the positive electrodes are less significant compared to the well-known impact of these metals on the solid electrolyte interphase (SEI) on negative electrodes.

Locally Concentrated Ionic Liquid Electrolytes for High-Energy Batteries

Xu Liu[a,b], Cheng Xu[a,b], and Stefano Passerini[a,b]

[a] Helmholtz Institute Ulm (HIU), Helmholtzstraße 11, D-89081 Ulm, Germany

[b] Karlsruhe Institute of Technology (KIT) P.O. Box 3640, D-76021 Karlsruhe, Germany

[c] Austrian Institute of Technology (AIT), Transport Technologies, Giefinggasse 4, 1020 Wien, Austria

E-mail: stefano.passerini@kit.edu; Stefano.passerini@ait.ac.at

Non-flammable ionic liquid electrolytes (ILEs) are well-known candidates for safer and long-lifespan lithium metal batteries (LMBs). However, the high viscosity and insufficient Li^+ transport limit their practical application. Recently, non-solvating and low-viscosity co-solvents diluting ILEs without affecting the local Li^+ solvation structure are employed to solve these problems. The diluted electrolytes, i.e., locally concentrated ionic liquid electrolytes (LCILEs), exhibiting lower viscosity, faster Li^+ transport, and enhanced compatibility toward lithium metal anodes, are feasible options for the next-generation high-energy-density LMBs. In the presentation, the progress of the recently developed LCILEs are summarised, including their physicochemical properties, solution structures, and applications in LMBs with a variety of high-energy cathode materials. Lastly, a perspective on the future research directions of LCILEs will be given as well as the most recent results on Li and post-Li metal anode cells.

References

1. Liu X., Mariani A., Diemant T., Di Pietro M.E., Dong X., Mele A., Passerini S. Reinforcing the Electrode/Electrolyte Interphases of Lithium Metal Batteries Employing Locally Concentrated Ionic Liquid Electrolytes (2023) Advanced Materials DOI: 10.1002/adma.202309062
2. Liu X., Mariani A., Zarrabeitia M., Di Pietro M.E., Dong X., Elia G.A., Mele A., Passerini S. Effect of organic cations in locally concentrated ionic liquid electrolytes on the electrochemical performance of lithium metal batteries (2022) Energy Storage Materials, 44, pp. 370 – 378 DOI: 10.1016/j.ensm.2021.10.034
3. Liu X., Mariani A., Diemant T., Pietro M.E.D., Dong X., Kuenzel M., Mele A., Passerini S. Difluorobenzene-Based Locally Concentrated Ionic Liquid Electrolyte Enabling Stable Cycling of Lithium Metal Batteries with Nickel-Rich Cathode (2022) Advanced Energy Materials, 12 (25), art. no. 2200862 DOI: 10.1002/aenm.202200862
4. Liu X., Mariani A., Diemant T., Dong X., Su P.-H., Passerini S. Locally Concentrated Ionic Liquid Electrolytes Enabling Low-Temperature Lithium Metal Batteries (2023) Angewandte Chemie - International Edition, 62 (31), art. no. e202305840 DOI: 10.1002/anie.202305840
5. Liu X., Mariani A., Adenusi H., Passerini S. Locally Concentrated Ionic Liquid Electrolytes for Lithium-Metal Batteries (2023) Angewandte Chemie - International Edition, 62 (17), art. no. e202219318DOI: 10.1002/anie.202219318
6. Liu X., Zarrabeitia M., Mariani A., Gao X., Schütz H.M., Fang S., Bizien T., Elia G.A., Passerini S. Enhanced Li+ Transport in Ionic Liquid-Based Electrolytes Aided by Fluorinated Ethers for Highly Efficient Lithium Metal Batteries with Improved Rate Capability (2021) Small Methods, 5 (7), art. no. 2100168 DOI: 10.1002/smtd.202100168

7. Liu X., Diemant T., Mariani A., Dong X., Di Pietro M.E., Mele A., Passerini S. Locally Concentrated Ionic Liquid Electrolyte with Partially Solvating Diluent for Lithium/Sulfurized Polyacrylonitrile Batteries (2022) Advanced Materials, 34 (49), art. no. 2207155 DOI: 10.1002/adma.202207155

Atomic Layer Deposition of Alumina for Enhanced Electrochemical Performance of $LiFePO_4$ Cathodes

Prangya P. Sahoo[a], Boris Hudec[b], Miroslav Mikolášek[c], Magdaléna Precnerová[a], Matej Mičušík[d], Peter Nádaždy[a,e], Peter Siffalovic[a,e], Karol Fröhlich[a, b]

[a]Centre for Advanced Materials Application, Slovak Academy of Sciences, 845 11 Bratislava, Slovakia

[b]Institute of Electrical Engineering, Slovak Academy of Sciences, 841 04 Bratislava, Slovakia

[c]Institute of Electronics and Photonics, Slovak University of Technology, Ilkovičova 3, 812 19, Bratislava, Slovakia

[d]Polymer Institute, Slovak Academy of Sciences, Dúbravská cesta 9, 845 41, Bratislava, Slovakia

[e]Institute of Physics, Slovak Academy of Sciences, 845 11 Bratislava, Slovakia

*Contact author: prangya.sahoo@savba.sk

This study explores the electrochemical performance of $LiFePO_4$ (LFP) cathodes enhanced with ultrathin alumina coatings deposited via atomic layer deposition (ALD) at 100 °C using trimethyl aluminum and water vapors. Alumina coatings ranging from 2 to 20 cycles were applied to LFP cathodes. Various electrochemical measurements, including cyclic voltammetry, galvanostatic charging-discharging, and electrochemical impedance spectroscopy (EIS), were performed on both coated and uncoated LFP electrodes. Results demonstrated that alumina-coated LFP electrodes exhibit lower charge transfer resistance and superior rate capability compared to uncoated electrodes. Elevated temperature tests at 50 °C confirmed the enhanced capacity of alumina-coated LFP. X-ray photoelectron spectroscopy (XPS) revealed differences in the composition of the cathode electrolyte interphase (CEI) and solid electrolyte interphase (SEI) layers. Operando X-ray diffraction showed that uncoated LFP electrodes form an inactive $FePO_4$ phase during cycling, while alumina-coated electrodes maintain stable phase volumes, indicating effective protection against chemical degradation.

Introduction

The quest for high-performance lithium-ion batteries has driven significant research into optimizing cathode materials. Among these, $LiFePO_4$ (LFP) offers several advantages such as excellent thermal stability, long cycle life, and safety. It has a theoretical specific capacity of 170 mAh/g. Li-ion batteries with LFP cathodes have a long cycle life with excellent charging/discharging performance. However, the intrinsic low electronic conductivity and moderate ionic diffusion rate of LFP limit its rate capability and overall electrochemical performance. To address these challenges, surface modification techniques such as coating with ultrathin layers have been explored. Atomic Layer Deposition (ALD) technique, known for its precise control over film thickness and uniformity, has emerged as a promising method to enhance the properties of LFP

cathodes. In our contribution, we show that the surface modification of the LFP cathode using ultrathin alumina films grown by atomic layer deposition (ALD) improves Li-ions charge transfer and rate performance.

Experimental

The composition of the cathode sheet was Lithium Iron Phosphate ($LiFePO_4$), poly(vinylidene fluoride) (PVDF), and Carbon Black (Super P) in a ratio of 90:5:5. Ultrathin alumina (Al_2O_3) thin films were grown on LFP electrodes using trimethylaluminum (TMA) and deionized water as a precursor and reactant, respectively. The deposition was carried out at 100 °C. The growth per ALD cycle (GPC) of the deposited alumina films as determined by ellipsometry was 0.1 nm/cycle.

The electrochemical measurements were carried out in a 2-electrode configuration using the LFP electrodes (pristine or coated by ALD alumina) as working electrodes and lithium metal or graphite electrodes as counter electrodes in half-cell and full-cell configurations respectively. Lithium hexafluorophosphate solution in ethylene carbonate and dimethyl carbonate (1.0 M $LiPF_6$ in EC/DMC) was used as the electrolyte. The cells were cycled at a constant current between 2.5-4.1 V vs. Li/Li+ (1C equal to 170 $mAhg^{-1}$). The EIS measurements were carried out in potentiostatic mode at a bias of 2.5 V (lithiated state). The electrochemical tests were also performed at 50 °C in a full-cell configuration.

Operando X-ray diffraction (XRD) experiments were conducted using a commercial in-situ battery cell. Both pristine and ALD-coated batteries were measured in a custom-designed setup that utilized a microfocus X-ray source and a 2D X-ray detector. The LFP electrodes were analyzed by scanning electron microscopy (SEM), X-ray photoelectron spectroscopy (XPS).

Results and Discussion.

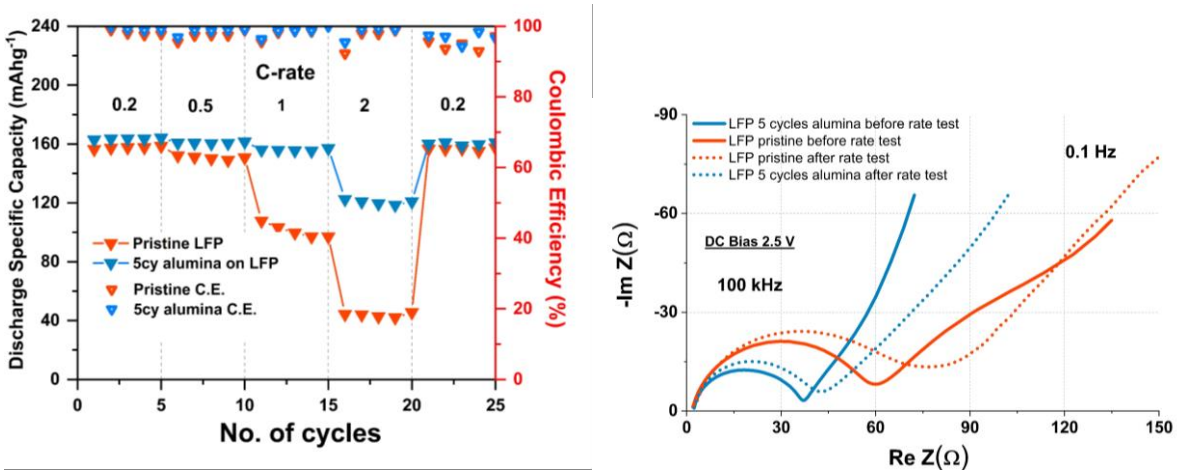

Figure 1. *Cyclic performance of the pristine LFP and 5 cycles alumina coated LFP at different C-rates in a half-cell configuration and Nyquist plots of the pristine and alumina coated LFP cathodes before and after rate test.*

The electrochemical performance indicates a beneficial effect of the alumina coating on the fast kinetics of intercalation/deintercalation of lithium ions into the LFP structure. Figure 1 shows the rate performance of the cells with the pristine and 5 ALD cycles alumina coated samples at the C-rates of 0.2, 0.5, 1, 2, and 0.2 C. The LFP electrode coated by 5 ALD cycles of alumina showed a

higher discharge specific capacity at all the C-rates performed compared to the pristine LFP electrode. Similarly, lower charge transfer resistance was observed for the 5 cycles alumina coated LFP sample compared to the uncoated LFP cathode.

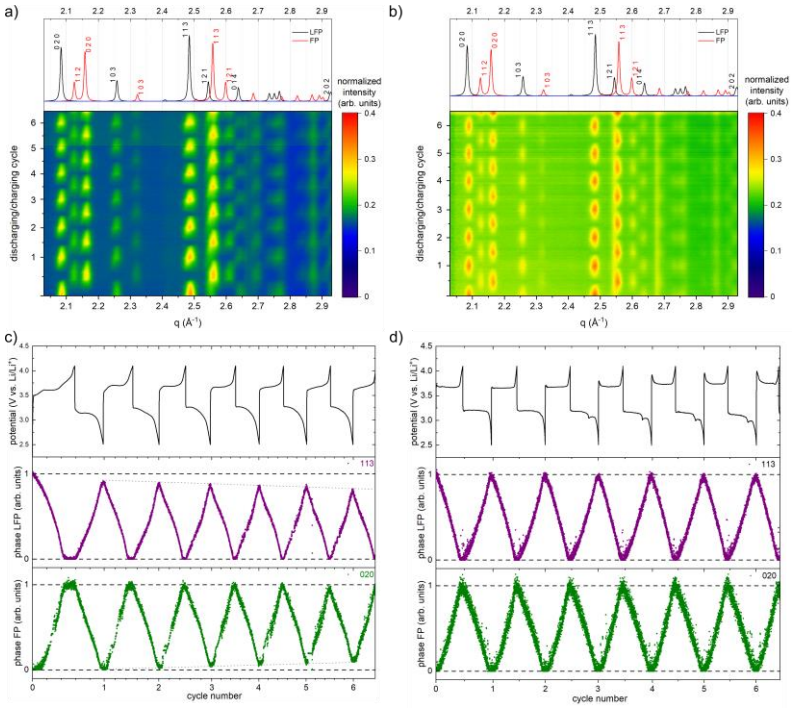

Figure 2. *Time-resolved diffracted intensity for a) pristine and b) ALD-coated cathodes for the first six cycles. The phase volumes of LFP and FP phases as a function of cycle number for c) pristine and d) ALD-coated cathodes.*

Operando XRD can track inactive material phases, offering more detailed insights into the lithiation/delithiation process. The phase volume of the LFP phase decreases continuously during the first cycles, as shown by the dotted line in Fig. 2c. This decrease signifies the formation of an inactive FP phase that cannot be re-lithiated. In contrast, the ALD-coated cathode shows no changes in the phase volumes of FP and LFP, as these phases always return to their initial maxima and minima (dashed line in Fig. 2d).

Electrochemical measurements carried out in full-cell configuration at room temperature and at elevated temperature of 50 °C showed superior performance of ALD alumina coated LFP electrode compared to the pristine uncoated LFP electrode. XPS analysis revealed the robustness of the ALD alumina layer since it could be detected on the surface of the coated LFP electrodes even after long electrochemical cycling. XPS analyses also provided significant insight into the composition of the cathode electrolyte interphase (CEI) and solid electrolyte interphase (SEI) layers. Atomic layer deposited ultrathin alumina layers significantly improve the electrochemical properties and can provide effective protection to the underlying LFP electrode.

Acknowledgments

The authors acknowledge the support from VEGA 2/0162/22 and APVV-20-0111 projects.

Innovative approaches to recycling graphite from lithium-ion batteries by enhancing capacity with silicon from PV panels

Jiří Báňa[1], Antonín Šimek[1], Tomáš Kazda[1]

[1]Department Of Electrical and Electronic Technology, University of Technology Brno, Czech Republic

With the rising consumption of lithium-ion batteries (LIBs), it has become essential to develop efficient and environmentally friendly recycling methods. Graphite, despite being abundant and inexpensive, often receives less attention in recycling efforts compared to other materials, particularly precious metals. However, the direct recycling of graphite presents a green and cost-effective solution. By incorporating recycled silicon from solar panels, we can merge recycling processes from two different sectors, thereby enhancing the capacity of the anode material.

Introduction

Graphite plays a dominant role in the commercial lithium-ion battery (LIB) market due to its excellent electrochemical properties and excellent availability. However, graphite gradually degrades during cycling. The aim of graphite recycling is to remove impurities and restore its crystal structure.

The first step in reconditioning used graphite is to remove impurities, including SEI residues, polymer binders, conductive substances, dirt and metal deposits from the cathode material or current collectors. Various methods are used for this cleaning process, such as heat treatment or chemical treatment. [1] [2]

The photovoltaic sector, like the lithium-ion battery sector, is experiencing a major boom. At the end of the life of the panels, a huge amount of waste is generated and needs to be recycled efficiently. Recycling silicon from PV panels can be more economically viable than producing new high purity silicon. [3] [4]

Experiment

This study is based on published article in *Monatshefte für Chemie - Chemical Monthly* [5] using a commercial Motoma LFP 18650 battery (1500 mAh) with an LFP cathode and graphite anode, cycled at a 1C-rate for 500 cycles to simulate aging, resulting in an 8.4% capacity drop to 1375 mAh. The battery was dismantled, and the graphite anode weight 6.156 g. Capacity was calculated to 234 mAh/g after aging. The graphite was electrochemically tested reaching capacity over 300 mAh/g.

The graphite was calcined in an inert nitrogen atmosphere for 15 hours at 1000°C. The Si wafer was crushed in a ball mill. The slurry was made by mixing graphite with silicon using a magnetic stirrer. PVDF and NMP solvent were used as the binder. The representation of graphite in the slurry is 70 %, silicon 10%, PVDF 10 % and 10 % SupP as a conductive additive. The slurry was deposited on a copper collector to form electrodes which were dried for 12 h at 60 °C and then pressed with four different pressures - 1843 N/cm^2, 3840 N/cm^2, 5684 N/cm^2 and 7681 N/cm^2. The fabricated electrodes were used to form electrochemical EL-Cells with Li counter electrode.

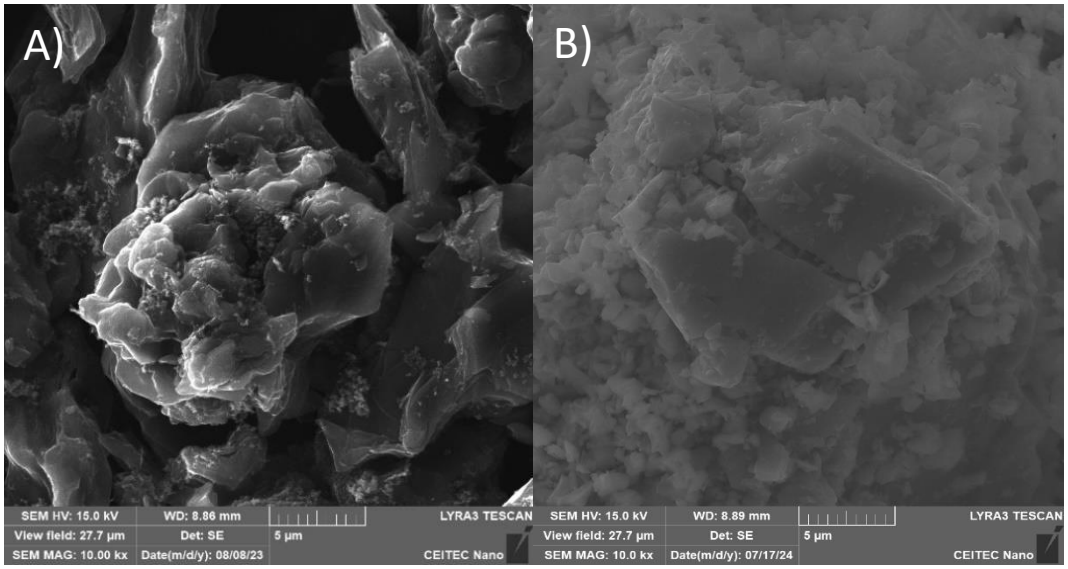

Figure 1. *SEM of Motoma LFP 18650 graphite after calcination in nitrogen atmosphere*

Fig. 1A shows the structure of graphite after calcination at 1000°C for 15 hours. Fig. 1B shows the structure of the ground silicon wafer.

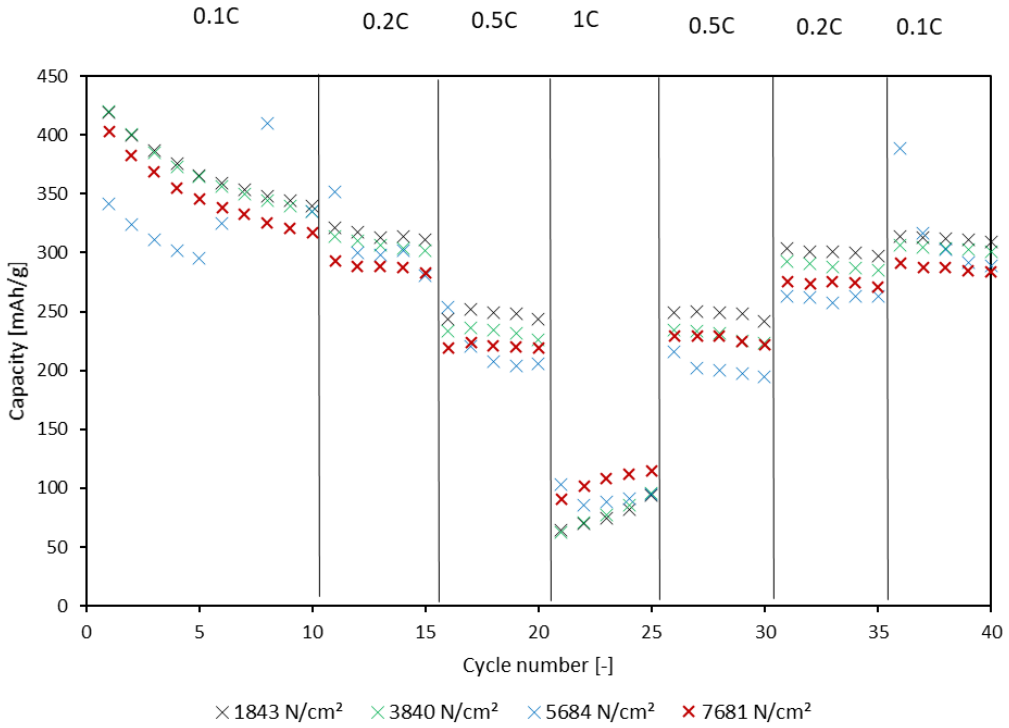

Figure 2. *Capacity of electrodes with different pressing pressures with different C-rates*

As shown in Fig. 2, the capacity of recycled graphite with recycled silicon exceeds 400 mAh/g, while theoretical capacity is 772.9 mAh/g. At a pressing pressure of 1843 N/cm^2 and 3840 N/cm^2, the capacity identically reaches 420 mAh/g. With increasing currents, the capacity gradually decreases for all pressing pressures, with the electrode with the highest pressing pressure reaching the highest capacity at 1C. At 40 cycles, the capacity reaches 309 mAh/g at a pressing pressure of 1843 N/cm^2 resulting in 26.4 % capacity drop. The capacity decreases with increasing pressing

pressure in 40 cycle. The electrode pressed at 5684 N/cm^2 shows an anomaly of occasional jump in capacity, which may be due to silicon particle cracking. Generally, this electrode shows the lowest capacity.

Conclusion

Doping graphite with silicon significantly increases the electrode capacity, where we are well above the theoretical capacity of graphite. However, the capacity decreases significantly in the first 10 cycles, a plateau can be observed after the first 15 cycles when the decrease in capacity slows. This is a possible approach of recycling graphite and recycling PV panels and reusing silicon, since the cost of silicon per kWh is lower than the cost of graphite. It can be observed that different pressing pressures affect the resulting electrode capacity.

Acknowledgments

This work was supported by the specific graduate research of the Brno University of Technology No. FEKT-S-23-8286. CzechNanoLab project LM2023051 funded by MEYS CR is gratefully acknowledged for the financial support of the measurements at CEITEC Nano Research Infrastructure.

Bibliography

1. WU, Jiawei; ZHENG, Mengting; LIU, Tiefeng; WANG, Yao; LIU, Yujing et al. Direct recovery: A sustainable recycling technology for spent lithium-ion battery. online. *Energy Storage Materials*. (2023)
2. LU, Yingqi; PENG, Kaiyuan a ZHANG, Lingen. Sustainable Recycling of Electrode Materials in Spent Li-Ion Batteries through Direct Regeneration Processes. online. *ACS ES&T Engineering*. (2022)
3. ANIELA-ABIGAIL, Hernández-López; TARIQ, Rasikh; MEKAOUI, Amina El; BASSAM, A.; VEGA DE LILLE, M. et al. Does recycling solar panels make this renewable resource sustainable? Evidence supported by environmental, economic, and social dimensions. online. *Sustainable Cities and Society*. (2022)
4. RAJASEKAR, R.; MOGANAPRIYA, C. a MOHANKUMAR, A. (ed.). *Materials for Solar Energy Conversion*. online. Wiley, (2021)
5. BÁŇA, Jiří; ČUDEK, Pavel; ŠEDINA, Martin; ŠIMEK, Antonín a KAZDA, Tomáš. Effect of pressing pressure on the capacity of recycled graphite anode. online. *Monatshefte für Chemie - Chemical Monthly*. (2024)

Spray drying Synthesis and Electrostatic Precipitation in Li-ion Battery Cathode Material Production

H. Hálová[a], L. Preisler[b], L. Chladil[a]

[a] Department of Electrical and Electronic Technology, Brno University of Technology, Technická 10, 616 00 Brno, Czech Republic

[b] Department of Power Engineering, Brno University of Technology, Technická 2896, 616 69 Brno, Czech Republic

As society's reliance on electronic devices and electric vehicles grows, improving lithium-ion (Li-ion) batteries' efficiency, sustainability is essential. This paper investigates innovative methods for producing submicron particles for Li-ion batteries, focusing on spray drying synthesis. This technique involves atomizing a solution into droplets, which are then dried and collected. The study also examines electrostatic precipitation, for capturing particles as small as 10 μm, and its integration with spray drying. Following particle collection, heat treatment is necessary to achieve optimal properties, with temperatures ranging from 750°C to 1,000°C. The study demonstrates the potential of spray drying synthesis and electrostatic precipitation in producing high-quality, low-cobalt cathode materials.

Introduction

Nowadays, when our society relies more and more on electronic devices and electric vehicles, the efficiency, performance and safety of lithium-ion (Li-ion) batteries becomes essential. The demands of users on these devices are also increasing. Charging speed, battery life and the total lifetime of accumulators are key factors affecting the user comfort and practicality of these modern technologies, and at the same time, they can form a barrier to entering completely new areas of their use. [1]

Due to the dynamics of the lithium-ion battery market, there is a growing focus on developing low-cobalt cathode materials to reduce costs and address environmental concerns. These materials dominate Li-ion batteries and account for over 50% [2] of their cost. The internal structure and particle size of the cathode material are crucial, as smaller particles with larger interfacial areas enhance the diffusion of lithium ions, improving charge/discharge rates and specific capacity. [1]

Cathode material preparation options

Common methods for creating cathode materials include the solid-state reaction [3] and sol-gel method [3]. The solid-state reaction is affordable and simple but struggles with controlling particle size and uniformity and requires high temperatures. The sol-gel method ensures even particle distribution, accurate stoichiometric control, and high purity but involves longer processing times and high initial costs.

Spray drying synthesis, commonly used in the food and pharmaceutical industries [4], offers simple scalability. It involves generating droplets, drying them to form particles, and collecting these

particles. Precursors are dissolved in water or ethanol, with common cation sources being acetates, nitrates, and ammonium salts as anion sources. Organic substances like citric acid are added as reducing agents or to increase electrical conductivity through carbon content. [1], [3], [4]

The liquid is sprayed into a drying chamber heated to 190-220°C for aqueous solutions [1]. Particles can be collected using methods like cyclones, gravity settling (40-50% efficiency), filtration (up to 99% efficiency for particles as small as 2 μm), or electrostatic precipitation (90-99% efficiency for particles from 10 μm). [1]

Electrostatic precipitator

One of the main requirements of the synthesis in the laboratory conditions is to collect sufficient quantity of the synthesized particles for electrode preparation with as little intervention from the operator as possible. On the other hand, we have to reckon with higher purchase costs, possibly also with our own equipment modifications. For proper operation of the electrostatic precipitator, the following principles must be observed: use of *DC voltage* (the DC voltage excites the electric field), a sufficiently high voltage to produce a corona discharge (but not sparking discharge), ensure adequate air flow (slow enough to charge the particles and subsequently trap the particles on the collection electrode). [5]

Figure 1 shows a model of a cylindrical electrostatic precipitator (the centre of the precipitator consists of a thin electrode used to charge the particles and the perimeter consists of a sheet of opposite polarity used to subsequently) designed in Matlab. The dimensions of the separator, together with the voltage, also determine the efficiency of particle collection. This efficiency increases with increasing radius of the charging electrode and also with increasing voltage, but care must be taken not to exceed the spark discharge limit.

Heat Treatment of Prepared Powder

After the collection of the atomized particles, further heat treatment is required. The storage of hygroscopic powders in particular is not recommended, due to the binding of atmospheric moisture and deterioration of the product. However, additional heat treatment is required in most other cases as well [1].

The temperature of additional heat treatment reported in the publications [6], [7], [8] varies from 750 °C to 1,000 °C in the time range from 5 to 15 hours. Seeenivasan in his publication [6] recommends also preheating at 500 °C for 5 hours.

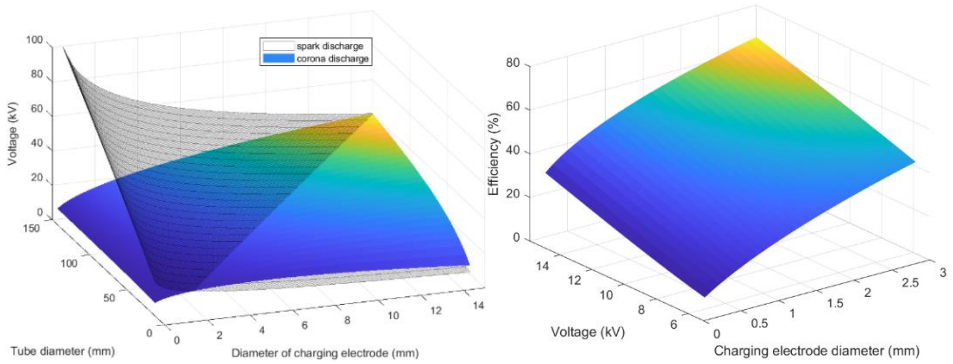

Figure 1. *Dependance of the voltage on the variables tube diameter and diameter of charging electrode for length of electrostatic precipitator of 0.4 m (left) and dependance of efficiency on the voltage and charging electrode diameter (right)*

Conclusion

This paper explores spray drying for synthesizing low-cobalt cathode materials, noting its scalability and effectiveness in producing uniform submicron particles. Electrostatic precipitation efficiently collects these particles, with insights into the impact of voltage and electrode dimensions on collection efficiency. Future research should focus on optimizing heat treatment processes, including temperature and duration, and investigate the hygroscopic properties of the particles to understand their impact on performance and stability.

Acknowledgments

Place acknowledgments at the end of the text, before the references.This work was supported by the specific graduate research of the Brno University of Technology No. FEKT-S-23-8286

References

1. B. Vertruyen and F. Boschini et al, *Materials*, **11**, 7 (2018)
2. M. Bielewski and Pfrang A et al, *Publications Office of the European Union*, Luxembourg (2022)
3. T. Wani and G. Suresh et al, *Journal of energy Storage*, **44** (2021)
4. A. Stunda-Zujeva and Z.Irbe et al, *Ceramics International*, **43**, 15, (2017)
5. J. Böhm, *Elektrické odlučování a odlučovače*, *Státní nakladatelství technické literatury* (1959)
6. M. Seenivasan and J. Jeyakumar, *Journal of Alloys and compounds*, **926** (2022)
7. M. Ihalainen and M. Kortelainen et al, *Advanced Powder Technology*, **34**, 10 (2023)
8. Y. James Li and W. Chien et al, Ceramics International, **48**, 5 (2022)

Electrochemical Impedance Spectroscopy for Lithium-ion Batteries

K. Jaššo[a,b], D. Biolek[b]

[a] Department of Electrical Engineering, University of Defence, 662 10 Brno, Czech Republic

[b] Department of Electrical and Electronic Technology, Brno University of Technology, 616 00 Brno, Czech Republic

Electrochemical impedance spectroscopy (EIS) is a relatively simple and powerful technique used for investigating physicochemical processes occurring in electrochemical systems, such as batteries. It separates complex electrochemical processes into basic ones based on their different relaxation times. However, approaches to EIS evaluation vary across the literature. The purpose of this paper is to provide a more detailed look at the proper procedures for using EIS to measure Li-ion batteries.

Introduction

Among scientists, Electrochemical Impedance Spectroscopy (EIS) is often regarded as a relatively simple technique for translating complicated physicochemical phenomena into simple electrical elements. However, there are often significant differences between scientists in the use of EIS and in the interpretation of measured impedance spectra. EIS is often perceived differently by chemists than by electrical engineers, and differently by theorists than practitioners. Thus, for more complex electrochemical systems such as Li-ion batteries, there are many different approaches, equivalent circuit models (ECMs), and interpretations of EIS [1]. Furthermore, due to the complexity of EIS, it can often be difficult to evaluate the accuracy of the measured data, which depends on the proper EIS settings, the accuracy of the measuring instrument and the extraneous contributors (e.g. wires, etc.).

Different ECMs are used to fit the measured data in the case of Li-ion. This is mainly due to the fact that different ECMs can fit a single impedance spectrum. But how is it possible to tell which ECM is the correct one? Clearly, without a comprehensive understanding of the internal processes in the measured electrochemical system, it is impossible to assign the correct equivalent electrical elements to the individual physicochemical phenomena. However, with the increasing popularity and use of EIS in Li-ion battery research, incorrectly measured or evaluated impedance spectra are appearing in papers.

Measurement

The basic prerequisite to ensure the validity of the experimental data is the appropriate measurement settings. The main input parameters of EIS measurements are the input signal amplitude and the frequency range. The amplitude of the input signal in potential EIS (PEIS) is often set in the range of 1-10mV to ensure pseudolinearity of the measured system. Too high a value may affect the quality of the measured spectrum due to the non-linearity of the measured system, but too low a value may be masked by noise. The amplitude of the input signal must therefore be chosen with respect to the measured system and the accuracy of the instrument.

The frequency range of the measurement is another input parameter that highly depends on the instrument and measured system. Every potentiostat has accuracy limits, particularly at extreme frequencies or impedances, which are often shown in its Accuracy Contour Plot [2]. This plot is crucial for understanding the capabilities and limitations of a potentiostat when performing EIS.

Besides the accuracy of the potentiostat, obtaining valid EIS measurements requires the system under investigation to be linear, stable, causal, stationary, and time-invariant. In the case of Li-ion cells, these conditions may not always be met, which could result in a distortion of the measured impedance spectrum, particularly in the low-frequency region where the measurement time is longer.

Battery connection

Another often overlooked prerequisite is the proper connection of the measured system to the instrument. A potentiostat can control both the current and the voltage applied to a cell and usually consists of at least 4 cables. The 4-point connection of the Li-ion cell with the potentiostat separates current-carrying wires (+P,-P) from voltage-sensing wires (+S, -S), eliminating voltage drops across connectors, cables, or interfaces, and ensuring no current passes through the voltage-sensing leads. Separating the contact of current-carrying wires and voltage-sensing wires is important as it results in more accurate and reliable electrochemical measurements, as the measurement is performed directly on the cell itself. While a 2-point connection between the cell and the potentiostat is feasible, it is advisable to use a 4-point measurement to ensure the quality of the experimental data.

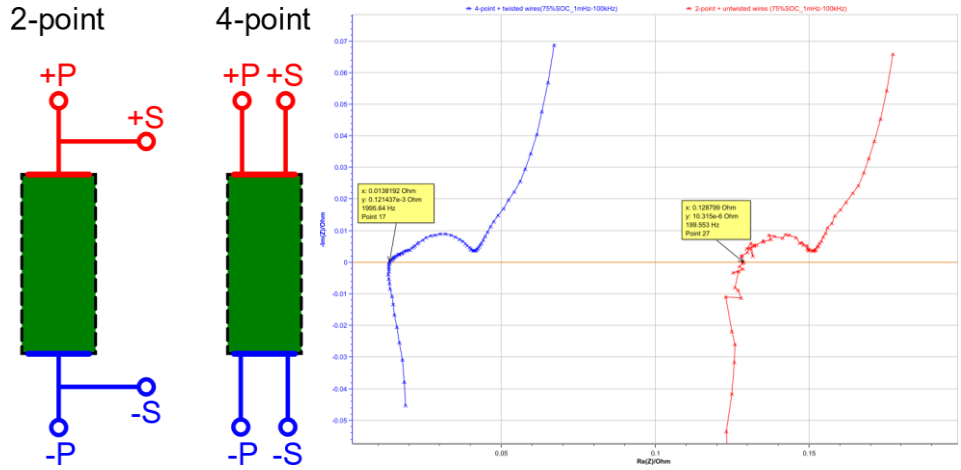

Figure 1. *Differences in connection and measured impedance spectra for 2-point (+untwisted cables) [red] and 4-point (+twisted cables) [blue] Li-ion cell connection to potentiostat*

The connecting cables can also affect the measured impedance, especially in the high-frequency region. In the high-frequency region of the measured impedance spectra of Li-ion cells, an inductive character is often observed, which is not expected in the case of an ideal battery system. This inductive character in the high-frequency region is typically attributed to the inductive contribution of the connecting cables and instrument and is often removed from the measured impedance spectra without hesitation. This can be problematic as the impedance spectrum is complex and the values of the individual ECM elements are often tied to each other. Thus, removing the inductive character from the measured impedance spectrum and inductor from the ECM leads to distortion of the results, as this inductance often affects the values of the series resistance and the impedance of the first time constant. Therefore, instead of ignoring this problem, it is better to minimize its effect. This stray impedance is mainly caused by mutual inductance of the

connection cables caused by magnetic flux due to current flowing through wires. It can be suppressed by twisting pair of current-carrying cables and maximize the distance between them and the voltage-sensing pair. In certain experimental setups, the need for extended cables may arise. However, this is generally not advised as it can negatively impact the quality of the measured data.

Equivalent circuit models

A wide variety of different Li-ion battery ECMs have been proposed in the literature, differing in complexity, parameterization speed and accuracy. These circuits can be divided into three key categories:

1. Thevenin-like ECMs (RC circuits)
2. Randles-like ECMs (Faradaic reaction circuits)
3. Complex ECMs

Thevenin-like ECMs are often used in mathematical modelling of Li-ion batteries. These models consist of only simple resistors, inductors and capacitors. For some Li-ion battery applications, such as electric vehicles or large-scale electrical grid storage, these models are often sufficient.

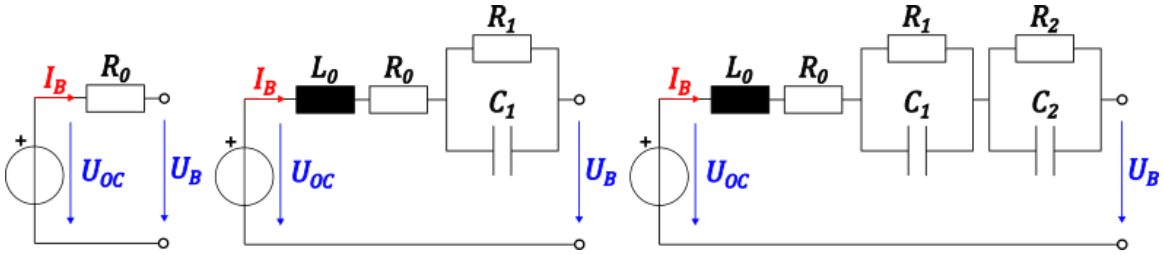

Figure 2. *Thevenin-like ECMs: a) Simple R model b) First-order RC model (1RC) c) Second-order RC model (2RC)*

To better describe Li-ion cells and the dependence of their properties on SOC, SOH, temperature and current, more complex Randles-like circuits are used. These ECMs incorporate fictional elements such as CPE or Warburg impedance, which can better mimic real physicochemical phenomena, such as diffusion.

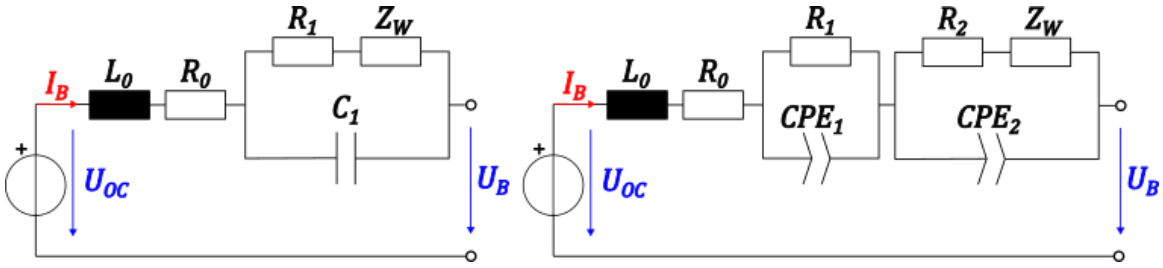

Figure 3. *Randles-like ECMs: a) Classic Randles circuit b) Second-order Randles with CPEs (2RCPE-W)*

The last category is complex ECMs for which there are several different approaches. The first approach is to attempt to describe the contributions of all the individual parts of a Li-ion cell by separate elements [1]. However, many physicochemical phenomena occur at similar frequencies and thus merge in the impedance spectra due to the overlap of time constants, which can lead to ambiguities in analysis. The second approach is to capture the non-linear nature of the Li-ion battery in the ECM itself, e.g. by using variable resistors, capacitors and diodes [3]. A last approach is the proposal of new unique models or elements that can better describe electrically or chemically the various processes taking place in Li-ion batteries.

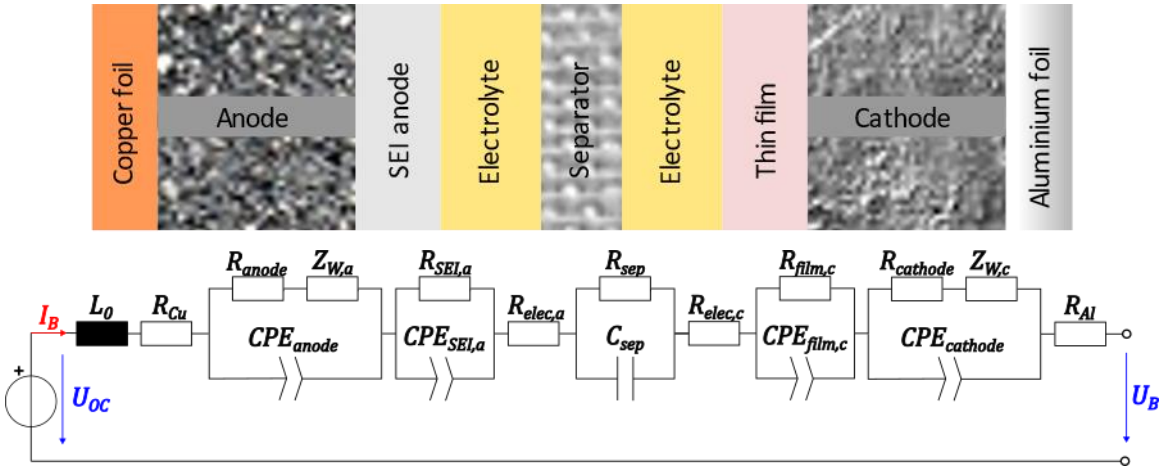

Figure 4. *Complex ECM attempting to define the individual components of a cell [1]*

Conclusion

To obtain accurate results with the EIS method, meticulous attention to detail is required. Factors such as the selection of measurement parameters, the accuracy of the measuring instrument, and the method of connecting the Li-ion cell to the potentiostat can greatly influence the resulting impedance spectra. As demonstrated on actual measured data, the difference in impedances between 2-point and 4-point connections is significant and even caused the measured data to shift by up to one frequency order. Therefore, it's essential to carefully establish experimental conditions that align with the system under study and the measuring instrument before initiating a measurement. Furthermore, it is necessary to find a balance between sustaining reasonable experiment durations and obtaining meaningful results. Once valid data has been measured, the next challenge lies in selecting and fitting an equivalent circuit. This topic will be addressed in greater detail in subsequent work.

Acknowledgments

This work was supported by the Czech Science Foundation under grant No. 24-12982S and specific research project at Brno University of Technology (FEKT-S-23-8286) and institutional support from the Ministry of Defence of the Czech Republic.

References

1. J. Doe and R. Hill, *J. Electrochem. Soc.*, **152**, H1902 (2005).
2. R. Smith, Electrochem. Solid-State Lett., **10**, A1 (2007).
3. E. Gaura and R. M. Newman, *ECS Trans.*, **4**(1), 3 (2006).
4. D. Warren and J. M. Woodall, in *Semiconductor Cleaning Technology/1989*, J. Ruzyllo and R. E. White, Editors, PV 90-9, p. 371, The Electrochemical Society Proceedings Series, Pennington, NJ (1990).
5. F. P. Fehlner, *Low Temperature Oxidation: The Role of Vitrous Oxides*, p. 23, Wiley Interscience, New York (1986).
6. N. J. DiNardo, in *Metallized Plastics 1*, K. L. Mittal and J. R. Susko, Editors, p. 137, Plenum Press, New York (1989).

Kinetic Model for Improved Dynamic Current Response in Lithium-ion Battery Electrical Circuit Models

J. Kasper[a], P. Hrzina[a], L. Černá[a], T. Finsterle[a], and V. Knap[a]

[a] Department of Electrotechnology, Faculty of Electrical Engineering, Czech Technical University in Prague, Technická 2, 166 27 Prague, Czech Republic

Nowadays, Lithium-ion (Li-ion) batteries are used in many applications due to their advantageous properties such as high energy density, long lifetime, and low self-discharge. For their effective use, battery models that can accurately describe battery behavior are utilized in management systems. In this work, a classical electrical circuit model is expanded by a kinetic battery model to improve model accuracy under highly dynamic conditions.

Introduction

Electrochemical power sources are of great importance in many electrical systems because the chemical energy stored inside them can be converted into electrical energy and delivered into electrical systems. For effective usage of batteries models are created. With accurate and efficient models, battery runtime can be predicted and optimized. There is a tradeoff between accuracy and hardware requirements where electrical circuit models (ECM) are less hardware intensive, but they do not reach the same accuracy as for example electrochemical models which are very hardware intensive. Thus, we propose to expand the ECM by a kinetic battery model (KIBAM). The ECM uses Coulomb Counting for calculating the state of charge (SOC) which is sufficient for steady loads but in cases where dynamic loads are applied, KIBAM shows better results because it accounts for charge recovery and C-rate effects. Those two effects are bound with the non-linear behavior of battery capacity.

Modeling

Electrical circuit model

The ECM of a Lithium-ion (Li-ion) battery used in this work consists of a source representing open circuit voltage, a series resistor, and 2 RC branches, as illustrated in Fig 1.

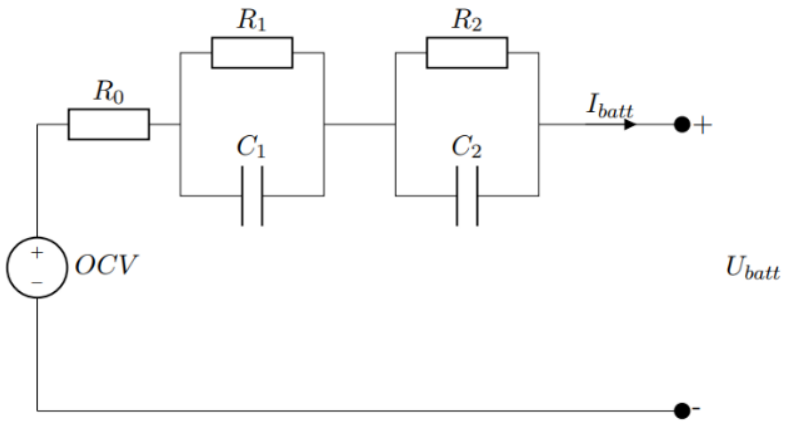

Figure 1. *Scheme of the ECM used.*

The considered ECM can be described by equations (1-3) where equation (1) is the output equation and equations (2), (3) are state equations.

$$U_{batt} = OCV - I_{batt} \cdot R_0 - I_{R_1} \cdot R_1 - I_{R_2} \cdot R_2 \quad (1)$$

$$\frac{dI_{R_1}}{dt} = -\frac{I_{R_1}}{R_1 \cdot C_1} + \frac{I_{batt}}{R_1 \cdot C_1} \quad (2)$$

$$\frac{dI_{R_2}}{dt} = -\frac{I_{R_2}}{R_2 \cdot C_2} + \frac{I_{batt}}{R_2 \cdot C_2} \quad (3)$$

Kinetic Battery model

KIBAM describes nonlinear dynamic cell capacity behavior. KIBAM divides cell capacity into two capacities called bound charge and available charge.

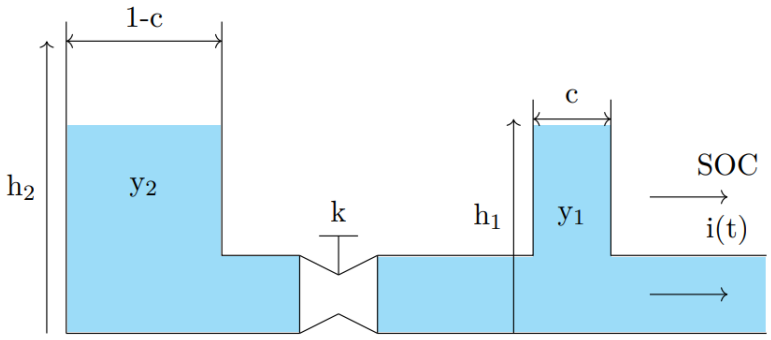

Figure 2. *Scheme of KIBAM.*

Figure 2. shows a representation of KIBAM as two connected wells. The right well represents available charge which is usable at any moment and the left well represents bound charge which is in a cell but cannot be directly used. Bound charge transfers to available charge through valve *k* which is diffusion constant. *c* is a capacity factor – distribution of whole capacity between available and bound charge. KIBAM is described with two following equations:

$$\begin{bmatrix} \frac{dSOC_E(t)}{dt} \\ \frac{dSOC_T(t)}{dt} \end{bmatrix} = \begin{bmatrix} 1 & 0 \\ k \cdot T_s & -k \cdot T_s \end{bmatrix} \cdot \begin{bmatrix} SOC_E(t) \\ SOC_T(t) \end{bmatrix} + \begin{pmatrix} \frac{-T_s}{C_{tot}} \\ \frac{-T_s}{c \cdot C_{tot}} \end{pmatrix} \cdot i(t) \qquad (4)$$

Here, $SOC_T(t)$ represents available SOC and $SOC_E(t)$ represents bound SOC. C_{tot} is total capacity of the cell.

Results and Discussion

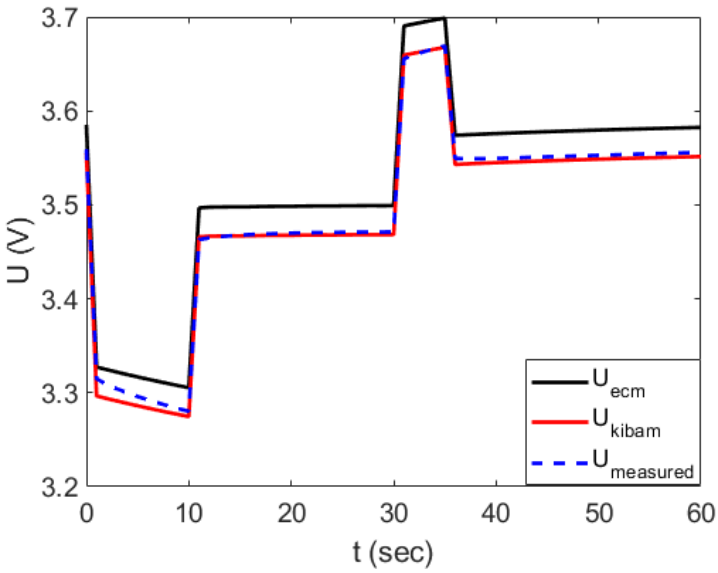

Figure 3. *Comparison of Measured Voltage and Computed Voltages.*

In Figure 3. there is comparison of measured voltage ($U_{measured}$), calculated voltage by ECM (U_{ecm}) and calculated voltage by ECM expanded with KIBAM (U_{kibam}). The extended model captures the real behavior of the battery more accurately than the ECM itself.

Preparation of Battery Cross-sections Using Broad Ion Beam Polishing

O. Klvač[a,b], D. Trochta[a,b], and T. Kazda[a]

[a] Department of Electrical and Electronic Technology, Faculty of Electrical Engineering and Communication, BUT, Technická 10, 616 00 Brno, Czech Republic

[b] Thermo Fisher Scientific Brno, Vlastimila Pecha 12, 627 00, Brno, Czech Republic

This conference contribution explores the usage of the Broad Ion Beam (BIB) polishing technique for the preparation of battery samples before their analysis. We discuss the limitations of scanning electron microscopy (SEM) without proper sample preparation and present the benefits of creating cross-sections using the BIB method. The paper focuses on the specific application of BIB for battery sample preparation, highlighting its importance in obtaining proper information.

Introduction

From electrochemical power sources, we require high energy density, long lifetime, and resistance to external influences. Li-ion batteries meet these requirements for most current applications, making them the most widely used battery type. However, over time the demands associated with even higher energy density, environmental friendliness, cost, and the limited supply of feedstock, are increasing. Hence, there is an effort to start using new materials such as sulfur, silicon, and others to address these challenges [1-4].

Although we have known for a long time that these materials are electrochemically active and can meet the mentioned requirements, they have not been commercialized yet, mainly due to their instability, which has a variety of causes (typically large expansion associated with mechanical stress on the electrodes, and others). The goal is to understand these mechanisms and subsequently develop solutions to limit their negative effects. One of the universal analytical methods is SEM along with associated methods such as EDS [3-6].

A battery system can be described as a system of many layers and interfaces. The base consists of an anode, a cathode, and an electrolyte-filled separator, or a solid electrolyte. The electrode itself is composed of a metal current collector and a layer of electroactive material. The current collector may be coated, as well as a separator. The separator itself may be a system of multiple materials. During battery operation, the growth of additional layers occurs – solid electrolyte interphase (SEI) layer, growth of lithium dendrites or metal dissolution, and their subsequent deposition on surfaces [7-9].

It is clear that simply scanning the sample in SEM from the surface is in many cases insufficient because it does not allow us to see the internal layers and their interfaces. For this reason, it is necessary to examine the materials in cross-section after proper preparation, for example using BIB. It is important to note that battery materials are air-sensitive and quickly react with moisture and oxygen. Therefore, appropriate inert transfer between devices must be ensured.

BIB is a technique that uses the kinetic energy of charged particles (ions) to remove material at the point of impact. Unlike mechanical grinding, BIB does not suffer from shear friction associated with the formation of scratches, and the amorphous layer on the newly formed surface is usually very

thin. Due to the susceptibility of battery materials to mechanical stress, it can be impossible to prepare a cross-section using mechanical techniques, but it can serve as a preliminary preparation. The usage of BIB can be divided into surface polishing (SP) and cross-section polishing (CP) [9].

In the case of SP, the ion beam incident at an angle, typically 3-10°, on a flat surface - a battery in the cross-section or an electrode from the surface. In the case of a battery in the cross-section, it is necessary to fix the structure in an epoxy resin, a clamp, or in the cell's housing (typically the metal case) and then pre-polish it mechanically (Fig. 1a). This pre-prepared sample is then attached to the holder. The fixation must be resistant to temperature changes and be thermally conductive. In the case of whole-structure cross-sections, cryogenic cooling is not an exception to prevent the melting of the separator. It is important to set the correct height so that the ion beam hits the center of the sample, which rotates during polishing. A possible result is shown in Fig. 1b.

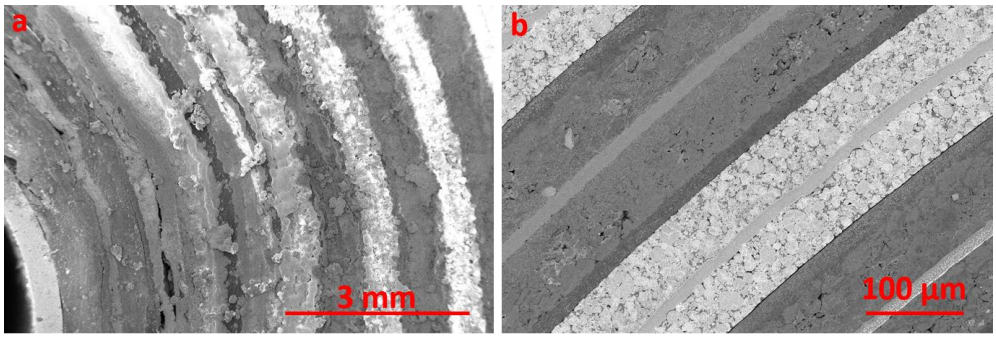

Figure 1. *SP cross-section of cell 18650; after mechanical grinding (a); after BIB (b)*

The CP uses a protective mask, behind which the sample is placed in a small overlap (Fig. 2a). This part is gradually sputtered off to create a new surface with a Gaussian profile (resulting from the beam intensity, Fig. 2b). The process of preparation is more challenging and strongly influences the result.

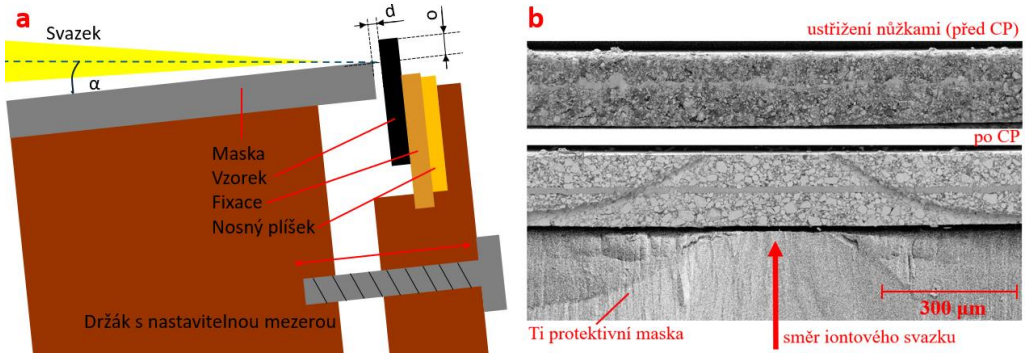

Figure 2. *Schematic drawing of sample setup for CP, side view (a); an example of electrode after CP compared to an unpolished sample after mechanical grinding, top view (b)*

The first step is cutting or chopping the sample. The goal is to create a rectangular edge with minimal depth of damage (cracks, peeled material). The height of the overlap o must correspond at least to the depth of the damage, but at the same time, the preparation time increases exponentially with height of the overlap. It is also important to set the gap d from the mask. A large gap will create an unsharp edge, too small a gap will cause a large redeposition, and contact with the mask will put a strong thermal stress on the specimen. The overlap and distance must be parallel in the edge/surface relation between the mask and the sample. This is done by the entire mechanical system and the

combination of the adhesive pads forming the fixation. Other parameters are beam voltage and current related to both polishing time, radiation damage as well as thermal heating. The angle of alpha incidence is directly proportional to the sputtering speed, but also the level of the so-called curtaining artifact. During polishing, the whole system is horizontally alternately tilted (rocking/oscillation) to reduce the curtains.

Conclusion

SEM is a suitable method for studying processes in Li-ion batteries, however, from the point of view of the battery as a system of individual layers and interfaces, its combination with BIB is often necessary. The preparation of battery samples using BIB has its own specifics and preparation procedures, which are further addressed in the conference contribution.

Acknowledgments

This work was supported by the specific graduate research of the Brno University of Technology FEKT-S-23-8286. The work was developed in cooperation with Thermo Fisher Scientific Brno.

References

1. Y. Liang et al., InfoMat, 1, 6-32 (2019)
2. H. -J. Kim et al., Electronics, 9 (2020)
3. G. Q. Liu et al., Journal of Solid State Electrochemistry, 14, 2191-2202 (2010)
4. M. Rana et al., Energy Storage Materials, 18, 289-310 (2019)
5. C. D. Rahn, Battery systems engineering, John Wiley & Sons Ltd., Publication, Chichester, West Sussex, United Kingdom, (2013)
6. C. Lin et al., Journal of Chemistry, 2015, 1-11 (2015)
7. T. Waldmann et al., Journal of The Electrochemical Society, 163, A2149-A2164 (2016)
8. A. Schilling et al., Journal of The Electrochemical Society, 166, A5163-A5167 (2018)
9. Kovachev et al., Batteries, 5 (2019)

Non-Faradaic Capacitance of Porous Manganese Dioxide Nanoparticles

O.L. Riabokin[a], K.D. Pershina[a], T.V. Lysnicha[a]

[a] Joint Department of Electrochemical Energy Systems NAS of Ukraine, Vernadskii Ave, 38, Kyiv, 03142, Ukraine

The X-ray powder diffraction analysis, scanning electron microscopy, Emmet-Teller method, and electrochemical impedance spectroscopy were used for investigating morphology impact on non-Faradaic capacitance in the three types of Manganese dioxides phases. Pore radii distributions were obtained from isotherms in terms of the density functional theory. The XRD - patterns detected the changes in Manganese Dioxide phase content (Mn_2O_3, mixture of Mn_2O_3 and Mn_3O_4, and Mn_3O_4) with a rising ratio of citric acid during melting treatment of Mn_2O_3 in solid citric acid media. The changes in Manganese dioxide phases impact the nanoscopic network, size of crystallites, pore sizes, and surface area of the samples. Experimental results demonstrate a correlation between micropore volume, surface area, average pore radius, crystallite size, and non-Faradaic capacitance of various Manganese dioxides. The Mn_3O_4 sample with oxygen deficit has maximum capacitance, average micropore volume, surface area, crystallite size, and minimum average pore radius.

Introduction

A major factor in the electrochemical operation of nanostructured metal oxides is the efficient electronic communication between the conducting substrate and the internal surface of the oxides. Electron transport in the nanoparticle network ensures that the functionalized surface from the contacts is addressable. Therefore, electron transport in nanostructured metal oxides has been the subject of numerous investigations [1-3]. The recent interest has the specific effect of the geometry of the nanoparticles array on the macroscopic charge transport [2-4]. Authors, [5] the relation between particle conglomeration and crystallite formation number and porosity in nanoparticle films was considered and described macroscopic transport in terms of the percolation model. Other authors have considered the variations of the network morphology16,17 and the influence of such morphology on the performance of conductivity and non-Faradic capacity (pseudo-capacity) in the nanostructured metal oxides [6]. Manganese dioxide is one such pseudo-capacitive material, which has been the focus of significant research due to its high performance, abundance, low cost, and low toxicity. Manganese dioxide exhibits a range of oxidation states including II, III, and IV, which primarily form octahedral arrangements with O^{2-}, OH^{-}, and H_2O species, to give rise to a wide range of crystallites. The octahedral geometry can have some distortion depending on the oxidation state, particularly Mn(III) due to Jahn-Teller distortion [6]. Pseudo-capacitance in manganese dioxide is dependent upon the diffusion of protons and electrons through the crystal lattice of the Mn_xO_y phases, their specific surface areas, and morphologies. Therefore the different manganese dioxide phases each have a different double-layer charge storage contribution, in addition to different non-Faradic capacitance. Such work has a target to detect major morphological factors that impacted the non-Faradaic capacitance formation of Mn_2O_3, Mn_3O_4, and their mixture.

Experimental and discussion of results

The Mn_2O_3 nanopowder (99,4 %) was used as a start material. Molten treatment in solid citric acid media of the Mn_2O_3 was used to change the nanoscopic network structure of powders. Molten rout of Mn_2O_3 transformation performed into two stages: at temperature 240 ^{0}C and at 540 ^{0}C with two mass ratio of citric acid relatively Mn_2O_3 (1:1 and 1:2). The structural investigation and X-ray powder diffraction analysis were performed on a (Cu-Ka radiation (l ¼ 0.15418 nm) and a Bragg 2θ configuration. The phase content and crystallite size estimations were performed use Match 3.0 software. SEM images were obtained using JEOL F-6301 scanning electron microscope. Specific surface areas and pore size distributions for the synthesized samples were calculated from nitrogen adsorption/desorption curves (NOVA 2200e, Quantachrome, USA) using the Nova Win 2.0 software. The total surface area of the materials S_{total} was calculated by the Brunauer-Emmet-Teller method (BET). Pore radii distributions were obtained from isotherms in terms of the density functional theory (DFT). EIS measurements were performed on an electrochemical module Autolab 30 PGSTAT301N Metrohm Autolab in a two-electrode cell (disk cell) in the frequency range 10^{-2} - 10^3 Hz. The results were processed using ZView2 software.

The XRD - patterns detected the changes in Manganese Dioxide phase content with a rising ratio of citric acid. The start sample has only the Mn_2O_3 phase, in the ratio of citric acid 1:1 sample has a mixture of two phases Mn_2O_3 and Mn_3O_4, and in the ratio 1:2 sample contains only the Mn_3O_4 phase. The changes in Manganese dioxide phases impact the nanoscopic network, size of crystallites, pore sizes, and surface area of the samples (Fig. 1, Table 1).

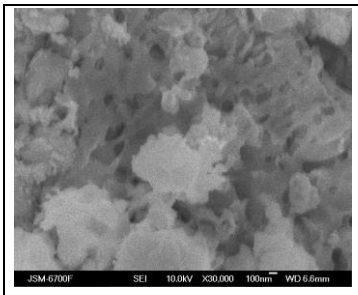

The start sample, Mn_2O_3 phase

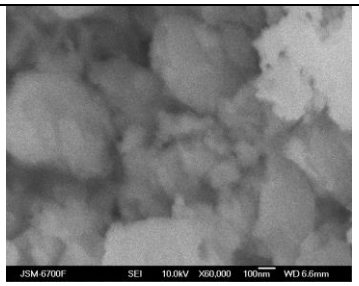

Sample with 1:1 citric acid, the mixture Mn_2O_3 and Mn_3O_4 phases

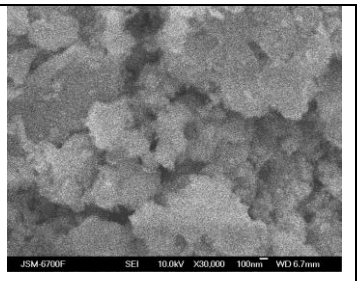

Sample with 1:2 citric acid, Mn_3O_4 phase

Figure 1. *SEM images of the Manganese dioxide samples*

TABLE I. *Morphological and capacitance data of Manganese dioxide samples*

Mass ratio Mn_2O_3: Citric acid	Average micropore volume, cc/g	Average mezopore volume, cc/g	Surface area, ml/g	Average pore radius, nm	Average crystallite size, nm	Non Faradaic capacitance, F/g
1:0	$1.16 \cdot 10^{-2}$	$0{,}92 \cdot 10^{-2}$	29,36	13,68	104.4	$9.22 \cdot 10^{-9}$
1:1	$1{,}33 \cdot 10^{-2}$	$1{,}12 \cdot 10^{-1}$	38,82	6,56	51.04	$1.38 \cdot 10^{-7}$
1:2	**$2.53 \cdot 10^{-2}$**	$1{,}14 \cdot 10^{-1}$	**70,88**	**4,91**	**141.17**	$3.56 \cdot 10^{-7}$

Experimental results demonstrate a correlation between micropore volume, surface area, average pore radius, crystallite size, and non-Faradaic capacitance of various Manganese dioxides. The Mn_3O_4 sample with oxygen deficit has maximum capacitance, average micropore volume, surface area, crystallite size, and minimum average pore radius (Table 1). So, such parameters may have a major priority in non-Faradaic capacitance formation.

Because the most porous media – especially powder oxides – represent interpenetrating networks of void space and solid matrix. The morphology of such porous media – the shapes and sizes of the voids, the way they are connected, and the structure of their surface – is usually highly chaotic [7]. The cross-section of the voids varies, and the number of ways out of a void differs from void to void. In this case, the formation of the non-Faradic interface takes place. The presence of a large number of surface voids increases non-Faradaic capacitance (Fig. 2).

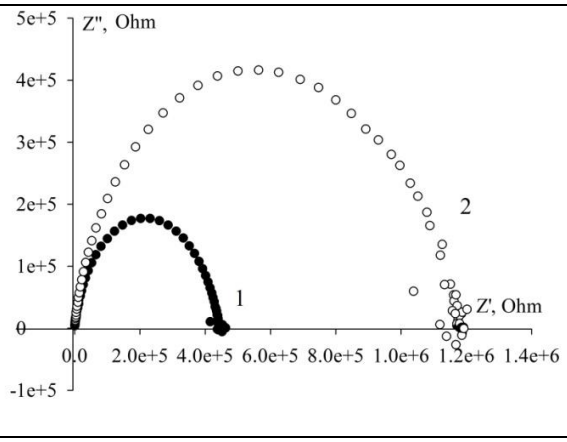

1- Mixture Mn_2O_3 and Mn_3O_4 phases
2- Mn_3O_4 phase

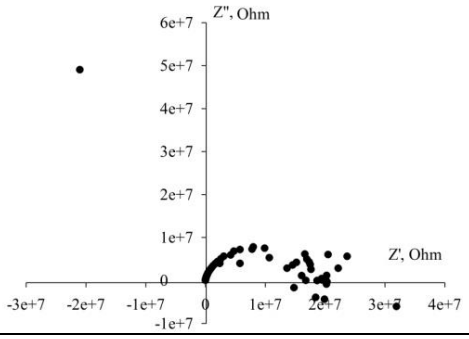

The start sample, Mn_2O_3 phase

Figure 2. *EIS spectra of the Manganese dioxide samples*

Acknowledgments

The authors would like to express their deep appreciation to the National Academy of Sciences of Ukraine (NASU) for the financial support our work (SR N^0 0122U200365).

References

1. M. Kandasamy, S. Sahoo, S. K. Nayak, B.Chakraborty, & C. S. Rout. *Journal of Materials Chemistry A*, **9** (33), 17643-17700. (2021).
2. Z. Qi, S. Huang, A. Younis, D. Chu, & S. Li, *Supercapacitor Design and Applications*, **7**, 411-456 (2016).
3. M. Zhi, C. Xiang, J. Li, M. Li, & N. Wu, *Nanoscale*, **5**(1), 72-88. (2013).
4. P. Simon, & Y. Gogotsi, *Nature materials*, **7**(11), 845-854. (2008).
5. S. De, P. J. King, P. E. Lyons, U. Khan, & J. N. Coleman, *ACS nano*, **4**(12), 7064-7072. (2010)
6. Dupont, M. F., & Donne, S. W. *Journal of The Electrochemical Society*, **163**(6), A888. (2016).
7. M. Sahimi *in Flow and Transport in Porous Media and Fractured Rock.* WILEY-VCH Verlag GmbH & Co. KGaA, Boschstr. 12, 69469 Weinheim, Germany (2011).

Exploring the Influence of Temperature on Li-ion Batteries

M.Šedina[a] and T.Kazda[a]

[a] Department of Electrotechnology, Brno University of Technology, Brno 61600, Czech Republic

With the increasing demand for reliable energy storage, it is essential to understand the relationship between temperature and the operation of Li-ion batteries. This paper explores how temperature affects key parameters such as lifetime, capacity, and performance. It also includes experiments testing automotive cells at different temperatures and the effect of depth of discharge (DoD) on battery performance and lifetime. Understanding these factors will help optimize Li-ion batteries for different environments and ensure their longevity and efficiency.

Introduction

Lithium-ion batteries have become the fundamental technology for the storage of electrical energy. They are used daily in smartphones, wearable devices, laptops, and increasingly in personal vehicles and energy storage systems. The use of Li-ion batteries in electric vehicles and energy storage systems has increased the need to optimize battery service life, which is strongly affected by many factors such as current load, operating temperature, and cell chemistry.

Operating temperature is a critical area of research as it directly affects the Li-ion battery lifetime. Overheating can result in a permanent reduction in battery capacity and cause battery damage. On the other hand, low temperatures can be harmful too, especially due to the risk of freezing the electrolyte, which can damage the battery and lead to its failure. These challenges are becoming increasingly important due to the growing number of large battery applications. [1]

Battery degradation

Degradation of Li-ion batteries is a process that occurs over time and reduces the battery's ability to hold a charge. It is a significant problem in many applications, especially in electric vehicles where battery performance and lifetime are crucial. Therefore, understanding and reducing the degradation of Li-ion batteries is a key area of research in battery development. Degradation processes are also associated with the operating temperature of the battery, as this can directly affect the chemical processes taking place in the battery. All degradation processes are illustrated in the figure 1.

All degradation processes in batteries are interconnected. Among the most prominent degradation processes is the growth of the SEI layer (solid electrolyte interphase). It is a passivation layer that grows on anode and this layer is essential for the functioning of the battery, but its excessive growth results in an irreversible decrease in battery capacity. [2][3]

Another problem is electrode material cracking, this is caused by aging of the materials and by their volume change during the cycling. Particle cracking leads to the growth of the SEI layer, reduction of conductivity, and capacity loss. [2][3]

Another problematic degradation process is the breakdown of the electrolyte, which is responsible for ion transfer inside the battery. Electrolyte degradation in Li-ion batteries can be caused

by the formation of an SEI layer, high temperature, overcharging, and over-discharging or other chemical reactions inside the battery. [4]

Last but not least is the lithium plating. It is a process in which lithium metal is deposited on the surface of the negative electrode instead of being incorporated into the structure. This is caused by the wrong operating conditions. Lithium plating leads to a loss of battery capacity and, in the worst case, to an internal short circuit. [2][3]

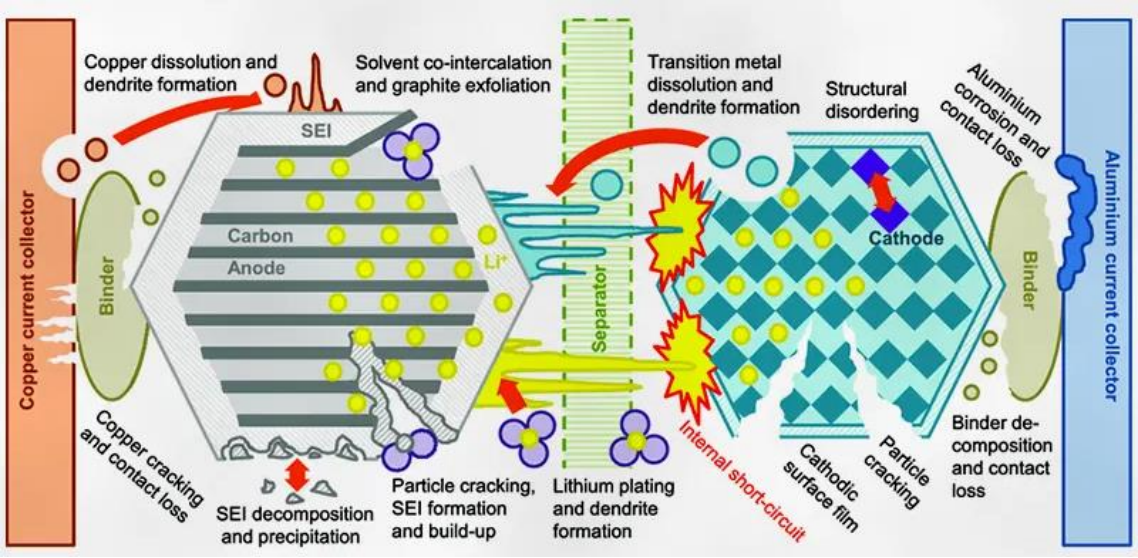

Figure 1. *Example of individual degradation processes [5]*

Effect of the operation temperature

The operating temperature of Li-ion batteries has a large impact on their reliability and performance, with an ideal range of 15 °C to 35 °C and a typical operating range of 20 °C to 60 °C. It is essential to maintain this temperature range to avoid negative effects on chemical processes, ionic conductivity, and the overall performance of the cell. At low temperatures, cycling performance is particularly affected by increased internal resistances, especially charge transfer resistance, which slows down the kinetics of Faradaic reactions at the electrode-electrolyte interface and makes charging more difficult. In addition, freezing of the electrolyte, which stops the reactions, or the lithium plating can occur, both of which reduce the capacity of the battery or destroy it. High temperatures present complex problems since heat generation from reversible and irreversible processes contributes to cyclic and calendar aging. This heat can cause thermally component decomposition, leading to the growth of the SEI, resulting in capacity loss. High temperatures can also trigger thermal runaway, which causes uncontrollable heat generation, structural damage, and potential explosion. [6][7][8]

Conclusion

The temperature effect on lithium-ion batteries is a significant factor affecting their performance and lifetime. High temperatures accelerate degradation, while low temperatures reduce performance. Appropriate battery thermal management settings offer one potential solution to these problems.

Acknowledgments

This work was supported by the specific graduate research of the Brno University of Technology No. FEKT-S-23-8286. This work was supported by the EIT Urban Mobility project SEVES.

References

1. G. Leoncini, R. Mothier, B. Michel, and M. Clausse, Applied Thermal Engineering, vol. 236, (2024)
2. J. S. Edge, S. O'Kane, R. Prosser, N. D. Kirkaldy, A. N. Patel, A. Hales, A. Ghosh, W. Ai, J. Chen, J. Yang, S. Li, M. -C. Pang, L. Bravo Diaz, A. Tomaszewska, M. W. Marzook, K. N. Radhakrishnan, H. Wang, Y. Patel, B. Wu, and G. J. Offer, Physical Chemistry Chemical Physics, vol. 23, no. 14, pp. 8200-8221, 4(2021).
3. S. E. J. O'Kane, W. Ai, G. Madabattula, D. Alonso-Alvarez, R. Timms, V. Sulzer, J. S. Edge, B. Wu, G. J. Offer, and M. Marinescu, Physical Chemistry Chemical Physics, vol. 24, no. 13, pp. 7909-7922, 3(2022).
4. Y. Liao, H. Zhang, Y. Peng, Y. Hu, J. Liang, Z. Gong, Y. Wei, and Y. Yang, "Electrolyte Degradation During Aging Process of Lithium-Ion Batteries: Mechanisms, Characterization, and Quantitative Analysis", Advanced Energy Materials. 2(2024).
5. "SPECIFIC EXPLANATION OF THE LITHIUM ION BATTERY DEGRADATION", TYCORUN, 5(2023). (accessed Mar. 01, 2024).
6. S. Ma, M. Jiang, P. Tao, C. Song, J. Wu, J. Wang, T. Deng, and W. Shang, Progress in Natural Science: Materials International, vol. 28, no. 6, pp. 653-666, (2018).
7. H. Luo, Y. Wang, Y. -H. Feng, X. -Y. Fan, X. Han, and P. -F. Wang, Materials, vol. 15, no. 22, (2022).
8. S. Ma, M. Jiang, P. Tao, C. Song, J. Wu, J. Wang, T. Deng, and W. Shang, Progress in Natural Science: Materials International, vol. 28, no. 6, pp. 653-666, (2018).

Shellac - Application of a Sustainable Biopolymer as a Binder for Si/Gr-Anodes in Li-Ion Batteries

M. Vuksanovic[a,b], B. Boz[a], K. Fröhlich[a], E. K. Ehmoser[c]

[a] Transportation Technologies, AIT Austrian Institute of Technology GmbH, Giefinggasse 2, 1210 Vienna, Austria

[b] Food Science and Biotechnology, University of Natural Resources and Life Sciences, Gregor-Mendel-Straße 33, 1180 Vienna, Austria

[c] Institute of Synthetic Bioarchitectures, University of Natural Resources and Life Sciences, Muthgasse 11/II

1190 Vienna, Austria

To overcome the problematic volume changes and particle deformations of silicon anodes, shellac, a new and sustainable binder, was tested in coin cell format. Moreover, different physiochemical and mechanical tests were performed. This naturally available polymer has the potential to serve as a self-healing binder in LiBs, due to its self-polymerization properties during the aging process.

Introduction

Silicon keeps great potential to increase the lifetime and capacity of LiBs, due to the fact that it can store more than ten times more theoretical capacity (≈4200 mAh·g-1) compared to conventional graphite (≈370 mAh·g-1). (2) However, its application often leads to drastic volume changes (>300%) during the charge-discharge process which cause significant changes and errors on the surface of the electrode. In addition, it leads to an unpredictable growth of the solid electrolyte interphase (SEI) and as a result, a decrease in capacity is observed for the upcoming charge and discharge cycles. (2,3)

Over the last decades, there has been a growing demand to find sustainable and water-based binder materials for both, cathode and anode. In terms of anode processing, Na-carboxymethyl cellulose (CMC), combined with a second binder (e.g. styrene-butadiene-rubber (SBR)) is still state of the art. (4) However, when using water-based binders, the Si-content also has its limitations. Depending on the binder, the problems associated with an increased Si-content include a lack of structural integrity, as well as particle deformation that lead to capacity losses. These problems can be solved by choosing a more suitable binder system. (4)

Shellac as a Self-Healing Binder

In addition to water-based binders, there are also other options and materials that could solve the aforementioned problems. One of these materials is shellac.

Shellac is a water-insoluble resin that was secreted by a lac insect. It´s main advantages are renewability, abundance, and non-toxicity. Due to the fact that shellac is not water-soluble, but would only swell in it, ethanol is used as a solvent. (5)

During the aging process the biopolymer melts and therefore flows easily. After some time, however, the shellac changes to a rubbery state, which is caused either by cross-linking or inter-esterification mechanisms of polyhydroxy carboxylic acids with the free alcohols. This process is also known as self-polymerization or self-esterification (5) and has the potential to serve as a self-healing material in LiBs. Therefore, the occurrence of these mechanisms as well as their effects on the electrochemistry have been tested in coin cell format.

Experimental Details

To test the potential of shellac serving as a self-healing binder, Si/Gr-anodes with a loading of ~4.5 $mAh \cdot cm^2$ were coated. The anodes produced were tested against Li metal to obtain the discharge capacities. Si/Gr anodes with the binder system CMC/SBR, which were attached in parallel, serve as a reference. Moreover, EIS measurements with Li metal-Si/Gr anode were performed. For a better explanation of the physiochemical properties, measurements were carried out on the rheometer, as well as examinations under the microscope. Mechanical tests were carried out with a peeling machine.

Acknowledgments

This work was financially supported by the Austrian Federal Ministry for Climate Action, Environment, Energy, Mobility, Innovation and Technology (bmk).

References

1. Z. Chen, C. Wang, J. Lopez, Z. Lu, Y. Cui, Z. Bao, *Advanced Energy Materials* **5**(8) (2015).
2. M. Tian, X. Chen, S. Sun, D. Yang, P. Wu, *Nano Research*, **12**, 1121-1127, (2019).
3. B. Boz, K. Fröhlich, L. Neidhart, P. Molaiyan, G. Bertoni, M. Ricci, F. De Boni, M. Vuksanovic, M. Romio, K. Whitmore, M. Jahn, *ChemPlusChem*, e202400195 (2024).
4. A. Ahuja, V. K. Rastogi, *Sustainability* **15** (4) (2023).

Advancing Sustainability in Lithium-Ion Battery Production through Innovations from the BatWoMan Project

Bernd Eschelmüller[1], Katja Fröhlich[1],

[1] Battery Technologies, AIT Austrian Institute of Technology GmbH, Vienna, Austria

The BatWoMan project aims to create new, eco-friendly methods for producing lithium-ion battery cells. This presentation provides an overview of the novel strategies and technologies being used to meet this goal. It underscores the potential to support the European Union's goal of creating carbon-neutral energy storage systems, while also being economically viable and environmentally safe [1].

BatWoMan focuses on developing energy-efficient processes for electrode production, eliminating volatile organic compounds, via handling highly concentrated slurries (up to 70% solid content for anode and 80% for cathode by weight). This way, the energy use and environmental impact is reduced. Additionally, the project aims to cut costs and the carbon footprint of cell production by implementing new concepts to reduce dry room requirements. The dry room is a significant cost factor in battery manufacturing, and minimizing its operational needs will lower both costs and environmental impact [2]. A battery data space will also be created to ensure the traceability and condition monitoring of the cells, enhancing transparency for customers and second-life users.

Within BatWoMan, efficient methods for wetting, formation, and ageing processes are developed. New three-dimensional electrode designs will improve these conditioning steps, ensuring optimal performance and longer lifetimes for lithium-ion cells. These advancements are set to make future batteries more sustainable and economically viable. By reducing production costs by 63.5% and energy consumption by 52.6%, BatWoMan aims to establish Europe as a leader in sustainable battery production.

Acknowledgments

This project is funded by the European Union’s Horizon research and innovation programme under Grant Agreement no. 101069705.

References

1. VDMA, Roadmap “Battery Production Equipment 2030”, Update 2020.
2. Marcus Vogt, Klemens Koch, Artem Turetskyy, Felipe Cerdas, Sebastian Thiede, Christoph Herrmann, Model-based energy analysis of a dry room HVAC system in battery cell production, 2021 Elsevier Inc. Joule 5 Procedia CIRP 98 (2021) 157–162

Synthesis of Graphene by Controlled Gas Detonation Method for Batteries Application

K. Vavilon[a,c], V. Zinin[a,b], Yu. Polishchuk[b], O. Potapenko[c]

[a] MaxAh Ltd., Kyiv 03113, Ukraine

[b] Ukrainian State University of Science and Technologies, Dnipro, 49010, Ukraine

[c] Joint Department of Electrochemistry Energy System of NAS of Ukraine, Kyiv, 03680, Ukraine

This work is based on the method of gas-detonation synthesis using hydrocarbon precursors. This study will present the relationship between the synthesis conditions of graphene and the properties of the obtained materials by the method of controlled gas-detonation and their subsequent thermomechanical processing.

Abstract

In modern chemical technologies, significant attention is devoted to carbon-based materials with unique properties arising from their structural features, including carbon nanotubes and fullerenes. However, two-dimensional materials, particularly graphene, garner the most interest. Graphene, a nanomaterial with a two-dimensional structure, consists of sp2-hybridized carbon atoms arranged in a hexagonal lattice and is one atom thick. Its unique properties include high rigidity, exceptional thermal conductivity, zero effective mass, gas impermeability, high charge carrier mobility, and optical transparency. These properties make graphene suitable for applications in lightweight body armor, construction, optical and electronic devices, energy generation and storage, and biological sciences.

This study explores gas-detonation synthesis as an alternative method that promises industrial-scale graphene production at lower costs. The research focuses on modifying synthesis techniques and post-synthesis processing of graphene materials. By establishing a relationship between synthesis conditions and material properties, this method aims to tailor graphene for specific applications such as ultra-strong concrete additives, electrochemistry, electronics, filtration membranes, and composite materials. This approach parallels the artificial diamond industry, highlighting its potential for significant advancements in various fields.

Method of Synthesis and Graphene Characterization

The controlled gas detonation method is based on the detonation reaction of a hydrocarbon precursor at high temperatures and pressures, resulting in the formation of graphene nanosheets. To achieve the best synthesis results, several parameters must be optimized: pressure, temperature, composition of the hydrocarbon precursor, and duration of the detonation process. In our research, various ratios of synthesis gas and oxygen were used during the synthesis of graphene. Increasing the amount of oxygen leads to an increase in pressure and temperature during detonation, which in turn affects the physicochemical parameters (specific surface area, volume, pore size, etc.) of the synthesized graphenes.

The optical spectrum of synthesized graphene (Fig.1) is characterized by three main peak resonances: the D-band, G-band, and 2D-band. The D-band (1350 cm^{-1}) arises due to disorder in the graphene structure, indicating the presence of defects. The G-band (1580 cm^{-1}) reflects the valence vibrations of sp^2 bonds and characterizes the crystalline domains of graphene. The 2D-band (2700 cm^{-1}), formed by a two-phonon electron-phonon resonance, is characteristic of bilayer graphene. The intensity ratio ID/IG indicates the defectiveness of the material, with a high ratio suggesting a significant number of defects. Data on Raman spectroscopy of graphene synthesized at different ratios of oxygen and synthesis gas and thermo-mechanical activation shown in Table. 1.

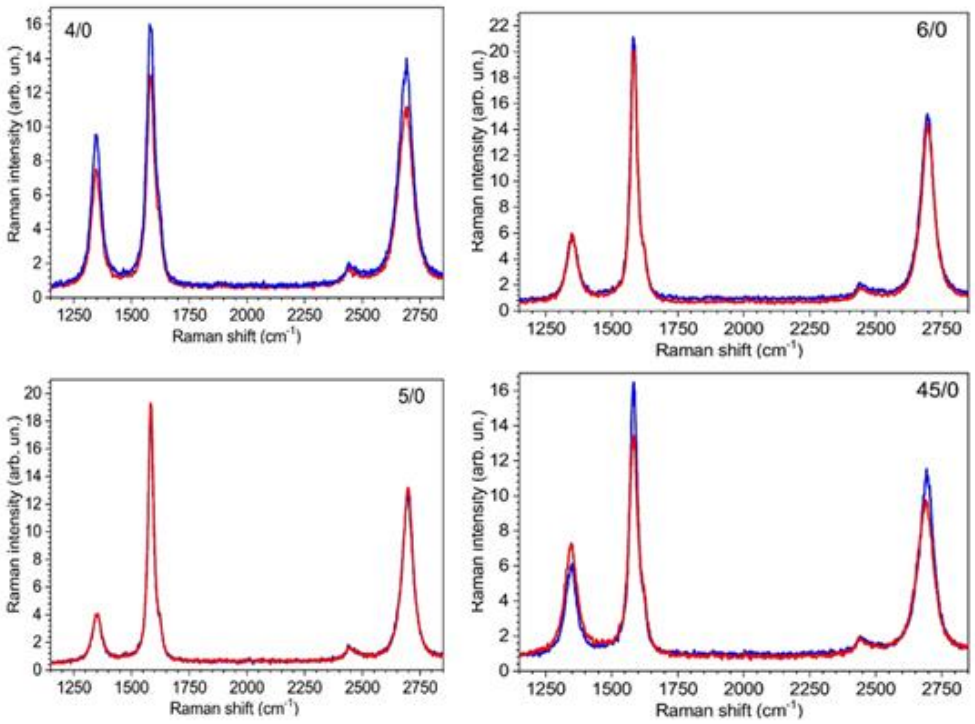

Figure 1. *Raman spectroscopy of "pompom" graphene synthesized at different ratios of oxygen and synthesis gas (number on curves).*

TABLE I. *Data on Raman spectroscopy of "pompom" graphene synthesized at different ratios of oxygen and synthesis gas and thermo-mechanical activation*

.

Parameter	**Sample / Activation time, min**							
	04/1		045/1		05/1		06/1	
	0	40	0	40	0	40	0	40
ω_D, cm^{-1}	1347.7	1347.2	1346.5	1348.8	1350.5	1346.5	1350.5	1348.5
I_D, a.u.	7.0	13.7	5.2	12.2	3.7	11.2	5.1	9.6
Γ_D, cm^{-1}	50.2	76.4	52.7	74.6	49.9	70.7	50.5	67.9
ω_G, cm^{-1}	1583.5	1585.9	1583.3	1588.8	1583.7	1585.5	1583.7	1584.7
I_G, a.u.	12.6	12.5	15.7	11.5	18.2	12.2	20.6	14.7
Γ_G, cm^{-1}	38.3	61.0	32.9	56.2	27.5	49.6	29.1	35.7
ω_{2D}, cm^{-1}	2687.6	2688.0	2692.1	2693.5	2695.3	2691.2	2695.1	2695.0
I_{2D}, a.u.	10.5	6.6	10.4	5.7	11.9	6.6	14.4	8.9
Γ_{2D}, cm^{-1}	75.2	100	65.1	98.0	57.1	88.3	58.2	68.1
I_D/I_G	0,55	1.10	0.33	1.06	0.20	0.92	0.25	0.65
I_{2D}/I	0.83	0.53	0.66	0.50	0.65	0.54	0.70	0.60

Thermo-mechanical activation has proven to be an effective method for enhancing the properties of graphene "flakes." This processing, conducted under controlled conditions, allows the separation of flakes into individual graphene sheets. This treatment also alters the physicochemical parameters of the material, as evidenced by transmission electron microscopy and Raman spectroscopy results. The choice of optimal processing time influences the number of graphene layers and their structural properties. These findings enable the control of the quality and properties of graphene materials, which is critical for their further applications in electronics, catalysis, acoustics, and other technological fields.

Thermomechanical Treatment and Its Influence

Thermomechanical treatment significantly influences the structure and electrochemical properties of graphene. Controlled conditions during this treatment allow for changes in the material's physicochemical properties, including the separation of "pompom" structures into individual graphene sheets or groups of sheets (Fig.2). Transmission electron microscopy (TEM) images have shown that the size of "pompoms" can be reduced from 100-400 nm to 50-150 nm after 40 minutes of thermomechanical activation, increasing the number of individual graphene sheets

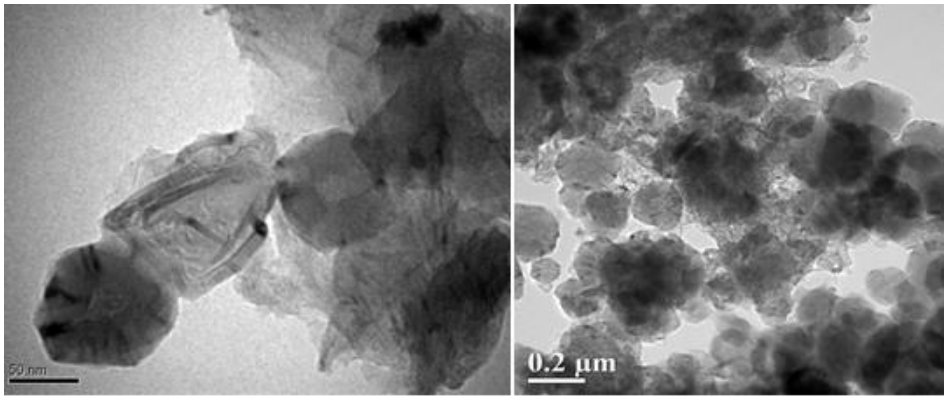

Figure 2. *TEM image of "pompom" graphene.*

These results indicate that thermomechanical activation is necessary to separate "pompoms" and obtain a higher number of individual graphene sheets. The increase in the degree of disorder with longer activation times suggests the potential of activated "pompom" graphene as an active material in energy storage devices such as batteries and supercapacitors.

Applications and Performance in Lithium-Ion Batteries

Graphene has demonstrated significant efficiency as an anode material for lithium-ion batteries (LIBs). Studies have shown (Fig. 3, 4) that it exhibits high specific capacity of up to 600 mAh/g at low charge/discharge currents, surpassing values of traditional materials like graphite. This is attributed to its unique structural and chemical properties, which facilitate efficient interaction with lithium ions and minimize degradation during cycling.

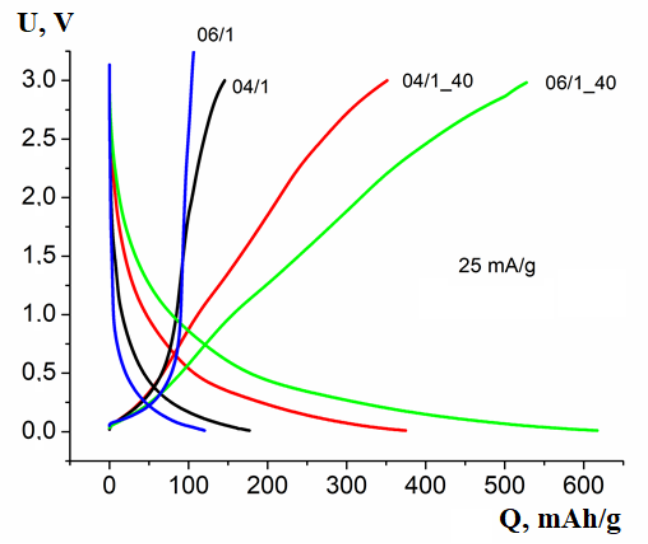

Figure 3. *Charge-discharge curves of graphene materials synthesized under different conditions: 04/1, 06/1 – initial graphene; 04/1_40, 06/1_40 – activated graphene materials. Electrolyte 1M $LiPF_6$ in EC:DMC. t=25°C, I=25mA/g.*

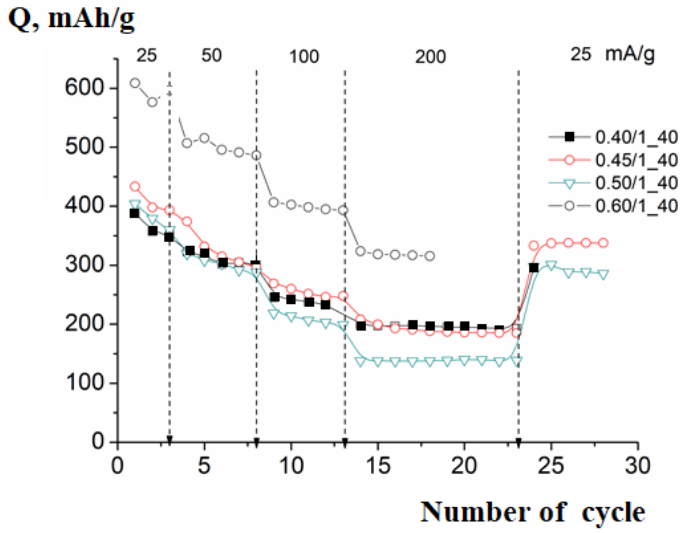

Figure 4. *Changes in the discharge specific capacity of activated graphene materials during cycling. The numbers on the graph indicate the current density.*

Furthermore, graphene anodes have shown high stability in cyclic operation, reducing reversible capacity losses and confirming their potential as a key component for the next generation of battery technologies. These results highlight graphene's potential to enhance the energy efficiency and longevity of LIBs, making it a pivotal subject for further research and development in electrochemical energy storage systems.

Conclusion

This study explored controlled gas detonation for synthesizing pompom-like graphene structures. Analyzing the graphene revealed controllable structure and physicochemical properties. The method effectively produced graphene with diverse layered pompom structures influenced by synthesis parameters, enhancing its properties through thermomechanical activation.

Innovative Anode based on Nanographite and Silicon Powder Without Binder for High Energy Batteries.

Y. Pustovalov[a], E. Shembel[b,c] D. Kaszuba[a], K Sukhy[c], V. Redko[b], T. Pastushkin[b],,

A. Markevich[c], Y. Sknar[c], N. Zaderey[c], V. Khandetskyy[b], A.Redko[c].

[a]*INT Sp. Z o.o., Ul Pilsudskiego 17/4, 34-074 Rzeszów, Polska*

[b]*Enerize Corporation, Coral Springs, FL, 33067, USA.*

[c]*Ukrainian State University of Science and Technologies. Scientific Research Laboratory of Chemical Power Sources. Dnipro, 49005*

Our goals are to developed the batteries with anodes based on nangraphites and silicon, without binder. These batteries have significant advantages compared to the use of lithium for the anode:operational safety, environmentally friendly materials, low cost, and high energy We already preparing and tested batteries with these anodes and cathodes like $LiMn_2O_4$ and Sulfure.

We are developing: 1. Anodes based on a composition of nanographite (1) (2) and Silicon without binder, and 2. Batteries with these anodes.

1. Compositions of nanographite and Silicon and study the conductivity, density and structure of these anode materials.
2. Technologies for manufacturing anodes based on nanographite (3) and Silicon without binder
3. Technologies for manufacturing and testing batteries with anodes based on a composition of nanographite and Silicon.
4. On the current stage we are developing and testing the batteries with anodes, based on the composition nanographite + Silicon without binder, and cathodes based on $LiMn_2O_4$ and Sulfur.

Nanographites, which are used to develop these anodes, have high electronic conductivities and affect the structure of the anode material. 1. Electrodes have high mechanical properties without binders. 2. Nanographite, which is used together with Silicon for the anode, affects the structure of the composition. As a result, the conductivity of this mixture of nanographite + Silicon powders is higher than the conductivity of the original nanographite. This is shown in Fig.1, curve 1.(4), (5)

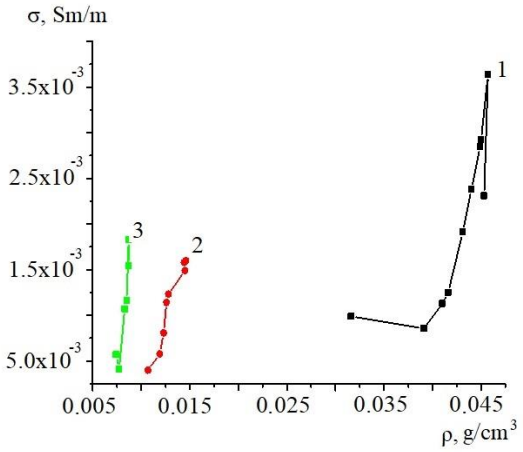

Figure 1. *Influence the parameters of the mixture process on the conductivity of the composition of nanographite and Silicon.. A method for measuring the conductivity of powders was developed by Enerize Corporation.* ***Curve*** *1. Powder of a mixture of Nanographite +Silicon. Mixing program No. 1. High results of the conductivity.* ***Curve 2****. Powder of mixture Nanographite + silicon. Mixing program No. 2.* ***Curve 3****. Powder of Nanographite. Mixing program №3*

The mixing parameters of a mixture of nanographite and silicon powders affect the change in the structure of the mixture. As a result, the conductivity of the mixture of these powders can be significantly increased. Accordingly, the power of the current source with this anode will increase.

Comparative discharge capacity of commonly used anode materials.

Li Anode - 3862 mAh/g. Commercial carbon anode with binder 372 mAh/g

Below we present results of cycling our innovative current sources.

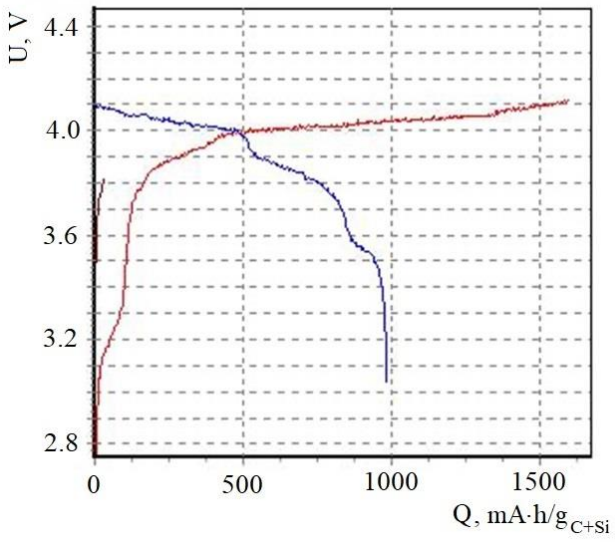

Figure 2. *Cycling our innovative current sources with anodes based on a composition of nanographites + Silicon without a binder. $LiMn_2O_4$ was used as the cathode material. Discharge capacity of this nanographite + Silicon without binder is 1000 mAh/g.*

Results of cycling these our batteries have stable parameters.

Silicon-containing in composition with nanographites whithout binder, which will become the basis of the anode electrode, will provide it with the following characteristics:

- High specific electrochemical capacity during charge-discharge cycling in our anode 1000 mAh/g;
- Environmental safety due to the inertness of silicon in relation to environmental components;
- High safety of operation of a lithium-ion battery due to the absence of the appearance of lithium dendrites on the surface of the negative electrode due to the intercalation charge mechanism;
- Low cost of producing a negative electrode due to the use of cheap nd common electrode materials, in particular Silicon

References

1. Peera S G, Koutavarapu R and Akula S J 2021 Carbon Nanofibers as Potential Catalyst Support for Fuel Cell Cathodes: A Review Energy Fuels **35**, 15 pp 11761–99
2. Pustovalov Y, Shembel E, Redko V, Pastushkin T, Zaderey N, Markevich A, Vishnyakov L and Sagirov I J 2019 Innovating Carbon Materials Open New Possibilities for Increasing Performance of Li-ion Batteries RS Global J. Word Sience **2** pp 4-8
3. Pustovalov Y, Shembel E, Vishnyakov L etc. Carbon material for electrodes of lithium-ion power sources and method of production thereof. US Patent application No. 10/898631
4. Redko V, Shembel E, Pastushkin T, etc. Method and Device for Rapid Non - Destructive Quality Control of Powdered Materials. US Patent No. 8,102,181
5. Redko V, Shembel E. etc. Method and Apparatus for Measuring Conductivity of Powder Materials Using Eddy Currents. US Patent No. 7,288,941

Ni and La Doping Effect on Characteristics of $LiMn_2O_4$ as Cathode Material for Lithium-Ion Batteries with Aprotic and Aqueous Electrolytes

Yu. V. Shmatok[a,b], N. I. Globa[a,b], V. A. Sirosh[a,b], I. V. Romanova[b]

[a] Joint Department of Electrochemical Energy Systems of the NAS of Ukraine,
38A Vernadsky Ave., Kyiv 03680, Ukraine

[b] Institute for Sorption and Problems of Endoecology of the NAS of Ukraine
13 Gen. Naumov St., Kyiv 03164, Ukraine

Introduction

Despite the progress achieved in the development of electrode materials for lithium-ion batteries (LIBs), solving problems associated with the stability of their specific capacity during cycling, high current loads and elevated operating temperatures remain a priority for researchers. Lithium manganese spinel $LiMn_2O_4$ exhibits good versatility and is suitable for use in LIBs with aprotic and aqueous electrolytes [1]. Along with such advantages as relative simplicity of production, low cost and environmental safety, $LiMn_2O_4$ is prone to relatively rapid loss of capacity during cycling. This is due to the gradual degradation of the original cubic structure as a result of a series of negative processes, the main ones of which are Jahn–Teller distortion caused by high-spin Mn^{3+} and loss of manganese caused by disproportionation reaction ($2Mn^{3+} = Mn^{4+} + Mn^{2+}$) [2]. Therefore, there is a need to increase the stability of the crystal structure of $LiMn_2O_4$, which will allow to improve its characteristics under various operating conditions. Doping of spinel, which consists in the partial replacement of Mn^{3+} ions by ions of other metals, is considered as one of the methods capable of stabilizing the crystal structure of $LiMn_2O_4$ and improving the cycling performance [3]. However, the influence of doping on the behavior of $LiMn_2O_4$ is determined by the nature and concentration of the dopant.

This work is devoted to the study of nickel and lanthanum doped lithium-manganese spinels, which were synthesized by means of a citric acid-aided route. The influence of the nature of the dopant on the structural, morphological and surface characteristics of spinels is studied. The effect of doping on the cyclic and kinetic characteristics of spinels as cathode materials for aprotic and aqueous lithium-ion systems is shown

Experimental

$LiMn_2O_4$, $LiNi_{0.05}Mn_{1.95}O_4$ and $LiLa_{0.05}Mn_{1.95}O_4$ samples were synthesized by decomposition of citrate precursors obtained from solutions of metal nitrates and citric acid, similarly to the procedure described earlier [4]. First, the obtained citrate precursors were pyrolyzed at 400 °C for 8 h and then the intermediate products were annealed at 750 °C also for 8 h. The obtained $LiMn_2O_4$, $LiNi_{0.05}Mn_{1.95}O_4$ and $LiLa_{0.05}Mn_{1.95}O_4$ samples are further marked as LMO, LNMO and LLMO, respectively.

Synthesized spinel samples were characterized by X-ray diffraction (XRD) method on a DRON 4-07 diffractometer with Cu-Kα radiation, scanning electron microscopy (SEM) on a JEOL JSM-6700F microscope and low temperature nitrogen adsorption method on a Micromeritics ASAP 2000 device.

Electrochemical studies in non-aqueous system were carried out in 2016 coin cells with a metal lithium anode, and in teflon cells with an activated carbon counter electrode and Ag/AgCl as a reference electrode in a case of aqueous system. The working electrode was prepared by mixing the as-synthesized active materials, carbon black Super C65 and PVDF binder at a weight ratio of 80:10:10 using dimethylacetamide as the solvent. The cathode slurry was casted on Al foil in a case of non-aqueous system and on Ni foil or stainless steel grid for tests in aqueous system. As a separator in 2016 coin cells was used a Celgard 2400 polypropylene film. A 1M solution of $LiPF_6$ in a mixture of ethylene carbonate/dimethyl carbonate/diethyl carbonate with the volume ratio (1:1:1) was used in coin cells. A 5M aqueous solution of $LiNO_3$ was used in studies in aqueous systems.

Results and Discussion

Based on the XRD data, the formation of a cubic structure of space group *Fd*3*m* (JCPDS No. 35-0782) characteristic of $LiMn_2O_4$ has been confirmed for all samples. In the case of nickel doping, no impurity peaks are observed in the diffractogram, indicating successful incorporation of nickel into the material's structure. However, for the lanthanum-doped spinel, an impurity phase corresponding to lanthanum manganite (LaMnO3) is detected. This impurity phase possesses a cubic structure (space group Pm3m), like to that of perovskite. According to the SEM data, the introduction of the dopant contributes to the decreasing the particle sizes to 100-150 nm and 100-200 nm for the LNMO and LLMO samples, respectively, compared to the LMO sample, which has an average particle size of 200-300 nm. LMO particles are well-formed crystals of a truncated octahedral shape. The LLMO sample has a similar particle morphology, but the shape of their crystals is not so perfect, which may be due to the formation of an additional $LaMnO_3$ phase, which can slow down the crystallization of the spinel phase. $LaMnO_3$ itself does not crystallize as individual particles, but forms a coating on the surface of spinel particles. The LNMO sample has the most perfect crystals of regular octahedral shape with sharp peaks and clear edges.

Electrochemical tests show that the nature of the dopant ion affects the specific cyclic and kinetic characteristics of $LiMn_2O_4$ in both aprotic and aqueous electrolytes (Figure 1). In the system with aprotic electrolyte, the specific capacity of LMO, LNMO, and LLMO spinels is 100, 100 and 124 mAh/g, respectively. When cycling with a current of 1 C for 200 cycles, the specific capacity of the LMO, LNMO, and LLMO samples decreases by 30.2, 7.3 and 16.9 %, respectively. In the aqueous system, the obtained specific capacity values are less than in the aprotic system, and the cycling stability is worse. Thus, the initial specific capacity of LMO, LNMO, and LLMO samples is 76, 81, and 106 mAh/g, respectively, and the corresponding capacity losses after 200 cycles (charge/discharge currents 3/1.5 C) are 46.5, 43.8, and 36.3%.

Significant differences are found in the behavior of spinel samples under different discharge rates (Figure 1c-d). In the non-aqueous system, the doped LNMO and LLMO samples have significantly better rate characteristics compared to pure LMO. For example, 80 % of the capacity retention is achieved at discharge current of 8 C, 20 C and 18 C for LMO, LNMO and LLMO, respectively. However, at a discharge rate of 50 C, the capacity retention for all samples remains nearly identical, around 20%. According to this parameter, systems with an aqueous electrolyte have a significant advantage. At the similar current load of 50 C, LMO, LNMO, and LLMO spinel samples yield 89, 87, and 92 % of the initial capacity. Such differences in the kinetic characteristics of $LiMn_2O_4$ in aprotic and aqueous electrolytes are explained by the physico-chemical properties of the electrolytes, in particular their electrical conductivity, and their influence on the formation of the electrode/electrolyte interface. Also, all the results are in good agreement with the obtained values

of the solid-state diffusion coefficient of Li^+, which were calculated from the voltammetry curves taken at the different potential sweep rates from 0.1 to 1 mV/s.

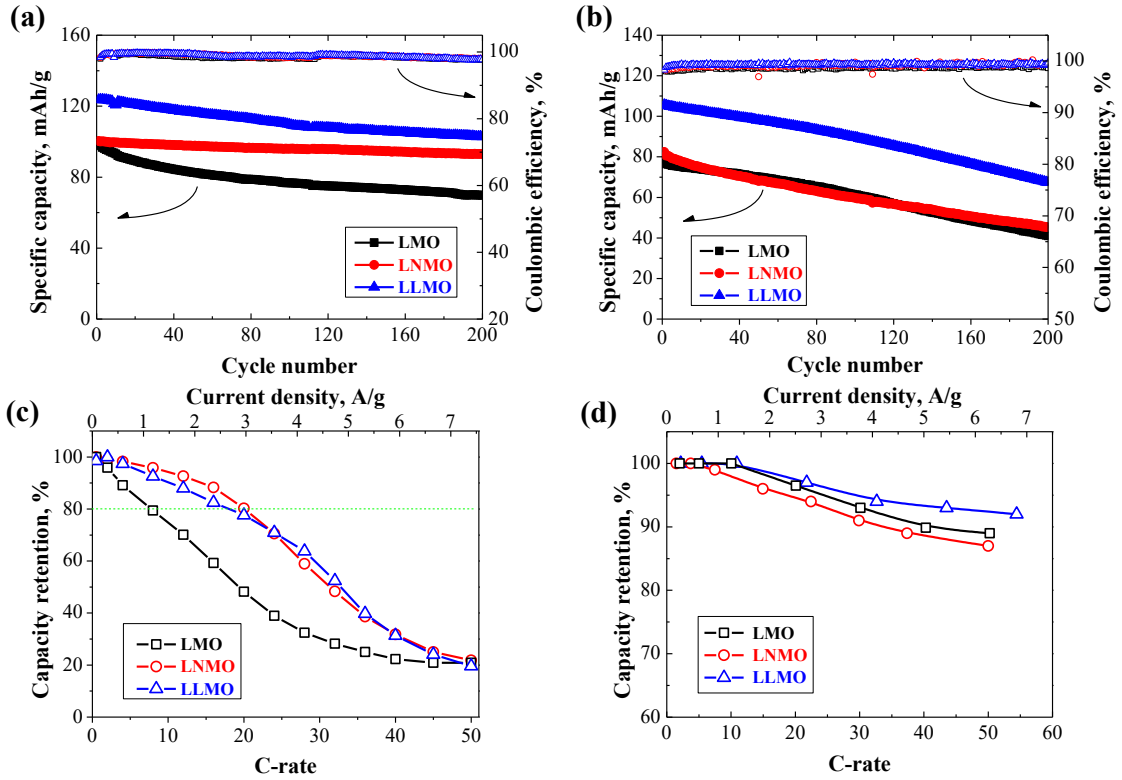

Figure 1. *Electrochemical performance of various spinel samples: (a) Cycling performance at 1 C in aprotic electrolyte, (b) Cycling performance at charge/discharge rates of 3/1.5 C in aqueous electrolyte. Rate capability in (c) aprotic and (d) aqueous systems.*

References

1. J. Zhao, M. Shi, Y. Wu, P. Zhang, X. Tan, X. Kang, W. Chu, Z. Wu, Y. Li, *Colloids Surf. A: Physicochem. Eng. Asp.*, **634**, 127932 (2022).
2. X. Hou, X. Liu, H. Wang, X. Zhang, J. Zhou, M. Wang, *Energy Storage Mater.*, **57**, 577 (2023).
3. S. Zhang, W. Deng, R. Momen, S. Yin, J. Chen, A. Massoudi, G. Zou, H. Hou, W. Deng, X. Ji, *J. Mater. Chem. A*, **9**, 21532 (2021).
4. Y.V. Shmatok, N.I. Globa, V.A. Sirosh, I.V. Romanova, S.A. Kirillov, *Monatsh. Chem.* **155**, 281–287 (2024).

Specific Conductivities of Tetraalkylammonium Bis(oxalato)borates in Acetonitrile, Dimethyl Sulfoxide, and Propylene Carbonate

N.I. Globa, Yu.V. Shmatok, O.B. Pushyk, O.I. Milovanova, M.I. Gorobets, V.A. Sirosh, S.A. Kirillov

Joint Department of Electrochemical Energy Systems, 38A Vernadsky Ave., Kyiv 03680, Ukraine

The paper presents data on the electrical conductivity (κ) of solutions of tetraalkylammonium bis(oxalato)borate salts [$(CH_3)_4NB(OCO)_4$, $(C_2H_5)_4NB(OCO)_4$, and $(C_4H_9)_4NB(OCO)_4$)] in acetonitrile (AN), glutaronitrile (GN), adiponitrile (AdN), propylene carbonate (PC) and dimethylsulfoxide (DMSO). It is shown that depending on the nature of the solvent, the specific electrical conductivity of electrolytes varies in the order $\kappa_{AN}>>\kappa_{DMSO}>\kappa_{PC}>\kappa_{GN}\geq\kappa_{AdN}$, in accordance with the inverse viscosity of the solvents (Φ): $\Phi_{AN}>>\Phi_{DMSO}>\Phi_{PC}>\Phi_{AdN}\geq\Phi_{GN}$. Depending on the radius of the salt cation, within one solvent, the value of κ changes in the order $\kappa_{Me4NBOB}>\kappa_{Et4NBOB}>\kappa_{Bu4NBOB}$. The equations that most accurately describe the concentration and temperature dependences of the conductivity of the investigated solutions were selected.

Introduction

Electric double-layer capacitors (supercapacitors, SC) are known as efficient devices for accumulating and storing energy (1,2). Their advantages include: high energy density and long service life. In order to achieve the maximum specific energy density and capacity of SC, electrolytes with high electrical conductivity and a wide range of electrochemical stability potentials are needed. Aqueous solutions have high electrical conductivity, but the range of charge/discharge potentials is limited by the decomposition potentials of water. Numerous salts of quaternary ammonium and phosphonium bases with various anions are actively pursued by experimentalists, and environmentally-friendly compounds containing bis(oxalato)borate (BOB) anion are of special interest. Among aprotic solvents, acetonitrile (AN) and propylene carbonate (PC) are the most widely used two. Among advantages of BOBs over tetrafluoroborates, lower cost and hydrolytic ability in the presence of moisture are especially stressed, and studies of supercapacitors employing these salts are successfully continuing. This improves their technological properties when used in SC. At the same time, only with an optimal combination of salt and solvent properties, it is possible to optimize the composition of the electrolyte and influence the electrochemical characteristics of SC (3). Therefore, the determination of temperature and concentration dependences of the specific capacity of electrolytes aprotic solvent – bis(oxalate)borate salt is relevant.

In the paper, we present data on the specific conductivity of solutions of tetraalkylammonium bis(oxalato)borate salts [$(CH_3)_4NB(OCO)_4$, $(C_2H_5)_4NB(OCO)_4$ and $(C_4H_9)_4NB(OCO)_4$), denoted hereinafter as Me_4NBOB, Et_4NBOB and Bu_4NBOB, in acetonitrile, glutaronitrile, adiponitrile, as well as propylene carbonate and dimethylsulfoxide. The results of the analysis of the concentration and temperature dependences of electrical conductivity are discussed.

Experimental

The synthesis of bis(oxalate)borates was carried out as described in Ref. (3). Oxalic and boric acids were mixed with hydroxide $(C_xH_y)_4NOH$ at room temperature. The mixtures were exposed to microwave radiation with a power of 260 W with a pulse duration of 2-4 min in a Daewoo 4/A5 household microwave oven. The total number of pulses depended on the hydroxide cation and ranged from 4 to 6. The obtained products were recrystallized from saturated acetonitrile solution and dried under vacuum for 3 h (at 115 ºC for Me_4NBOB, 70-80 ºC for Et_4NBOB, and ~70 ºC for Bu_4NBOB). The yield of salts was approximately 70 %.

Electrolyte solutions were prepared in a dry argon box. The salt concentration was calculated in moles per kilogram of solvent (mol/kg). To find the volume fractions required for molar concentration calculations, the density of crystalline Me_4NBOB at 298.15 K was determined as 1.375±0.001 g/cm^3 in a glass pycnometer with hexane as the pycnometric fluid.

In the H^1 spectra, the signals from water hydroxyls (chemical shifts in the range of ≥5 ppm) were not found indicating the absence of water. The most valuable feature of the C^{13} spectra is a singlet at ~160 ppm responsible for the C=O bond in the bis(oxalato)borate anion; other signals correspond to skeleton carbons of organic cations and acetonitrile. This data can be considered as a proof of the chemical individuality of the target compounds.

The range of electrochemical stability of solutions was determined by cyclic voltammograms, which showed the absence of Faraday processes within the potentials of cathodic and anodic decomposition of the electrolyte.

The specific electrical conductivity κ was determined by the high-frequency part of the impedance spectrum in a two-electrode cell with platinum electrodes. The cell constant was found using the standard 0.1 n. aqueous solution of KCl.

Results and Discussion

The temperature dependences of the specific electrical conductivity of 0.7 mol/kg solutions of Me_4NBOB, Et_4NBOB and Bu_4NBOB are shown in Fig. 1. It is well seen that at 25 °C, the specific conductivity of AN solutions is ca. three times greater than that of DMSO solutions, four times greater than that of PC solutions, and five times greater than that of solutions in higher nitriles, AdN and GN. The same is true at all temperatures: $\kappa_{AdN} \leq \kappa_{GN} < \kappa_{PC} < \kappa_{DMSO} << \kappa_{AN}$. This raw coincides with the row of fluidities Φ of the solvents: $\Phi_{AdN} < \Phi_{GN} < \Phi_{PC} < \Phi_{DMSO} << \Phi_{AN}$. For differing cations, an expected trend follows: $\kappa_{Me4NBOB} > \kappa_{Et4NBOB} > \kappa_{Bu4NBOB}$. The analysis of temperature dependences carried out according to the equations of Arrhenius and Vogel-Fulcher-Taman (VFT) and Litovitz showed that acetonitrile solutions are characterized by an activation (Arrhenius) dependence. The conductivity of solutions in other solvents corresponds to the VFT and Litovitz models developed for viscous fluids capable of glass formation. Concentration dependences, which were analyzed according to the Castilla-Amis models of a disordered alloy, showed greater effectiveness of the Castilla-Amis model.

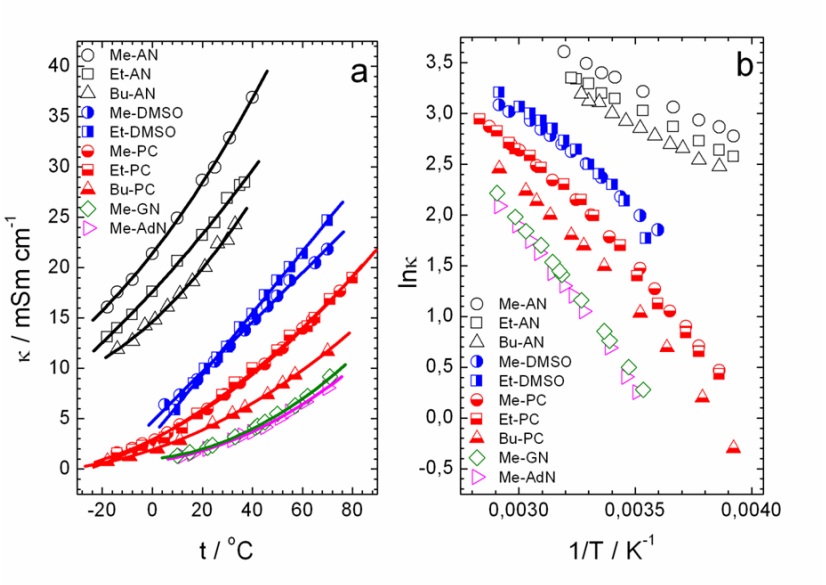

Figure 1. *Temperature dependences of specific conductivities of 0.7 mol/kg solutions of (a) and Arrhenius (b) coordinates.*

Conclusion

In this paper, the data are presented on the specific conductivities of acetonitrile, glutaronitrile, adiponitrile, dimethyl sulfoxide, and propylene carbonate solutions of tetraalkylammonium bis(oxalato)borates Me_4NBOB, Et_4NBOB and Bu_4NBOB obtained by means of a microwave-assisted method. Measurements signify that this method leads to the products of sufficient quality with conductivities, which perfectly coincide with existing data available. The temperature and concentration dependences of conductivity are fitted to polynomial and Casteel-Amis equations, respectively. Comparisons show that the conductivities of acetonitrile solutions at all concentrations and temperatures are superior to those of propylene carbonate solutions; the values for dimethyl sulfoxide lie between them, $\kappa_{PC}<\kappa_{DMSO}<<\kappa_{AN}$, the conductivities of the solutions of salts with longer substituents are smaller, $\kappa_{Me4NBOB}>\kappa_{Et4NBOB}>\kappa_{Bu4NBOB}$, and the conductivities of salt solutions in higher nitriles are very low. Based on a comparison with existing data regarding the molecular composition and conductivity of lithium salt solutions, it is suggested that the inequality $\kappa_{PC}<\kappa_{DMSO}<<\kappa_{AN}$ for one and the same cation can be explained by ion pairing phenomena.

References

1. J. Xie, P. Yang, Y. Wang, T. Qi, Y. Lei, C. M. Li, *J. Power Sources*, **401**, 213 (2018).
2. C. Zhong, Y. Deng, W. Hu, J. Qiao, L. Zhang, J. Zhang, *Chem. Soc. Rev.*, **44**, 7484 (2015).
3. N. I. Globa, V. D. Prisiazhnyi, V. A. Diamant, O. V. Potapenko, Patent UA90234C2. 12.04.2010.

Integration of Nickel-Ammonium Complex Precipitation, Reduction and Electrochemical Activation for Superior Nickel Hydroxide Supercapacitor Electrodes

O. Zima[a], A. Stranovsky[a], P. Ondrejka[a], M. Sojkova[b] and M. Mikolasek[a]

[a] Institute of Electronics and Photonics, Slovak University of Technology, Ilkovičova 3, 812 19 Bratislava, Slovakia

[b] Institute of Electrical Engineering SAS, Dúbravská cesta 9, 841 04, Bratislava, Slovakia

email: oleksandra.zima@stuba.sk, miroslav.mikolasek@stuba.sk

Nickel hydroxide $Ni(OH)_2$ is a key material for hybrid supercapacitors, used as nanoparticles or in composites with graphene oxide or carbon nanotubes. Its role in hybrid supercapacitors, electrocatalysis, and sensing technologies highlights its versatility. In our study, the electrochemical performance of $Ni(OH)_2$ electrodes was significantly improved by combining precipitation, reduction and electrochemical activation methods to form core-shell $Ni(OH)_2$ system. This optimization approach is auspicious for advanced supercapacitor applications.

Introduction

In the field of energy storage, nickel hydroxide is the main ferroelectric active material in hybrid supercapacitors, where $Ni(OH)_2$ is used as a stand-alone material in the form of nanoparticles or ultrafine particles, or as a composite material with nanocarbon structures such as graphene oxide or carbon nanotubes. In the case of thin-layer supercapacitors, $Ni(OH)_2$ films are formed during electrode fabrication on a conductive base, which improves performance and durability.

Nickel hydroxide $Ni(OH)_2$ is one of the most promising materials for use in supercapacitor electrodes (1). Its electrochemical properties and high specific capacity originated from the reversible redox reaction make it a promising material for achieving a high energy density. Nickel oxide electrode with $Ni(OH)_2$ as an active material is widely used as a Faradic electrode for hybrid supercapacitors (1), often in the form of nano-sized particles or composites with nanocarbon materials (2). The main limitation hindering performance of such supercapacitors is low conductivity of $Ni(OH)_2$.

In this work, we propose three step fabrication to prepare a core-shell $Ni(OH)_2$ system. Procedure is based on precipitation of $Ni(OH)_2$ described in (3), followed by reduction of $Ni(OH)_2$ by annealing to form highly structured Ni and subsequent electrode activation in KOH (4) to form core-shell $Ni(OH)_2$ system. The results of the study showed that the combination of these methods led to the formation of structured core-shell $Ni(OH)_2$ system, achieving high conductivity, capacity and high electrochemical stability.

Experimental set-up

All chemicals employed in this study were of ACS reagent grade and utilized without further purification. Metal precursors, including nickel nitrate hexahydrate ($Ni(NO_3)_2 \cdot 6H_2O$,≥98%), ammonium hydroxide (NH_4OH, 25%), potassium hydroxide (KOH), and polyvinylpyrrolidone (PVP, 29,000 a.m.u.), were procured from Sigma Aldrich. Nickel foam rings (thickness 1.6 mm, surface density 346 g/m²). Using an ultrasonic cleaner, the oils were removed with isopropyl alcohol (10 min) and the oxide with hydrochloric acid (10 min).

Formation of Electrode was performed as follows. First, 3.14 g of $Ni(NO_3)_2*6H_2O$ was dissolved in 20 mL of water and 2.46 g of KOH in 40 mL of water. The $Ni(NO_3)_2$ solution was stirred with the KOH solution at 770 rpm for 10 min. The $Ni(NO_3)_2$ solution was added under stirring at 770 rpm for 10 min. The resulting precipitate was filtered off and dissolved in 40 ml of NH_4OH. The prepared substrate was immersed in the solution for 24 h, rinsed with demineralized water and air-dried at room temperature.

Reduction of prepared $Ni(OH)_2$ was done by annealing at 350 °C for 120 min in a nitrogen atmosphere. Subsequently, electrochemical oxidation was performed by cyclic voltammetry in 1 M KOH for 150 cycles at a scanning rate of 50 mV/s in the voltage range from -0.2 V to 0.8 V.

Results and discussion

The prepared $Ni(OH)_2$ by precipitation and core-shell $Ni(OH)_2$ samples prepared by tree step system were characterized by cyclic voltammetry in a three-electrode set-up in 1 M KOH electrolyte. Figure 1 shows measured cyclic voltammetry for the electrode obtained from the nickel-ammonia complex (a) and obtained from the nickel-ammonia complex after oxidation (b). The curve area increased significantly when using the combined method. The position of the redox peaks also changed, indicating greater electrochemical stability and electrochemical activity. Redox peaks in voltammetry indicate the pseudo-capacitive nature of charge accumulation on the surface of the electrode under study. The distribution of the curve area along the y-axis is completely symmetrical at lower scanning frequencies, which indicates the reversibility of electrochemical reactions on the electrode surface. Detailed analysis of electrochemical measurements and supercapacitor performance will be provided in the final paper.

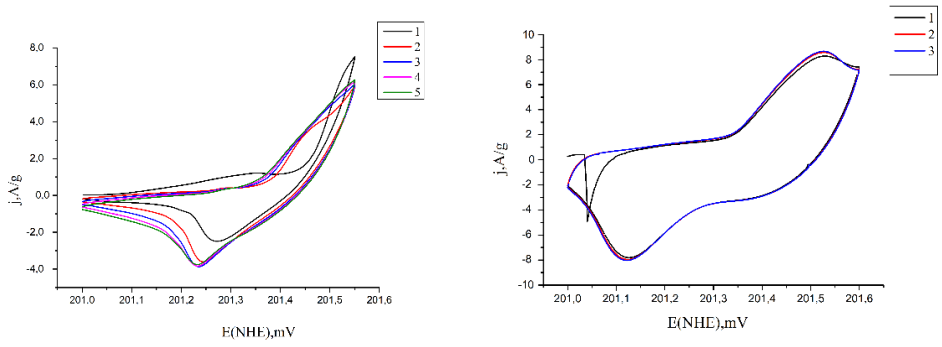

Figure 1. *Cyclic voltammetry curves for the electrode obtained from the nickel-ammonia complex (a) and obtained from the nickel-ammonia complex after oxidation (b)*

Figure 2 and Table 1 show the presence and ratio of each element on the electrode surface after electrochemical activation in 1 M KOH, and Figure 3 shows the positions of the EDX maxima in the

spectra, which are characteristic of the elements and indicate their presence on the electrode surface. In Table 1 we can observe the presence of potassium, which may have reached the supercapacitor electrode during the electrochemical activation in 1 M KOH solution, by the decomposition of KOH.

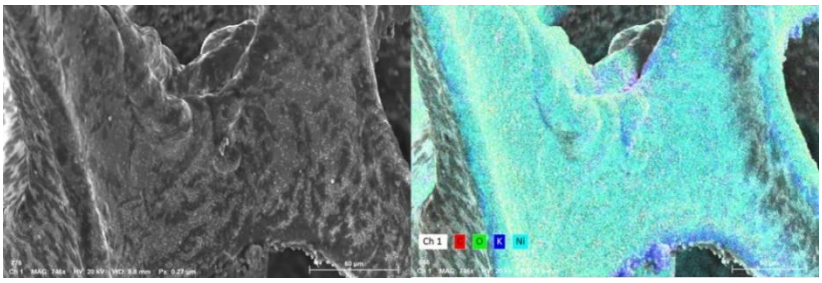

Figure 2. *SEM (left) and EDX (right) image of the electrode after electrochemical activation in 1 M KOH.*

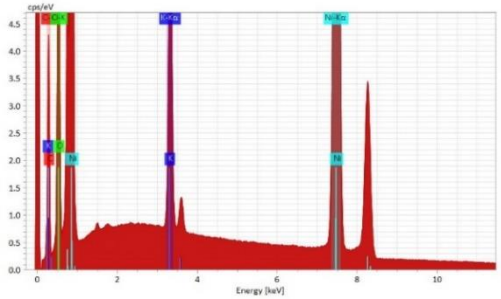

Figure 3. *EDX spectrum of the electrode after electrochemical activation in 1 M KOH*

TABLE I. *EDX data output for the electrode after electrochemical activation in 1 M KOH electrolyte.*

Element	Mass. Norm [%]	Atom [%]	Abs. error [%] (1 sigma)	Rel. error [%] (1 sigma)
Carbon	12,99	31,68	0,15	5,37
Oxygen	16,66	30,49	0,18	4,91
Potassium	10,87	8,14	0,04	1,54
Nickel	59,49	29,69	0,12	0,91

The proposed method, which combines the precipitation of nickel hydroxide from a nickel-ammonium complex, reduction of such hydroxide to Ni by annealing and subsequent electrochemical oxidation, proved to be very effective in improving the electrochemical characteristics of the electrodes. The results indicate that this method has the potential to produce supercapacitor electrodes with high capacity and stability. Further studies will be aimed at optimizing the synthesis conditions and a detailed analysis of the effect of various parameters on the structure and electrochemical properties of the obtained supercapacitor electrodes.

Acknowledgments

This work was supported by grant VEGA 1/0707/24 and by the Slovak Research, and Development Agency under contracts APVV-20-0220 and APVV-21-0231

References

1. Zheng C., Journal of Central South University, Vol.21,p. 2596–2603, (2014)
2. Kovalenko, V.; Kotok, V East.-Eur. J. Enterp. Technol, 5, 17–22, (2017).
3. Kotok, V.;Kovalenko, V., Coatings, 13, 84, (2023).
4. Urso, M., Torrisi, et al. Scientific Reports, 9(1), p.7736. (2019).

Graphitic carbon nitride - nitride partially unzipped carbon nanotubes nanocomposite: synthesis, properties and application for oxygen electrodes of alkaline fuel cells.

M.O. Danilov[a*], G.I. Dovbeshko[bc], I.A. Rusetskyi[a], O. P. Gnatyuk[b], S.S. Fomanyuk[a], G.Ya. Kolbasov[a]

[a] V.I.Vernadsky Institute of General and Inorganic Chemistry of the NAS of Ukraine, Kyiv, 03142, Ukraine.

[b] Institute of Physics of the NAS of Ukraine, Kyiv, 03039, Ukraine.

By the thermo chemical method composite based on graphite-like carbon nitride and nitrided partially unzipped multi-walled carbon nanotubes was obtained. Hybrid composites were confirmed by XRD, TEM, Raman and FT-IR. Electrochemical studies have established that the resulting composites are promising materials as a metal-free catalyst for oxygen electrodes in alkaline electrolyte and were stable in operation time for six months in a fuel half-cell.

Introduction

Investigation of electrode materials for oxygen electrodes is a major challenge for creating cheap energy sources. This study discusses the performance of materials using g-C_3N_4, carbon nanotubes (CNTs) and graphene as important materials to improve the characteristics of fuel cells with alkaline electrolyte (1). As can be seen from the literature, g-C_3N_4 and CNTs are good catalysts with high electrocatalytic properties. It has been shown that partially unzipped multi-walled carbon nanotubes (PUMWCNTs), due to their structure, are more effective catalysts for oxygen reduction than CNTs (2). It appears that carbon materials doped with nitrogen are good catalysts for the oxygen reduction reaction (3). Therefore, it can be assumed that by making a composite of PUMWCNTs and g-C_3N_4 and also by pre-nitriding nanotubes before thermochemical synthesis, a synergistic effect can be achieved in such a hybrid composite.

The aim of work was the synthesis and study the electrochemical characteristics of materials obtained from the thermochemical synthesis of g-C_3N_4 in the presence of nitrided PUMWCNTs as a metal-free catalyst for the oxygen electrode of a fuel cell.

Experimental

Before synthesis, the PUMWCNTs obtained by the electrochemical method were subjected to nitriding in a solution of concentrated nitric acid at boiling temperature for half an hour. To obtain PUMWCNTs, we used the electrochemical method of anodic oxidation of nanotubes in sulfuric acid, described in (2). The thermochemical synthesis of g-C_3N_4 in the presence of nitrided carbon nanotubes was carried out according to the given methods (4). Nitrided PUMWCNTs were mixed with urea and melamine in various compositions then placed in a crucible with a lid and heated without air to 550º C. The synthesis was carried out for 4 hours, followed by cooling to room temperature without. For the investigation synthesis materials, as an active layer for the oxygen electrodes, were used compositions given in Table 1. Oxygen electrodes were made from the synthesized materials and tested in a fuel half-cell with an alkaline electrolyte.

TABLE I. *Consist for synthesis*

Sample N	Initial consist	Additives
Sample 1	15 g of urea + 0.8 g of melamine sponge	0.5 g of nitrided PUMWCNTs
Sample 2	15 g of urea + 0.8 g of melamine sponge	0.5 g of PUMWCNTs
Sample 3	8 g of urea + 4 g of melamine powder	2 g of nitrided PUMWCNTs
Sample 4	8 g of urea + 4 g of melamine powder	2 g of PUMWCNTs
Sample 5	15 g of urea + 0.8 g of melamine sponge	-

The studies were carried out on a fuel half-cell, with a zinc electrode used as the anode. The fuel half-cell with gas diffusion electrodes are described in (5).

Results and discussion

In Figure 1 the load current-voltage characteristics of oxygen electrodes with an active layer of various electrode materials are presented.

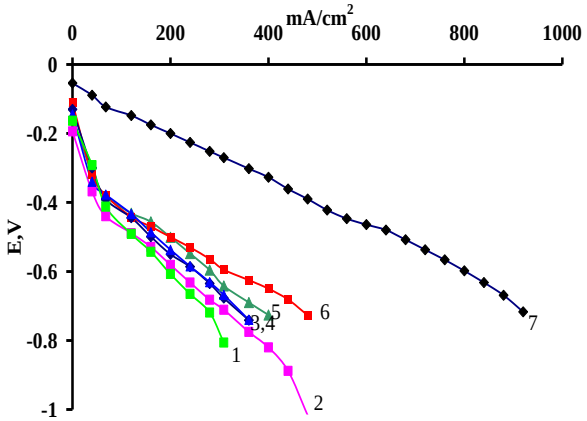

Figure 1. *Volt-ampere characteristics of oxygen electrodes with an active layer of various electrode materials: 1 – PUMWCNTs; 2 - Sample 5; 3 - Sample 2; 4 - Sample 4; 5 - Sample 3; 6 - Sample 1; 7 - MWCNTs with deposited Pt.*

As can be seen from the analysis of electrochemical characteristics, treatment with nitric acid PUMWCNTs improves the electrochemical characteristics of oxygen electrodes made of this material. For the composite based on content of treatment with nitric acid nanotubes and synthesized from melamine sponge, we see an increase in the electrochemical characteristics of oxygen electrodes (curve 6) compared to the composite not treated with nitric acid (curve 3). Thus, the hybrid composite based on g-C_3N_4 and electrochemically synthesized partially unzipped multi-walled carbon nanotubes treated with nitric acid is a promising metal-free support for catalysts, which shows on discharge characteristics approaches to platinum-containing carbon nanotubes (curve 7).

These results can be explained as follows. During the thermochemical synthesis of carbon nitride from urea and melamine together with nitrided PUMWCNTs, we obtains material which are a mixture of nitrided graphene particles and fragments of unzipped nanotubes with embedded molecular groups of NO_3^- from nitric acid. This nanoparticles serve as catalysts and centers for the formation of a hybrid composite of g-C_3N_4. Using XRD, TEM, IR and Raman spectroscopy, the preparation of hybrid composites of g-C_3N_4 with PUMWCNTs were proven. Figure 2 (a) is a hybrid composite based on carbon nitride with pure PUMWCNTs. Figure 2 (b) shows composite of carbon nitride and nitrided PUMWCNTs. Microphotographs of the initial PUMWCNTs presented

on Figure 2 (c). Carbon nitride synthesized under these conditions without nanotubes presented on Figure 2(d).

The long-term experiments were also carried out on the stability of the oxygen electrodes made of the g-C_3N_4 and nitride partially unzipped multiwalled carbon nanotubes. It is worth to mention that the produced materials were stable over six months subject to testing in the fuel half-cell under galvanostatic mode at the current density of 200 $mA \cdot cm^{-2}$ at the oxygen electrodes.

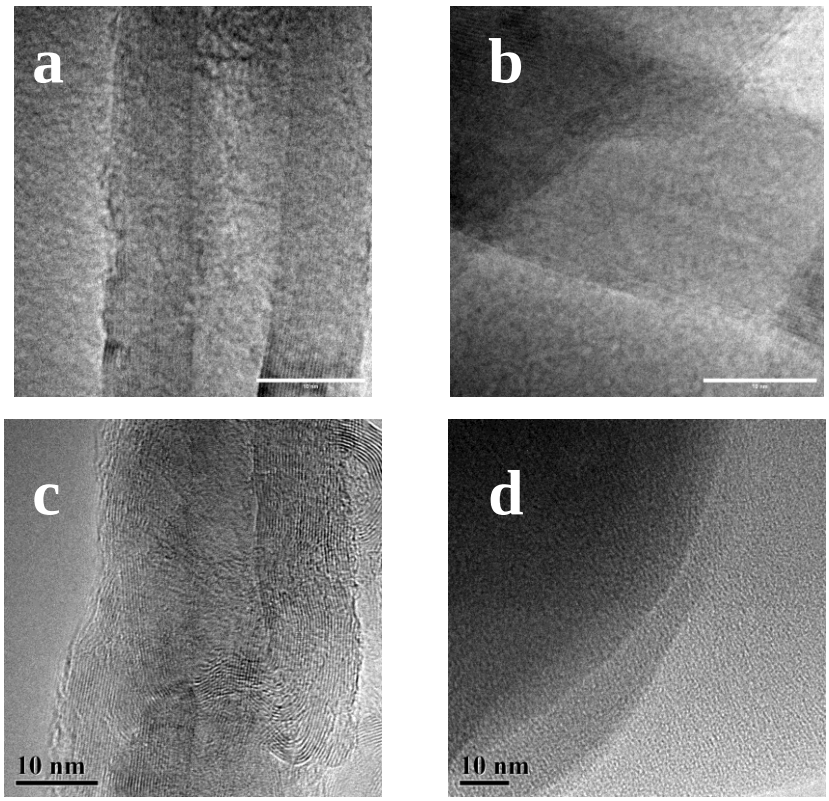

Figure 2. *Micrograph of a hybrid composite (Sample 2) based on: g-C_3N_4 and PUMWCNTs. (a); (Sample 1) g-C_3N_4 and nitrided PUMWCNTs (b); initial PUMWCNTs (c); (Sample 5) pure g-C_3N_4 (d).*

Conclusion

Thus, the hybrid composite based on g-C_3N_4 and electrochemically synthesized PUMWCNTs. treated with nitric acid is a promising metal-free catalyst carrier.

References

1. N. A. M. Harun, N. Shaari, Z. A. Ch. Ramli, *International Journal of Energy Research*, **46** (12), 16281 (2022).
2. M. O. Danilov, G. I. Dovbeshko, I. A. Rusetskyi, V. I. Pekhnyo, A. S. Nikolenko, G. Ya Kolbasov, *Applied Physics A*, **126**(10),764 (2020).
3. M. Wang, Z. Wu, L. Dai, *Journal of Electroanalytical Chemistr*, **753**, 16 (2015).
4. M.O. Danilov, G.I. Dovbeshko, I.A. Rusetskyi, V.N. Bykov, O.P. Gnatyuk, S.S. Fomanyuk, G.Ya. Kolbasov, *Nanocomposites*, **9**(1), 1 (2023).
5. M.O. Danilov, I.A. Rusetskii, G.I. Dovbeshko, A.S. Nikolenko, S.S. Fomanyuk, G.Ya. Kolbasov, *ECS Trans.*, 95(1), **273** (2019).

Analysis of the Electrochemical Method of Producing Environmentally Friendly Hydrogen Energy Carrier According to the Evans Diagram

M. K. Sukhyi, V. G. Nefedov, and Yu. V. Polishchuk

Ukrainian State University of Science and Technology, Dnipro, 49010, Ukraine

The possibility of increasing the hydrogen release rate and reducing energy consumption was analyzed using a system in which the anodic process of metal (aluminum alloy) dissolution occurred on one electrode and the process of H_2 release - on the other (nickel) electrode. In the study, the ratio of hydrogen release currents on aluminum and nickel was evaluated, the effect of alkali concentration and temperature on the value of current density, polarization and polarizability of electrodes from an aluminum alloy containing Cu was determined 3.8-4.9; Mg 1.2-1.8; Mn 0.3-0.9 and Fe 0.5%.

Introduction

Modern industry and energy are increasingly focused on using environmentally friendly technologies. To a large extent, this relates to reducing the use of natural hydrocarbons and coal, which form carbon oxides during combustion. Their accumulation in the atmosphere is one of the reasons for global negative climate change. Therefore, hydrogen is considered an energy carrier that does not increase the carbonization of the atmosphere. [1]. Currently, most hydrogen is produced from natural gas and coal. These technologies are well-developed, accessible, and cheap. However, along with hydrogen, their processing products also include carbon oxides [2].

Another method of hydrogen production is water electrolysis. If nuclear or green energy is used as a source of electricity, it is possible to produce a coolant with a high combustion temperature, which has an unlimited resource and produces water during combustion. The disadvantage of this method is the high energy intensity of this process: hydrogen produced by electrolysis is approximately one and a half to two times more expensive than natural gas. The high energy consumption is due to the high theoretical value of the water decomposition voltage, 1.23 V. Moreover, in modern electrolyzers, this value is about 1.8 V. To reduce energy consumption, we have proposed a method of electrolysis with a soluble anode from electronegative metal scrap, for example, iron and aluminum [3]. This makes it possible to replace the anodic process of oxygen release in an acidic medium with a potential of 1.23 V with the anodic dissolution of aluminum (minus 1.66 V) or iron process of dissolving iron (potential minus 0.44 V). Since scrap and waste aluminum of arbitrary composition is expected to be used as an anode, it is necessary to evaluate the factors influencing the dissolution rate of aluminum and its alloys, that is, the corrosion resistance of these materials.

The rate of aluminum dissolution and hydrogen release can be increased if an additional cathode with low H_2 release overvoltage is used. Such a material could be nickel. A further option when using an aluminum-soluble anode and a nickel cathode is the ability to generate electricity simultaneously with the release of hydrogen. In this case, this electrochemical system behaves as a chemical power source.

Experiment

Experiments were carried out in sodium hydroxide solutions with a concentration of 0.1; 0.5; 1 and 2 mol/l in a thermostat at temperatures of 20, 30, 40, and 50 °C. Electrodes made of an aluminum and nickel alloy in the form of plates with dimensions of 10x10 mm (electrode area 1 cm^2) were installed at a distance of 5 mm under the burette to collect the released gas. The current strength and density were calculated from the volume of gas released. During the experiment, the potentials of the electrodes relative to the silver chloride reference electrode were measured. The nickel cathode was connected to the aluminum anode via an ammeter, allowing partial currents:

$$I_{\Sigma}=I_{Al}+I_{Ni}, \quad (1)$$

where I_{Σ} is the total current determined by the volume of the gas released; I_{Al} is the current strength of aluminum dissolution (hydrogen release on aluminum); I_{Ni} is the current strength flowing through the nickel electrode.

Results and discussion

In the first stage, we assessed the dependence of aluminum dissolution's reaction rate (current density) on temperature and electrolyte concentration (Fig.1). The current strength was determined by the volume of gas released.

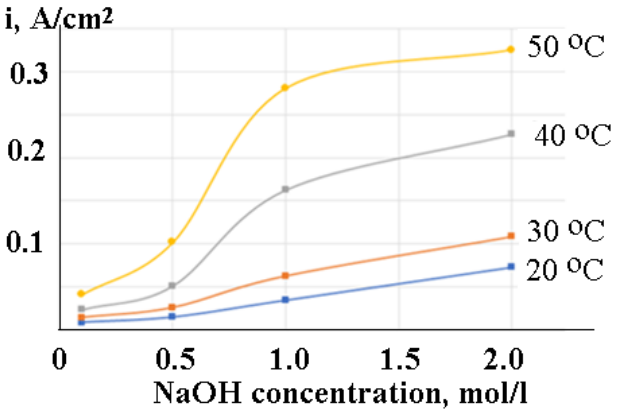

Figure 1. *Dependence of the current density of hydrogen release on a nickel electrode on the concentration and temperature of the sodium hydroxide solution. The numbers next to the curves indicate temperature*

In the second stage, we calculated the polarization values of the aluminum electrode during the hydrogen release on it, and the potential difference between the anode (aluminum alloy) and nickel cathode pair for temperatures of 20-50°C.

For example, polarization diagrams of Al alloy dissolution and hydrogen release in 0.5 mol/l of NaOH solution shown in figure 2. The letters in the figures indicate the following: A – standard potential of aluminum; C – equilibrium potential of hydrogen release; B – measured compromise potential of hydrogen release on aluminum, D – measured compromise potential of hydrogen release on Al alloy electrode short-circuited with a nickel electrode; E – measured potential of the nickel electrode; G – measured potential of an Al alloy electrode short-circuited with a nickel electrode. Connecting the points ABC represents the polarization diagram of aluminum dissolving with hydrogen release; ADC – total polarization diagram of hydrogen release on a pair of aluminum alloy and nickel electrodes; AGEC – the diagram, which takes into account the partial currents of

hydrogen release on the Al alloy and nickel. The potentials at points E and G differ by the voltage drop in the electrolyte. Current strength at points: B - dissolution of the Al alloy; D – hydrogen release on a pair of Al alloy and Ni; E – hydrogen release on nickel; G – hydrogen release on a pair of Al alloy and Ni, calculated according to formula [1]. Current densities were calculated taking into account the electrode area equal to 1 cm^2.

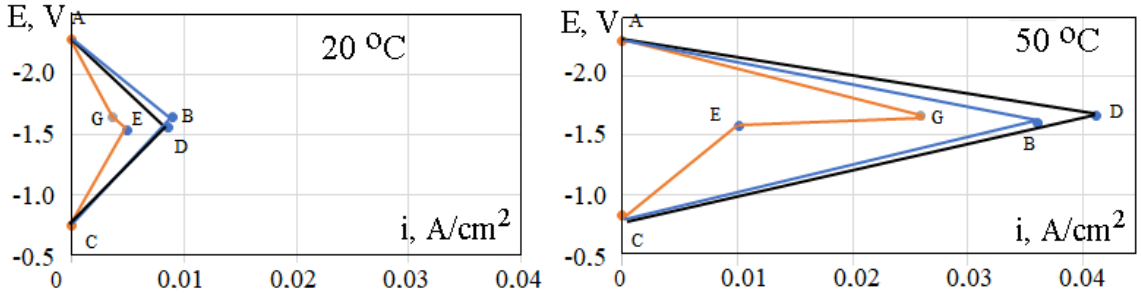

Figure 2. *Polarization diagrams of Al alloy dissolution and hydrogen release in 0.5 mol/l of NaOH solution*

From experimental data it follows that at relatively low alkali concentrations (0.1÷1 mol/l) and a temperature of 20°C, the current density of hydrogen release on the nickel electrode (point E) is greater than on the aluminum alloy (point G). With increasing temperature, the current ratio changes, and the current density of hydrogen release on the Al alloy becomes significantly greater.

Conclusions

1. The dissolution rate of the aluminum alloy is proportional to the square root of the NaOH solution concentration, at concentrations higher than 0.5 mol/l.

2. The part of the current of the hydrogen release on Ni, short-circuited with the anode, exceeds that on the Al alloy at the temperature of 20-30°C and decreases with increasing temperature and concentration.

3. In general, the polarizability of the hydrogen release process on an aluminum alloy is less than on nickel. This indicates the need to replace the cathode material or its activation.

References

1. J. M. Yue, H. Lambert, E. Pahon, R. Rocke, S. Jemei and D. Hissel, *Renewable and Sustainable Energy Rev.*, **146**, 111180 (2021).
2. R. B. Gupta, *Hydrogen fuel: Production, Transport and Storage*, p. 603 CRC Press, Boca Raton, London, New York (2009).
3. V. Nefedov, V. Matveev, K. Sukhyy, Yu. Polishchuk, A. Bulat, B. Bluss and A. Mukhachev, *IOP Conf. Ser.: Earth Environ. Sci.*, **1156**, 012034 (2023).

High-Temperature Electrochemistry for the Investigation of Redox Reactions on Metal Surfaces

Michael Georg Stadt[1,3], Michael Nelhiebel[2], Silvia Larisegger[3], Günter Fafilek[1]

[1]TU Wien, Institute of Chemical Technologies and Analytics – EC, Vienna, Getreidemarkt 9, 1060 Wien, Austria

[2]KAI Kompetenzzentrum Automobil- und Industrieelektronik GmbH, Europastraße 8, 9524 Villach, Austria

[3]Kompetenzzentrum Automobil- und Industrieelektronik GmbH, Argentinierstraße 8, 1040 Wien, Austria

Abstract

High-temperature cyclic voltammetry (HT-CV) is a versatile technique for accurately characterizing metal oxidation processes. This method uses YSZ (Yttria-stabilized zirconia), a solid-state oxygen ion conductor, as an electrolyte. By applying defined potentials, different oxide species are produced. Hence, thermodynamic processes such as the stability of oxides and kinetic properties, like growth rates, can be investigated. However, in electrochemical reactions the current cannot be assigned to specific reactions unequivocally. To address this issue, *in situ* analytical methods are necessary. This is crucial when investigating diffusion processes or electrical properties of the reaction products (oxides), as they require additional (electro-)analytical information. While extensive research has been conducted on thermal oxidation under varied conditions, in-situ investigation of the electrical and chemical properties during oxide layer formation has been challenging.

Our work introduces a novel method for controlled metal oxidation, combined with an in-depth analysis of the electrical properties of nanometer-thick oxide layers. Therefore, a potentiostat and a frequency response analyzer are coupled in a specific arrangement, allowing for their artifact-free combination in the solid electrolyte cell setup. This combined setup allows for the control of oxygen pressure at the metal surface, while in-situ electrochemical impedance is used to determine the electrical properties of the oxide layers. Through this approach, the defect density as a function of oxygen partial pressure is determined, providing valuable insights for precise tuning of electrical properties in oxide formation.

Moreover, we study present a novel combination of high-temperature electrochemistry with Raman spectroscopy to directly investigate metal oxidation processes and diffusion phenomena at the solid-electrolyte/metal interface. The adaptation of a commercial Raman heating stage enables electrochemical measurements in the cell, while the use of a transparent YSZ single crystal (solid-electrolyte) allows for Raman measurements at the metal(oxide)/electrolyte interface. This combined method not only enables the analysis of oxides produced under controlled conditions but also allows for the investigation of metallic interdiffusion. The results obtained with Raman spectroscopy confirm the species predicted from electrochemical experiments, providing valuable insights into metal oxidation processes and diffusion phenomena.

On The Stability of Perowskit Oxygen Evolution Electrocatalysts in alkaline Solutions

Da Xing[1], Leander Kucklick[1], Ioannis Spanos[2], Blaz Toplak[1*], Doris Segets[1] and Harry Hoster[1*]

[1.] University of Duisburg Essen, Duisburg, Germany

[2.] Max-Planck-Institut für chemische Energiekonversion, Mülheim an der Ruhr, Germany

Water splitting requires a highly active catalyst. Lanthanum-based perovskites have recently been used as catalysts for the oxygen evolution reaction (OER) due to their high activity.1 However, the stability of perovskite oxide catalysts for OER plays a critical role in their applicability in water splitting concepts.2-4

In the present study, the OER of $La_{0.8}Sr_{0.2}CoO_3$ (LSCO), $LaCoO_3$, $LaMnO_3$, and $LaFeO_3$ was investigated using a rotating disk electrode (RDE). LSCO shows the highest OER activity and $LaMnO_3$ shows the lowest OER activity. Self-activation towards OER with LSCO was also observed by potentiostatic and galvanostatic experiments. The metal dissolution was studied by operando ICP-OES and Raman using a self-designed flow cell5 and the chemical state was investigated by XPS before and after OER. Operando ICP-OES revealed the periodic dissolution of Sr and Fe in the cyclovaltomogram and in the long-term stability measurement. Interestingly, no co-dissociation was observed. The peaks of La, Sr, Co and O of LSCO in the XPS spectra shift with the dissolution of Sr in different electrochemical experiments. The dissolution of strontium cations leads to a decrease in the abundance of strontium on the catalyst surface. At the same time, cobalt is enriched on the catalyst surface during the activation process due to its lower solubility in water. After the activation process of LSCO, Co_3O_4, $Co(OH)_2$, Co(OOH) were formed, which are believed to be the active species for OER. It is not clear whether $La(OH)_3$ also plays a role in OER, since it does not participate in oxidation reactions.

Novel Carbon Material with Potential Application in Lead-Acid Battery Technology

Marek Baraniak[a*], Radosław Płowens[b], Katarzyna Lota[c], Marek Bajsert[b], Grzegorz Lota[a,c]

[a] Poznan University of Technology, Institute of Chemistry and Technical Electrochemistry Berdychowo 4,60-965 Poznan, Poland,

[b]Jenox Akumulatory Sp. z o.o. Notecka 33,64-800 Chodzież, Poland,

[c]Łukasiewicz Research Network Institute of Non-Ferrous Metals Division in Poznan Central Laboratory of Batteries and Cells Forteczna 12, 61-362 Poznan, Poland

Lead-acid batteries are one of the most important energy storage systems, widely used in automotive, industrial and backup applications. However, lead-acid batteries exhibit limitations, such as relatively low energy density, limited service life, etc. The aim to improve the performance of Pb/PbO_2 systems forces the searching for new materials with better physicochemical and electrochemical properties. One of the most important research directions is the use of various types of carbon materials as additives to electrode active masses. This article presents the results of a research on the effect of the addition of a new carbon material on the properties of the active mass of a lead-acid battery. The carbon material was obtained by carbonization of sheep's wool fibers.

Introduction

The increase in electricity production and consumption is closely related to the development of civilization. In the 21st century (2001-2023), global electricity production increased from about 124 PWh to 183 PWh (1). Significant increases in energy prices are caused by depleting fossil fuel reserves, global warming, pollution, geopolitical and military conflicts. Renewable energy provides a solution to these growing energy problems. However, this carries some drawbacks. Energy storage is a critical challenge in renewable energy production due to the intermittent nature of sources such as solar and wind power. These energy sources are weather-dependent, leading to periods of excess and deficit generation. To balance supply and demand, effective storage solutions are needed to provide a constant supply of energy. Energy storage systems (ESS) are becoming increasingly important components of power grids. Current storage technologies, such as batteries, encounter limitations in terms of capacitance, performance and cost. However, they are widely used especially in smaller systems (2,3). One of the most important types of batteries is continuously Pb/PbO_2 system. Lead-acid batteries are known for their lower specific energy and energy density, but at the same time offer a low cost and full recyclability, making them still an attractive energy storage system for both SIL applications and as energy storage for small-scale renewable energy installations (4-7). The widespread application of Pb/PbO_2 systems necessitates a multidirectional search for methods to improve performance or further reduce the cost of their production. The most important area in this research focuses on new types of carbon material additives to active masses. This is a result of the almost unlimited number of types of carbon material precursors and the possibility of modifying the process conditions (8-12).

The present research focuses on the effect of new type of carbon material added to the positive and negative electroactive mass on the properties of lead-acid cells.

Experimental and results

Novel carbon material was obtained during carbonization of natural wool fibers. Conditions for carbonization of precursor: time: 2h, T = 700°C, gas: N_2. Based on SEM and macroscopic images, it can be observed that there are significant differences in the morphology and microstructure of the prepared carbon material compared to commercially available ones. The material used was not activated but only carbonized. Conductivity values determined by electrochemical impedance spectroscopy indicate that the obtained carbon material is about 9 times worse conductor of electricity than commercial graphite (0.5 and 4.5 [S/cm], respectively). 2V cells with 3 electrodes (two positive and one negative or two negative and one positive) were assembled. Electroactive masses were based on lead powder produced in a ball mill with a composition of about 75% PbO and 25% Pb. The modified masses (positive and negative) were enriched with carbon materials at 0.2% by weight. Modified electrodes have been manually pasted. Other technological operations (including the process of paste preparations, pasting of standard electrodes, curing and formation) were carried out in accordance with the technology of a Jenox company. The electrode masses after the curing process exhibited a sulfuric acid adsorption capacity about 69-108% higher than standard plates. The formation process occurred at a higher voltage, indicating a higher over-voltage of hydrogen and oxygen release. The positive plates already achieved the assumed capacity at the first cycle, and in the discharged state the electrodes achieved values of charge transfer resistance lower than analogous cells with standard electrodes.

Conclusions

The new type of carbon material shows a significant difference compared to traditional materials used as additives to the active mass of lead-acid batteries. Despite relatively low conductivity and significant differences in macro- and microstructure, this material presented a positive effect on the physicochemical properties of the electrode material at various stages of its production. The basic electrical properties of the cells did not change, while an improvement in the efficiency of the positive mass formation process was obtained. The lower charge transfer resistance for electrodes in the discharged state additionally indicates a lower risk of sulfation of the system. This demonstrates the large potential for the use of some non-activated carbon materials in lead-acid batteries.

Acknowledgments

This work was supported by the Polish Ministry of Science and Higher Education. The authors would also like to thank Jenox for providing samples.

References

1. H. Ritchie, P. Rosado, M. Roser, *Energy Production and Consumption Explore data on how energy production and use varies across the world* https://ourworldindata.org/energy-production-consumption (accessed 12.07.2024)
2. L. Yao, B.Yang, H. Cui, et al. *J. Mod. Power Syst. Clean Energy* **4,** 519–528 (2016).
3. G.J. May, A. Davidson, B. Monahov, *J. Energy Storage*, **15,** 145–157 (2018).
4. R. Etacheri, R. Marom, R. Elazari, G. Salitra, D. Aurbach, *Energy Environ. Sci.,* **4**, 3243-3262 (2011).

5. J. Garche, E. Karden, P. T. Moseley, D. A. J. Rand, *Lead-acid Batteries for Future Automobiles*, Elsevier, Amsterdam (2017).
6. X. Luo, J. Wang, M. Dooner, J. Clark, *Applied Energy*, **137,** 511-536 (2015).
7. L.T. Lam, R. Louey, *J. Power Sources*, **158**, 1140-1148 (2006).
8. R. Marom, B. Ziv, A. Banerjee, B. Cahana, S. Luski, D. Aurbach, *J. Power Sources*, **296,** 78-85 (2015).
9. X. Zou, Z. Kang, D. Shu, Y. Liao, Y. Gong, C. He, J. Hao, Y. Zhong, *Electrochim. Acta,* **151,** 89-98 (2015).
10. J. Lach, K. Wróbel, J. Wróbel, P. Podsadni, A. Czerwiński, *J. Solid State Electrochem.,* **23,** 693–705 (2019).
11. P.T. Moseley, R.F. Nelson, A.F. Hollenkamp, *J. Power Sources,* **157,** 3–10 (2006).
12. K. Yanamandra, D. Pinisetty, N. Gupta, *Renew. Sustain. Energy Rev.,* **173**,113078 (2023).

Progress in redox flow battery development

J. Charvát[a,b], J. Pocedič[a], J. Vrána[a]

[a] Pinflow Pinflow energy storage, s.r.o., Plzeň, Czech Republic

[b] New Technologies – Research Centre, University of West Bohemia, Plzeň, Czech Republic

In this work, we will introduce progress in the development of redox flow batteries around the world and describe different redox flow battery chemistries that are currently used for large-scale applications. In the second part of this work will introduce problems connected with scale up of the redox flow batteries and we will explain how these problems are solved in Pinflow energy storage.

Redox flow batteries

The increase in the generation of electricity from renewable sources is creating demand for stationary energy storage that helps to use this electricity efficiently while stabilising the transmission system. Redox flow batteries (RFBs) appear to be promising candidates for such stationary energy storage. Redox flow batteries could be based on many different chemistries (all vanadium, organic, Zn-Br, all iron, Fe-Cr) but the main description for all these chemistries is as follows.

RFB is composed of a battery stacks and of tanks with the electrolyte. The tanks are connected to the battery stacks via pipelines, and pumps are used for the circulation of the electrolyte through the battery stack. The battery stack is composed of dozens of cells separated by a so-called bipolar plate. Due to this setup, battery power and capacity are independent (with exception of RFB with metal deposition (e.g. Zn-Br)), as the power is determined by the size and number of cells and capacity is determined by the volume of the tanks. Each cell is composed of two inert electrodes (positive and negative electrode where electrochemical reactions occur. The electrodes are mutually separated typically by an ion-exchange membrane, which prevents cross-mixing of a positive (posilyte) and negative (negalyte) electrolyte but enables ionical connection.

In this work we will present the progress from two perspectives. From the commercial one where individual installation and plans for the future installations around the would be present. We will also present progress from the scientific side and explain what it means to scale up the redox flow battery.

Progress in redox flow battery development around the would

Redox flow batteries are actively developed and manufactured all over the world. From the homeland of the vanadium redox flow batteries in Australia, through many countries in Europe, where the development is driven by the Green deal, to America. However, the most active in redox flow battery development and deployment is currently Asia and mainly China.

In China, the development is driven by the Dual Carbon Goal (analogy of the European Green Deal). Currently the biggest battery in the world (200 MW and 400 MWh) is based on vanadium redox flow battery technology and is installed in Dalian China and further

low dozens of GW and GWh of different redox flow battery are planned to be installed in China in the following years.

Scale-up of Redox-Flow Batteries

The battery stacks are the main components of the RFB and are responsible primarily for the performance and efficiency of the RFB.

RFB stacks are usually composed of dozens of single cells that are electrically connected in series while hydraulically in parallel. Thus, battery performance is significantly affected by every single cell, and a problem with even one single cell could completely destroy the battery stacks if a parasitic reaction (oxygen evolution) occurs. The standard battery stack can be monitored only on the current collectors, and each of these problems results only in a small increase in the resistance of the battery stack (higher or lower voltage during charging/discharging) and it is not possible to distinguish whether there is some small problem homogenously distributed between all the cells or if there is a problem with only one cell. In the Pinflow research-grade stacks, every single cell might be easily contacted and characterised. This arrangement enables us to develop an easy way to develop a reliable stack design with homogeneous distribution of the resistances.

Optimization of performance and stability of zinc-air flow battery

P. Mazúr[a], P. Richtr[a], D. Graf[a], M. Bureš[a], J. Hnat[a], M. Paidar[a], J. Charvat[b], J. Pocedic[b]

[a] University of Chemistry and Technology Prague, Technicka 5, 166 28 Prague, Czechia

[b]University of West Bohemia Pilsen, Univerzitni 8, 306 14 Pilsen, Czechia

Ongoing decarbonisation of energetics and mobility sectors emphasizes the needs for reliable, safe and environmentally energy storages for both mobile and stationary applications. The concept of flow battery offers several original features particularly interesting for grid stabilization applications. The zinc-air flow battery particularly provides cheap, non-toxic and non-explosive alternative to more matured vanadium-based system. However, both efficiency and durability needs to be improved to fully exploit the potential of the chemistry. In our contribution, the activities related to R&D of zinc-air flow battery on UCT Prague and UWB Pilsen are summarized, with the main focus on development of efficient and stable 3D electrodes for oxygen evolution reaction (OER used for battery charging) and oxygen reduction reaction (ORR used for battery discharging).

The electrocatalytic activity of OER electrode was enhanced by electrochemically assisted precipitation of Ni-Co spinel catalysts onto suitable 3D Ni supports (mesh of foam). The quality and composition of the deposited catalytic layer before and after electrochemical testing was inspected by suitable physico-chemical techniques incl. scanning electron microscope with EDS detector. The performance and stability of the prepared electrodes was preliminary tested in a flow water electrolysis cell showing reduced overpotential of the catalysed OER electrodes and mid-term stability within 180 hours test. Finally, the electrode performance was evaluated in a the developed 3-electrode Zinc-air flow battery full-cell showing significantly improved efficiency for both catalysed electrodes (slightly better parameters achieved with the foam-supported one).

For ORR electrode, we successfully optimized the hydrophobicity of the catalytic layer of the gas diffusion electrode using a commercial PTFE polymeric binder and carbon supported platinum electro-catalyst (0.5 mg Pt/ cm^2 loading). The electrochemical testing of the GDEs in a flow electrochemical cells revealed the optimized PTFE content to be around 50-70 wt.%, providing reduced overpotentials for the ORR reaction and suitable mid-stability.

The optimization of both positive electrodes together with application of suitable carbon felt for negative electrode construction resulted in improved cell parameters (approx. 45% energy efficiency of galvanostatic cycling at 100 mA cm^{-2} and peak discharge power density reaching 150 mW cm^{-2}.

Acknowledgments

This publication was supported by the project "The Energy Conversion and Storage", funded as project No. CZ.02.01.01/00/22_008/0004617 by Programme Johannes Amos Comenius, call Excellent Research.

Design of "water-in-salt" electrolytes for dual-ion batteries – influence of salt concentration and additives

M. Nádherná[a], T. Chvojka[a,b], R. Pfeifer[a], G. Abbas[a,c], Z. A. Zafar[a,d], J. Červenka[a]

[a] FZU – Institute of Physics of the Czech Academy of Sciences,162 00 Prague 6, Czech Republic

[b] University of Chemistry and Technology, 166 28 Prague 6, Czech Republic

[c] University of Waterloo, Ontario N2L 3G1, Canada

[d] IMDEA Materials Institute, Getafe, Madrid, 28906, Spain

The electrochemical systems for energy storage with aqueous electrolytes have attracted significant attention mainly due to their high safety, ionic conductivity, and lower costs in comparison to organic-based electrolytes. They also offer non-flammability, good recyclability, and environmental friendliness that presents them as a promising alternative for large-scale energy storage applications. However, their biggest challenge is the narrow electrochemical window of water (1.23 V), which prevents reaching higher energy density.

In this work, we present an electrolyte design strategy based on highly concentrated aqueous water-in-salt (WIS) electrolytes, which enables to significantly expand their electrochemical windows in the range of 2-4 V (ref. 1, 2). We explore how the concentration of salts, additives, and different types of cations and anions influence the electrochemical stability window, ionic conductivity, and other important physicochemical properties of aqueous electrolytes. To achieve an even wider electrochemical stability window, we tested several additives. These additives were selected based on their potential interaction with water molecules and water solvent activity and chemical reactivity. It was found that the high concentration of salts and specific additives can effectively suppress the dissociation of water and improve the stability of the electrolytes. Linear sweep voltammetry reveals that the oxygen evolution reaction (OER) and the hydrogen evolution reaction (HER) can be shifted with the increasing concentration of salts, pH, or via specific ion or additive effects in the aqueous WIS electrolytes. The electrolytes have also been evaluated using Raman spectroscopy to examine the modification in the local structure and hydrogen bonding of water. Electrochemical results indicate the existence of two distinct regions in the concentration behavior that show a good correlation to the local water structure analysis by Raman spectroscopy. We identify the best cation-ion pairs and additives for broadening the electrochemical stability window and demonstrate their application in high-voltage aqueous dual-ion batteries (2).

References

1. A. Z. Zafar et al., *Electrochim. Acta,* **404**, 139754 (2022).
2. Z. A. Zafar, et al., *J. Mater. Chem. A,* **10,** 2064 (2022).

Ionic Liquid and Palladium Nanoparticle Modifications for Nickel-Metal Hydride Negative Electrode

K. Tokarek[a], J. Wojciechowski[a], F. Walkiewicz[b], M. Baraniak[a], M. Pająk[c], K. Hubkowska[c], D. Monikowska[c], A. Czerwiński[c], G. Lota[a,d]

[a] Poznan University of Technology, Institute of Chemistry and Technical Electrochemistry, Berdychowo 4, 60-965 Poznan, Poland

[b] Poznan University of Technology, Institute of Chemical Technology and Engineering, Berdychowo 4, 60-965 Poznan, Poland

[c] University of Warsaw, Faculty of Chemistry, Pasteur 1, 02-093 Warsaw, Poland

[d] Łukasiewicz Research Network Institute of Non-Ferrous Metals Division in Poznan Central Laboratory of Batteries and Cells, Forteczna 12, 61-362 Poznan, Poland

The research deals with improving the corrosion resistance of nickel-metal hydride negative electrode by means of adding ionic liquid to commercial 6M KOH electrolyte, as well as improving hydrogen absorption kinetics and capacity by modifying the electrode material with palladium nanoparticles.

Abstract

Nickel-metal hydride battery cells, abbreviated Ni-MH, are one of the most commonly used secondary electrochemical cells in the world, along with lithium-ion and lead-acid cell systems. They are also closely related to nickel-cadmium electrochemical cells, sharing with them positive electrode material, electrolyte solution and some of the chemistry of charge-discharge reactions. Compared to those systems, they offer several advantages, like lower toxicity of the components (compared to highly toxic lead and cadmium metals) and stability. But they also have drawbacks. The most commonly used electrolyte for Ni-MH batteries, the concentrated solution of potassium hydroxide, is highly corrosive to the electrode materials. The corrosion of the system results in degradation of the half-cells, and in turn gradual loss of capacity of the system (1). Therefore, limiting the corrosion rate of the electrochemical cell is one of the ways of improving its working parameters.

Ionic liquids have widely studied and understood anti-corrosive properties (2). They have been used to prevent metals from degradation and proposed as replacement for more aggressive electrolytes of electrochemical cells (3). They usually exhibit decent ionic conductivity, along with non-flammability, low toxicity, low volatility and chemical, as well as thermal stability. Their main drawbacks, when it comes to their utility as alternative electrolytes, seem to be high viscosity as well as relatively low electrical conductivity when compared to aqueous and organic systems. One way to mitigate their negative aspects is to use ionic liquids as additives to classic aqueous electrolytes, as they show anti-corrosive properties even in small concentrations. While higher concentration of ionic liquid in aqueous electrolyte improves the corrosion inhibition, it also affects the capacity of studied electrochemical systems by blocking hydrogen absorption reactions. A balance between corrosion inhibition and good hydrogen absorption is one of the key aspects of this work.

Research and Methodology

The experimental part of this research focused on two aspects - physicochemical and electrochemical characterisations of studied systems. The conductivity of ionic liquids, as well as concentrated potassium hydroxide solution with addition of 0.01 wt%, 0.1 wt% or 1 wt% of ionic liquids (namely ethyl-methylimidazole (C_2C_1im) or propyl-methyl-methylimidazole ($C_3C_1C_1$im), both with bis(trifluoromethane)sulfonimide anion) was characterised by the means of electrochemical impedance spectroscopy in two-electrode Swagelock® system, utilising gold as both working and counter electrode. The surfaces of studied Ni-MH negative half-cells, that is AB_5 hydrogen-absorbing alloy ($LaMmNi_{4.1}Al_{0.3}Mn_{0.4}Co_{0.45}$), either unmodified or modified with palladium nanoparticles, were performed by means of scanning electron microscopy and energy-dispersive X-ray spectroscopy.

The electrochemical testing was divided into two parts – corrosion testing and capacity testing. Corrosion testing was performed in three-electrode Swagelock® system with AB_5 working electrode, golden counter electrode and Ag/AgCl reference electrode. The corrosion tests consisted of open circuit potential measurement, potentiodynamic electrochemical impedance spectroscopy and cyclic potentiodynamic polarisation. The capacity testing was performed in three-electrode system, with AB_5 alloy as working electrode, Ag/AgCl or Hg/HgO reference electrode and nickel counter electrode. The experiments involved galvanostatic cycling with potential limitation and open circuit potential measurement.

Results and discussion

The curves obtained from cyclic potentiodynamic polarisation are shown in Fig. 1. The values of corrosion potential and corrosion current obtained from analysis of the CPP curves are collected in Table I. It can be concluded that even small amount of addition of ionic liquid (0.01 wt%) has noticeable positive effect on corrosion parameters of the studied systems. The results of capacity testing are displayed in Table 2, and the comparison between corrosion currents and capacity of various systems is shown in Fig. 2. It is worth noting that even though the capacity decreases with the addition of the ionic liquids to the systems, it does so by relatively smaller value compared to the decrease in corrosion current. Moreover, modification of AB_5 hydrogen-absorbing alloy with palladium nanoparticles positively impacts the capacity of studied half-cells.

TABLE I. *Corrosion current densities (j_{corr}) and corrosion potentials (E_{corr}) obtained from cyclic potentiodynamic polarisation curves (Fig. 1). All of the values were estimated on the basis of Tafel extrapolation method.*

Electrolyte	**E_{corr} vs SHE [mV]**	**j_{corr} [µA/g]**
6 M KOH	-165	349.0
0.01% C_2C_1im 6M KOH	-147	239.9
0.1% C_2C_1im 6M KOH	-143	173.1
0.01% $C_3C_1C_1$im 6M KOH	-191	159.2

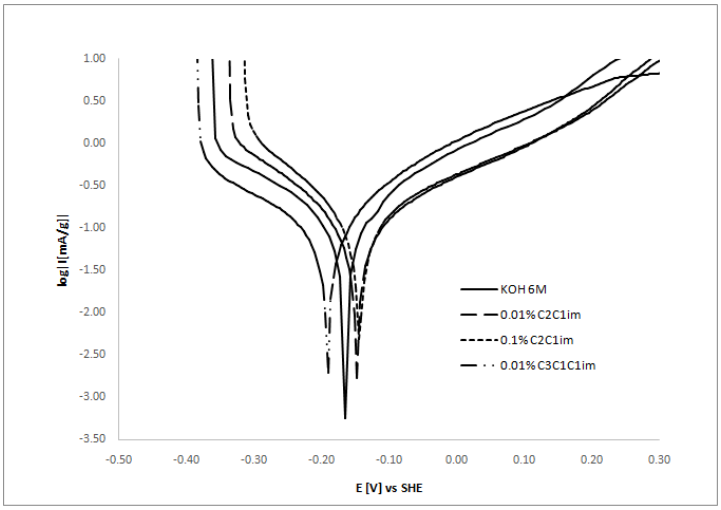

Figure 1. *Curves of cyclic potentiodynamic polarisation obtained for AB_5 hydrogen-absorbing alloy ($LaMmNi_{4.1}Al_{0.3}Mn_{0.4}Co_{0.45}$) in various types of electrolytes.*

TABLE II. *Charge and discharge process parameters for AB_5 hydrogen-absorbing alloy ($LaMmNi_{4.1}Al_{0.3}Mn_{0.4}Co_{0.45}$) in various types of electrolytes.*

Electrolyte	Discharging time [s]	Specific capacity [mAh/g]
6 M KOH	16490	206.12
0.01% C_2C_1im 6M KOH	12700	158.75
0.1% C_2C_1im 6M KOH	8700	108.69
0.01% $C_3C_1C_1$im 6M KOH	13290	166.13
6M KOH (Pd-modified)	18745	234.31
0.01% C2C1im 6M KOH (Pd-modified)	17680	221.00

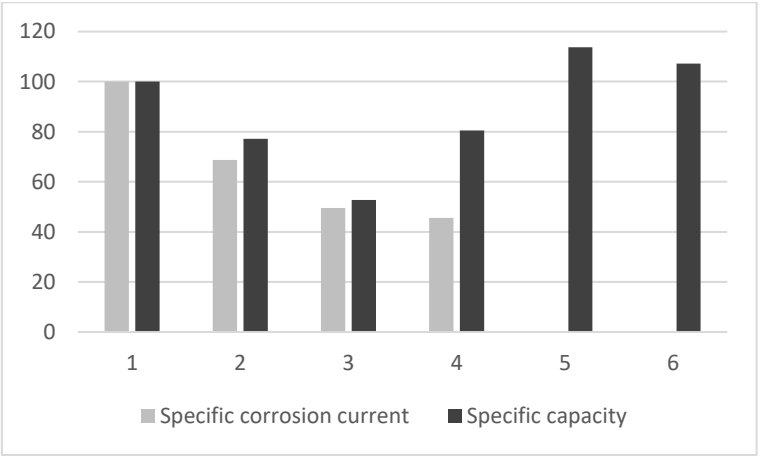

Figure 2. *Comparison between specific corrosion current and specific capacity of studied samples: 1 – 6M KOH, 2 – 0.01% C_2C_1im 6M KOH, 3 – 0.1% C_2C_1im 6M KOH, 4 – 0.01% $C_3C_1C_1$im 6M KOH, 5 - Pd-modified electrode in 6M KOH and 6 – Pd-modified electrode in 0.01% C_2C_1im 6M KOH*

Acknowledgements

This work was supported by the National Science Centre, Poland, grant number 2021/41/B/ST5/04047, and by the Polish Ministry of Science and Higher Education.

References

1. K. Young, S. Yasuoka, *Batteries*, **2**, 3 (2016)
2. M. Zunita, Y. J. Kevin, *Results in Engineering*, **15**, 100562 (2022)
3. T. Meng., K. Young., D. F. Wong, J. Nei, *Batteries*, **3**, 4 (2017)

Suspension electrolyte for zinc metal dual-ion batteries

Yitao He, Jiří Červenka

Department of Thin Films and Nanostructures, FZU – Institute of Physics of the Czech Academy of Sciences, Cukrovarnická 10/112, 162 00 Prague 6, Czech Republic

Yitao He: yitao@fzu.cz

Dual-ion batteries (DIBs) have garnered significant interest due to their cost-effectiveness, high operating voltage, and eco-friendly nature. The electrolyte, serving as the provider of active ions during the charge/discharge cycles, is pivotal to the performance metrics of DIBs, such as capacity, energy density, and lifespan. Despite this, the high-concentration electrolytes that rely heavily on main salts often compromise the cost-effectiveness of DIBs. Therefore, a solvated main salt particle suspension electrolyte (SPSE) system has been successfully developed based on a linear carbonate solvent with a trace amount of water. This innovative SPSE offers improved anion utilization efficiency at the electrode surface and ensures a sufficient anion supply even at relatively low concentrations. A prototype DIB utilizing this SPSE has demonstrated a remarkable discharge capacity of 178.66 mAh g^{-1} at a current rate of 10 mA g^{-1}, and an impressive 84.7% capacity retention after 240 cycles at 100 mA g^{-1}. When considering the cathode, the energy density of this DIB soars to 304.8 Wh kg^{-1}. This groundbreaking SPSE holds the potential to significantly lower the commercialization barriers and production costs associated with DIBs.

Temperature Changes in a Lead-Acid Battery During Cycling

Petr Křivík

[a] Department of Electrotechnology, Brno University of Technology, Faculty of Electrical Engineering and Communication, 616 00 Brno, Czech Republic

The paper deals with the study of temperature changes inside the battery during discharging and charging at different ambient temperatures. For this reason, 2 temperature sensors were placed in the battery and the temperature changes inside the battery during cycling were measured. It was found that, in addition to the discharge and charge current, the temperature changes are influenced by the ambient temperature.

Introduction

Thermal changes in a lead-acid battery during discharge and charge are influenced by the design of the cell, its age and by the method of cycling. They have an effect on the use properties of the electrode systems and affect both the capacity and the life of the cells of the lead-acid battery. The issue of thermal changes in a lead-acid battery cell has been addressed by several authors, often with different results [1-4]. To correctly determine the thermal changes of a lead-acid battery cell, it is necessary to take into account all the contributions of individual types of heat. These are heat generated due to electrochemical reactions, heat generated due to ohmic and polarization losses (Joule heat) and heat lost through contact with the environment.

The heat generated due to the electrochemical reaction is calculated according to the formula:

$$\boldsymbol{Q_R = -\frac{T\Delta S}{nF} It = -U_R It} \tag{1}$$

where T is the temperature (298.15 K), ΔS the entropy change of the electrochemical reaction with the unit [$Jmol^{-1}K^{-1}$], n is the number of electrons exchanged during the reaction (for the discharge reaction of a lead-acid battery cell n = 2), F is the Faraday constant (96485 $Asmol^{-1}$), I is the electric current [A], t is the discharge time [s] and U_R is the reversible reaction voltage [V]. For a lead-acid battery, the reversible voltage of the discharge reaction is

$$U_R = \frac{T\Delta S}{nF} = 0.057 \text{ V} \tag{2}$$

For a charging reaction, this value is negative. From equations 1 and 2, it can be seen that the discharge reaction is endothermic and contributes to cooling, and the charging reaction is exothermic and contributes to the heating of the accumulator. Joule heat is proportional to the change in voltage caused by the current flowing according to the equation:

$$Q_J = \Delta U I t = (U - U^0) I t \tag{3}$$

where U is the actual voltage and U^0 is the voltage during current off state. ΔU includes the change in voltage caused by the current flowing through the internal ohmic resistance of the

electrodes and the electrolyte, as well as the overvoltage on the electrodes. When discharging, the Joule heat can be calculated from the relation:

Experiment

A maintenance-free 12 V ZAP Plus Calcium 74 Ah battery with dimensions of 275 x 175 x 190 mm was used to investigate the temperature changes inside the lead-acid battery during cycling. 2 Pt 100 temperature sensors were placed in the vertical plane passing through the center of the battery. The 1st sensor was placed between the outer edge of the plate and the side wall in the area of the 1st cell in the center of the plate. The 2nd sensor was placed between the plate and the plastic partition in the area of the 2nd cell closer to the center of the accumulator also in the center of the plate. An experiment was carried out with the battery in a charged state, with measurement of the temperature changes during discharge with 10 A to a voltage limitation of 10.5 V (1.75 V per cell) and during charging with 10 A with a voltage limitation of 14.4 V, (2.4 V per cell), terminated at 1 A at an ambient temperature of 19 °C (Fig. 1).

During discharge of the lead-acid battery at an ambient temperature of 19 °C, the temperature inside the battery increased by about 1.5 °C on both sensors in 3.2 hours due to Joule heat. During charging, the temperature rises significantly by 6 °C in 3 hours, after which the charging current decreases due to reaching the voltage limitation. At the same time, the temperature inside the accumulator rises longer than at the edge at the contact with the side wall. At the beginning of charging, the internal resistance has its share in the heating, in the further course, the polarization resistance also starts to contribute to heating, and at the end of the charging, there is a small contribution of heating due to the electrolysis of water. However, it is limited by voltage limitation. The heat of the charging reaction, which is exothermic, can be added to these heats. As the current decreases in the further course of charging, the temperature drops due to cooling from the surroundings, this cooling occurs later inside the accumulator. It can be seen that the battery heats up more during charging than when discharging, which corresponds to theoretical assumptions. During subsequent discharge, the battery temperature continues to drop. The temperature drop of 4°C takes about 8 hours and starts during charging after reaching the voltage limitation and ends before the end of discharging. The cooling from the surroundings is higher than the Joule heat caused by the internal resistance of the battery. An endothermic discharge reaction also contributes to cooling. The temperature rises again only at the end of the discharge, where the internal resistance increases more significantly. During subsequent charging, the temperature continues to rise again until the voltage limitation is reached, which causes a gradual decrease in the charging current.

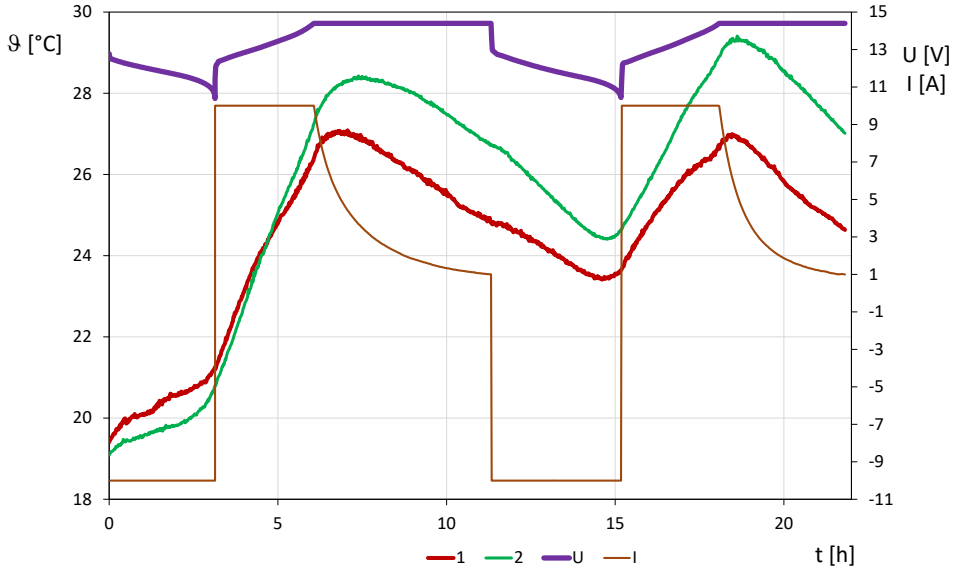

Figure 1. *Temperature dependence of 2 measured points in a lead-acid battery during discharge and charge at a temperature of 19 °C.*

Conclusion

From the dependences of the temperatures inside the battery and at the contact with the side wall during discharge and charging of the lead battery at an ambient temperature of 19 °C and at -37 °C, a significant change in temperature curves can be seen. Low temperature significantly affects the internal resistance and capacity, and the different thermal conductivity of the materials inside the battery and at the contact with the side wall also affect temperature changes. During discharge, the internal resistance of the battery and the endothermic discharge reaction affect temperature changes. Polarization resistance, electrolysis of water and exothermic charging reaction also affect temperature changes during charging. Discharging and charging current and the setting of the voltage limitation during charging affect temperature changes too.

Acknowledgments

This work was supported by the specific research of the BUT FEKT-S-23-8286.

References

1. H. A. Kiehne, Battery Technology Handbook, second edition, 2003
2. D. Valkovska, M. Dimitrov, T. Todorov, D. Pavlov, Thermal behavior of VRLA battery during closed oxygen cycle operation, Journal of Power Sources 191 (2009), 119–126
3. H. Frank Gibbard, Thermal Properties of Battery Systems, Journal of the Electrochemical Society, Volume 125, Issue 3, (1978) 353–358
4. D. A. J. Rand, R. Woods, R. M. Dell, Batteries for electric vehicles, 1998

Aerosol-based processes to produce battery materials

J.R. Buchheim[a], F. Beutler[b]

[a] Glatt Ingenieurtechnik GmbH, Department New Technologies and Business Development, Weimar 99423, Germany

[b] Glatt Ingenieurtechnik GmbH, Department Sales Pharma & FFF, Weimar 99423, Germany

With the introduction of the Sony lithium battery in 1990, the development of active materials has undergone a continuous process with the aim of increasing energy density. This is being realised through the development of new, nickel-rich and cobalt-free cathode materials, the production of silicon-carbon composite materials and the development of solid-state batteries.

The increasing demand for applications within electromobility or stationary energy storage requires the implementation of innovative, sustainable and continuous manufacturing processes as well as processes for coating active materials. Aerosol-based methods based on spray drying/spray calcination and spray granulation are presented using selected examples. Initial results on electrochemical characterization will be presented.

Materials and methods

Preparation of cathode active materials

The development of new cathode materials based on the layered oxide $LiCoO_2$ led to lithium-nickel-manganese oxides NMC and lithium-nickel-aluminium oxides NCA, among others, by substituting cobalt with other elements. In addition to these materials, which are mainly used for electromobility, there are also oxides of the olivine structure, e.g., lithium iron phosphate $LiFePO_4$, and materials of the spinel structure $LiMn_{2-x}Ni_xO_4$. The production of these active materials involves a variety of methods, some of which require several process steps. These include precipitation and solid-state reactions, hydrothermal processes and sol-gel processes. By using aerosol-based spray drying and spray calcination processes, the process steps can be reduced, and continuous production can be realised.

Preparation of anodic active materials

Graphite is a common anode material. The theoretical capacity of this material is limited to a theoretical capacity of 372 mAh/g due to the formation of the compound LiC_6. The drive towards higher energy densities has led to a focus on other elements. Silicon offers an alternative solution due to its good availability and a much higher theoretical capacity of 3600 mAh/g. A volume change of 320% during the charging and discharging cycle leads to particle breakage, loss of contact with the current arrester and continuous erosion of the protective boundary layer between the silicon and the electrolyte. The production of silicon-carbon composite materials offers a promising approach to compensate for the

volume change. Production can be carried out using continuously guided aerosol-based processes based on spray drying and spray granulation.

Production of solid electrolytes

Another method of increasing energy density is the development of solid-state batteries in which the liquid electrolyte is replaced by a lithium-conducting material, for example lithium lanthanum zirconium oxide LLZO. This allows metallic lithium to be used as the anode material (theoretical capacity of 3860 mAh/g). The challenge here lies in the synthesis of the solid electrolyte. The reaction time can be shortened by producing it using aerosol-based processes.

Coating of cathode materials

Another representative of solid-state electrolytes is lithium phosphorus sulphide LPS. The material is characterised by a high ionic conductivity. However, the material is chemically less stable against oxidic cathode materials, so that a coating of the active materials is necessary. Lithium phosphate Li_3PO_4, lithium niobate $LiNbO_3$, lithium borate $Li_xB_yO_z$ and lithium titanium oxide LTO are being discussed. Processes based on spray drying and spray calcination can also be used for this in order to realise continuous processing.

Novel lithiated high-entropy spinel type oxychloride and oxyfluoride and its electrochemical performance in Li-ion batteries

M. Zukalová[1], O. Porodko[2], M. Fabián[2], B. Pitňa Lásková[1], and L. Kavan[1]

[1]J. Heyrovský Institute of Physical Chemistry, v.v.i., CAS, Dolejškova 3, Prague 8, Czech Republic

[2] Institute of Geotechnics, Slovak Academy of Sciences, Watsonova 45, 040 01, Košice, Slovak Republic

The high entropy oxide $(Zn_{0.25}Mg_{0.25}Co_{0.25}Cu_{0.25})Fe_2O_4$ (HEOFe), lithiated oxyfluoride $Li_{0.5}(Zn_{0.25}Mg_{0.25}Co_{0.25}Cu_{0.25})_{0.5}Fe_2O_{3.5}F_{0.5}$ (LiHEOFeF), and lithiated oxychloride $Li_{0.5}(Zn_{0.25}Mg_{0.25}Co_{0.25}Cu_{0.25})_{0.5}Fe_2O_{3.5}Cl_{0.5}$ (LiHEOFeCl) with spinel-based cubic structure is prepared by combination of ball milling and temperature treatment(1). The products exhibit particle size from 50 to 200 nm and homogeneous distribution of particular elements in the structure. Electrochemical measurements carried out in the 2032 coin cell with Li-metal anode have shown excellent results. The charge capacities calculated from the oxidation branch of the cyclic voltammogram were 450, 694, and 593 mAh g^{-1} for HEOFe, LiHEOFeCl, and LiHEOFeF, respectively. The best electrochemical performance of LiHEOFeCl was ascribed to its smallest particle size. Galvanostatic chronopotentiometry at 1 C confirmed high initial charge capacities for all the samples but galvanostatic curves exhibited a capacity decay over 100 charging/discharging cycles. Raman spectroelectrochemistry measured on the LiHEOFeF sample proved the reversibility of the electrochemical process for initial charging/discharging cycles. Electrochemical impedance spectroscopy shows the lowest initial charge transfer resistance for LiHEOFeCl and its gradual decrease both for LiHEOFeCl and LiHEOFeF during galvanostatic cycling, whereas the charge transfer resistance of HEOFe slightly increases over 100 galvanostatic cycles due to different mechanism of the electrochemical reduction.

Acknowledgment

This work was supported by the project "The Energy Conversion and Storage", funded as project No. CZ.02.01.01/00/22_008/0004617 by Programme Johannes Amos Comenius, call Excellent Research.

References

1. O. Porodko, L. Kavan, M. Fabian, B. Pitna Laskova, V. Šepelák, H. Kolev, K. Lucenildo da Silva, V. Girman, M. Lisnichuk and M. Zukalova, *Nanoscale*, **submitted** (2024).

Preparation and analysis of biological derived carbon for lithium-sulfur batteries

P. Čudek[a], K. Jaššo[a,b]

[a] Department of Electrical and Electronic Technology, Brno University of Technology, Technická 10, 616 00 Brno, Czech Republic

[b] Department of Electrical Engineering, Faculty of Military Technology, University of Defence, Kounicova 65, 662 10 Brno, Czech Republic

Porous carbons derived from carbon-rich feedstock precursors are being extensively used in various applications including batteries. The unique hierarchical architecture and functional heteroatoms of these porous carbons have the potential to effectively address the main challenges of lithium-sulfur batteries, such as poor conductivity and dissolution of long-chain polysulfides. This paper specifically focuses on the production of porous carbon from coffee grounds through the process of hydrothermal carbonization. The resulting carbon has a high purity with a low sulfur content.

Introduction

Lithium-sulfur (Li-S) batteries have the potential to replace Li-Ion batteries in some areas due to their high theoretical energy density. The development of high energy Li-S batteries using biowaste derived materials will increase the sustainability of energy storage devices. Porous carbon with hierarchical architecture and functional heteroatoms can effectively penetrate the sulfur cathode and overcome the main problems of Li-S batteries, namely poor conductivity of the sulfur cathode and dissolution of long-chain polysulfides. The Li-S cell with porous carbon provides a high initial discharge capacity with a low rate of capacity loss. The strong carbon structure can accommodate the volume changes during the sulfur conversion reaction and the unoccupied pores in the porous carbon can act as a reservoir of polysulfide, which effectively captures the migration of polysulfide and achieves high stability. The highly interconnected hierarchical pores further facilitate faster electronic and ion transport to achieve high-rate performance, higher than that of the cathode with pristine sulfur. These results show the potential for the development of high-performance energy storage devices using ecological and renewable materials. (1)

Due to the diverse surface morphology, porous carbon materials are suitable for use not only in lithium-sulfur batteries, but also in electrode materials for supercapacitors or in adsorbents for hydrogen storages. (2, 3) For this reason, great efforts have been made to prepare various porous carbon materials derived from different biological materials. (4)

Carbon can be easily obtained from biological materials. The deciding factor for the selection of biowaste material was its primary particle size, easy availability and elemental composition, with any elements other than carbon being undesirable. One of these materials appears to be coffee grounds. Coffee contains predominantly organic compounds composed of hydrogen carbon oxygen and a minimum of nitrogen. The content of other elements is trace. (4) In addition, most of the organic acids and hydrocarbons are released during the preparation of the coffee. Also, coffee

grounds have a particle size of tens of microns, which is why coffee grounds were chosen for the experiments.

This article describes the method of obtaining carbon from coffee grounds by hydrothermal carbonization and monitoring the content of unwanted elements by energy dispersive spectroscopy methods. The disadvantage of hydrothermal carbonization is that sulfur remains in the resulting substance. However, if the sulfur content can be reduced to a minimum, this may not be a problem given the intended use in Li-S batteries.

Experiments

Coffee grounds from espresso was used as the basis to produce organic carbon. After each step in the carbon preparation, surface observation by scanning electron microscopy (SEM) and elemental microanalysis by energy dispersive spectroscopy (EDS) were performed at accelerating voltages of 5 kV and 20 kV.

An accelerating voltage of 5 kV was used due to better spectral resolution in the light element region. The disadvantage in this case is that the x-rays are only produced from the layer up to about 300 nm in the case of carbon element and even less in the case of elements with higher density, so the results of the analysis depend more on the composition on the sample surface, whereas when using an accelerating voltage of 20 kV it is up to a depth of about 3.8 microns for the carbon. The different accelerating voltages were used mainly to compare the results, where under optimal conditions the results of both analyses should be similar.

From the EDS results shown in TABLE. I, it can be observed that the original coffee grounds mixture contained mostly carbon and oxygen and around 3.5 wt% of nitrogen.

TABLE I. *Results of elemental microanalysis of coffee grounds fresh from coffee machine.*

Element	Weight concentration % Accelerating voltages 5 kV	Weight concentration % Accelerating voltages 20 kV
Carbon	67.48	69.86
Oxygen	29.71	25.86
Nitrogen	2.71	4.27

This was followed by mixing the coffee grounds with demi-water and, with constant stirring, boiled at a temperature of 100 °C until the mixture was dried.

TABLE II. *Results of elemental microanalysis of boiled and dried coffee grounds*

Element	Weight concentration % Accelerating voltages 5 kV	Weight concentration % Accelerating voltages 20 kV
Carbon	69.00	59.96
Oxygen	28.40	36.03
Nitrogen	2.61	4.01

In comparing the results in TABLE I. and TABLE II., there were no significant changes in the elemental representation when using an accelerating voltage of 5 kV. While when using an accelerating voltage of 20 kV, which allows the detection of elements from a greater depth, an increase in the percentage of oxygen of about 10% can be observed at the expense of the representation of carbon. This large decrease in detected carbon could be due to evaporation of the

remaining aromatic hydrocarbons left in the coffee grounds after the initial brewing of the espresso. The percentage of nitrogen remained almost unchanged.

TABLE III. *Results of elemental microanalysis after hydrothermal carbonization.*

Element	Weight concentration % Accelerating voltages 5 kV	Weight concentration % Accelerating voltages 20 kV
Carbon	39.97	47.87
Oxygen	28.36	31.44
Sulfur	31.67	20.69

Next the dried coffee grounds were subjected to hydrothermal carbonization (HC). 20 grams of coffee were drenched in 50 ml of 30 % H_2SO_4 and heated at 180 °C for 18h. After HC, elemental analysis was again carried out, the results of which are presented in TABLE III. showing up to 30% increase in sulfur on the surface of the mixture, or 20% sulfur in its volume.

TABLE IV. *Results of elemental microanalysis after the first filtration.*

Element	Weight concentration % Accelerating voltages 5 kV	Weight concentration % Accelerating voltages 20 kV
Carbon	77.84	73.13
Oxygen	20.01	20.36
Sulfur	2.15	6.51

The resulting mixture from HC was then filtered with one litter of deionized water and the EDS was performed again. The results in TABLE IV showed a significant decrease in the sulfur content, mainly on the surface of the mixture, after the first filtration, from the original 30% to 2%. The sulfur content of the mixture was 6%.

TABLE V. *Results of elemental microanalysis after final filtration.*

Element	Weight concentration % Accelerating voltages 5 kV	Weight concentration % Accelerating voltages 20 kV
Carbon	81.64	75.07
Oxygen	17.37	21.15
Sulfur	0.99	3.78

Subsequently, repeated filtering of the mixture with deionized water was performed until the pH of the resulting liquid was neutral. A total of 3 litters of deionized water was used. As can be seen from TABLE V, the sulfur content in the mixture decreased again to less than 4%. Due to the resulting neutral pH, it can be assumed that further washing would not reduce the sulfur content.

Conclusion

The measured data indicate that coffee grounds could be a promising precursor for producing porous carbon for use in Li-S batteries. So far, the coffee grounds have undergone hydrothermal carbonization and subsequent washing. Based on EDS analyses, it is evident that hydrothermal carbonization has eliminated nitrogen, but it has resulted in sulfur contamination of the carbon. Despite intensive washing with deionized water, the sulfur contamination could not be completely removed. However, this may not pose a problem considering the intended use of the porous carbon in the production of Li-S batteries. In future research, the carbon prepared in this manner will

undergo KOH activation, as well as conductivity and porosity analyses, before being used in production of positive electrodes for Li-S batteries.

Acknowledgments

This work was supported by the specific graduate research of the Brno University of Technology No. FEKT-S-23-8286 and by the institutional support of the Ministry of Defence of the Czech Republic.

References

1. A. Sandeep and A.V. Ravindra, *Diamond and Related Materials*, **146**, 111158 (2024)
2. K. Nema and K. Mohanty, R. Thangavel, *Journal of Industrial and Engineering Chemistry*, **121**, 235 (2023).
3. A. Turkyilmaz, K. Isinkaralar, M. Dogan, B. K. Kizilduman and Z. Bicil, *Sustainable Chemistry and Pharmacy*, **40**, 101634 (2024)
4. X. Zhang, G. He, H. Sun, W. Cui, H. Song, J. Li and J.Zheng, *International Journal of Electrochemical Science*, **19**, 100617 (2024)
5. A. Santanatoglia, S. Angeloni, G. Caprioli, L. Fioretti, M. Ricciutelli, S. Vittori and L. Alessandroni, *Food Chemistry*, **454**, 139717 (2024)

Solid-state composite materials for redox-mediated flow batteries

M. Spurný[a], J. Žitka[b], P. Mazúr[a]

[a] Department of Chemical Engineering, University of Chemistry and Technology Prague, 16628 Praha 6, Czechia

[b]Tailormem s.r.o., Zájezd 8, 273 43 Zájezd, Czechia

The aim of this work was to study the possibility of increase energy density of redox flow batteries by so called "capacity boosters" , i.e. solid redox species immobilized in the form of granules that are accessible for the redox mediator dissolved in the electrolyte, thus providing the flow battery additional capacity. The experimental study focused on capacity boosters for both negative and positive electrolyte. The complex optimization study includes the influence of polymeric binder material type and its content within the granules, porosity of the granules and pH of the electrolyte on mechanical stability, solid species retention and capacity utilization of the granules. The most perspective configuration achieved 52% capacity utilization of the booster granules for the combination of ferrocynide-based mediator and Prussian blue booster.

Introduction

The environmental problems associated with the use of fossil fuels in the energy sector are motivating the search for technical solutions that would allow a modern economy to operate without greenhouse gas emissions. One possible solution is the use of renewable sources of electricity, however, they energy production, particularly in case of photovoltaics and wind turbines, strongly depends on the weather or the hour of the day, which causes an unstable supply to the grid. This requires technology capable of storing this electricity efficiently and ensuring its full availability at all times. Redox flow batteries (RFB) are one of the potential candidates for this task.

Capacity boosting

The capacity of the RFB is determined by the volume of electrolytes stored and the maximum possible concentration of active substances dissolved in them. A promising way to circumvent the concentration limit is to use a redox active immobilized in the solid phase (so-called capacity booster) that is in contact with the electrolyte. The electrolyte thus acts as a redox mediator between the immobilized active and the electrode, thus ensuring its charge/discharge while itself storing capacity [1]. To maximize the capacity of the booster, the method of its immobilization in the form of mechanically stable granules needs to be optimized using a suitable binder. A schematic of the RFB and RFB with capacity booster is shown in Figure 1.

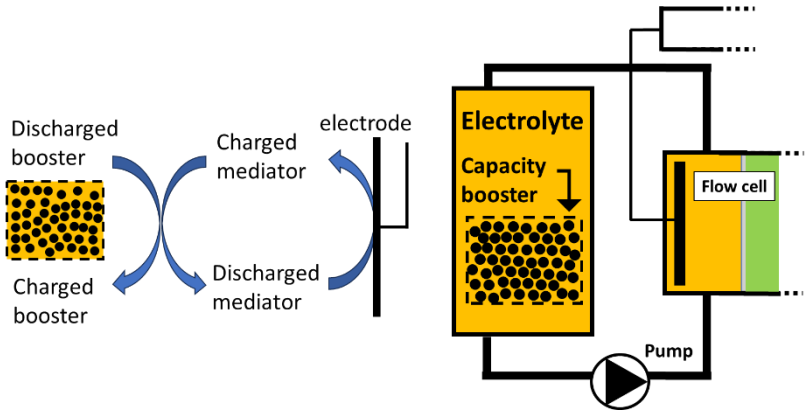

Figure 1. *Principle of redox flow battery with capacity booster*

Experimental part

The preparation of booster granules consisted of mixing the active species (anthraquinone 2,6-disulfonic acid sodium salt on negative side (2,6-AQDS-Na_2) and Prussian blue (PB) on positive side) with the binder and conductive additive. In some cases, porogenic additive was also added. A solubilizing agent was then added to produce paste-like material, which was extruded into a form of granules, which were left to dry overnight. All granules consisted of 67% (wt.) active species. The conductive additive, binder and porogenic additive were used in various contents from 10% to 22%. The tests were performed with a laboratory flow electrochemical cell (PinFlow Energy Storage, s.r.o.) in three-electrode setup. Both electrolytes contained soluble active species in 0.1M concentration. The negative side utilized soluble 2,7-sulfonated isomer of AQDS and was cycled between –1.2 V and –0.7 V vs. MSE reference electrode. The positive side utilized potassium ferrocyanide and was cycled between –0.45 V and 0.0 V vs. MSE. The test sequence started with a blank cell test with pristine electrolyte. Subsequently, the booster granules were added to the system and the cycling procedure was repeated. From the capacity difference of the two tests, the capacity utilization of the booster granules was obtained.

Results and discussion

The tests of negative electrolyte capacity boosters based on anthraquinone disulfonic acid sodium salt (2,6-AQDS-Na_2) revealed strong influence of used binder and its content on the mechanical stability, capacity utilization and retention of the active species inside the granules. It was found that the low density polyethylene, Nafion® and polyvinylidene fluoride binders at suitable amount provide mechanically stable granules, but with the exception of Nafion®, they suffered from active species wash-out and poor capacity utilization. This problem could be reduced by further research of the granule porogenic additives and binder materials.

The tests of positive capacity booster granules containing PB active material showed a significant effect of K^+ concentration and pH of the electrolyte on the capacity utilization of the booster. Increased concentrations of K^+, which intercalate into PB crystal structure within booster discharge reaction, resulted in enhanced booster utilization. It was also found that the granules using anion-exchange functionalized polystyrene-based polymer (PSEBS), kindly provided by Tailormem, s.r.o., showed significantly higher capacity utilization of 52% when compared to the polyethylene-acrylic acid co-polymer (PEcoAA) binder (12% capacity utilization). It was found that lower current densities and increased rest time after charging and discharging process also enhanced the utilization

of the capacity of the PB-based booster, which indicate on mass transfer limitations within the booster granules.

Acknowledgments

This publication was supported by the project "The Energy Conversion and Storage", funded as project No. CZ.02.01.01/00/22_008/0004617 by Programme Johannes Amos Comenius, call Excellent Research.

References

S. Gentil, D. Reynard and H. H. Girault, *Current Opinion in Electrochemistry*, **21**, 7 (2020).

Use of Raman spectroscopy to examine the suitability of carbonaceous materials for Li-ion vs. Na-ion anodes

A. Šimek[a], T. Kazda[a] and O. Čech[a]

[a] Department of Electrical and Electronic Technology, Brno University of Technology, Brno 616 00, Czech Republic

Carbon materials, including graphite and hard carbon, are essential components of Li-ion and Na-ion batteries due to their excellent electrical conductivity and structural stability. Raman spectroscopy can be used to determine the suitability of these materials for battery applications, providing a detailed view of the structural and compositional properties of the investigated materials. These spectroscopic analyses are then verified by electrochemical measurements such as cyclic voltammetry and galvanostatic cycling with potential limitation. This approach is essential for advancing the development of anode materials and quickly determining whether a given material is more suitable for use in Li-ion or Na-ion battery technology.

Introduction

Carbon materials such as graphite and hard carbon play a key role in the development of anode materials for Li-ion and Na-ion batteries due to their excellent electrical conductivity, structural stability and high ion storage capacity [1]. In Li-ion batteries, graphite is the preferred anode material, reaching a theoretical capacity of 372 $mAh.g^{-1}$ for LiC_6. Graphite also has a stable interface between the electrode and electrolyte due to the suitable formation of solid electrolyte interphase (SEI). Graphite is of the intercalation type, which allows it to accommodate lithium ions and provide high energy density and long cycle life [2]. For Na-ion batteries, where the performance of graphite is limited by the larger size of sodium ions, hard and soft carbon have emerged as promising alternatives. Hard carbon offers a disordered structure that can more efficiently accommodate sodium ions, thereby increasing capacity and cycle stability [3, 4]. Raman spectroscopy can be used to reveal whether a given material has an ordered (graphitized) structure or a disordered structure, thus providing an early indication of the suitability of a given material for Li-ion or Na-ion batteries.

Experiment

Four samples of carbonaceous materials (marked sample 1-4) of unknown structure were investigated in the experiment. The materials were first ground in a Fritsch Pulverissete 7 planetary ball mill to ensure small particle sizes (below X um). Subsequently, Raman spectroscopy was performed using a Witec Alpha 300R instrument using a green laser at a wavelength of 532 nm. The measured Raman spectra are shown in Figure 1. The materials were then used as the active material in the electrode material, which was composed of 80% carbonaceous material, 10% PVDF binder and 10% SuperP conductive additive. The electrode material was then deposited at a thickness of 200 um on a copper current collector (Li-ion and Na-ion applications are possible), dried, crimped to 30 kN and 18 mm diameter electrodes were die-cut. The electrodes were then assembled in a Jacomex glove box into electrochemical test cells using lithium metal (sodium) as

the counter electrode, a Whatman GF/C glass separator filled with electrolyte (1.5M $LiPF_6$ DMC/EC 2/1 for Li-ion and 1M $NaClO_4$ EC/PC 1/1 for Na-ion), and prepared negative electrodes as working electrode. Thus, a total of 8 test cells were prepared.

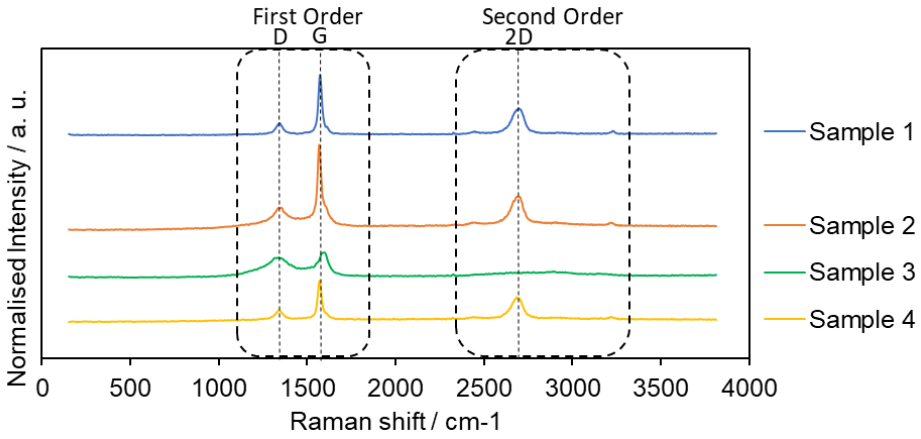

Figure 1. *Measured Raman spectra of the four investigated carbonaceous materials.*

Two main regions corresponding to first- and second-order Raman scattering are visible in the measured Raman spectra. There are then two main peaks in the first-order Raman scattering, the first at a Raman shift of approximately 1350 cm^{-1} is referred to as the D-band and corresponds to the degree of disorder in the material. The second peak at a Raman shift of approximately 1570 cm^{-1} is referred to as the G-band and corresponds to the degree of graphitization, i.e., the orderliness of the material [5]. Comparing these peaks, it is then possible to determine that samples 1, 2 and 4 have a high degree of graphitization compared to disorder, hence their structure is more ordered and closer to graphite. In contrast, sample 3 has a very low intensity of both peaks and the peaks are similarly large, indicating a disordered structure approaching hard carbon.

Figure 2a shows the cyclic voltammetry results of the prepared electrodes measured in Li-ion system, and Figure 2b shows the cyclic voltammetry results of the prepared electrodes measured in Na-ion system. Table 1 then summarizes the initial discharge capacity of the prepared electrodes against lithium and sodium.

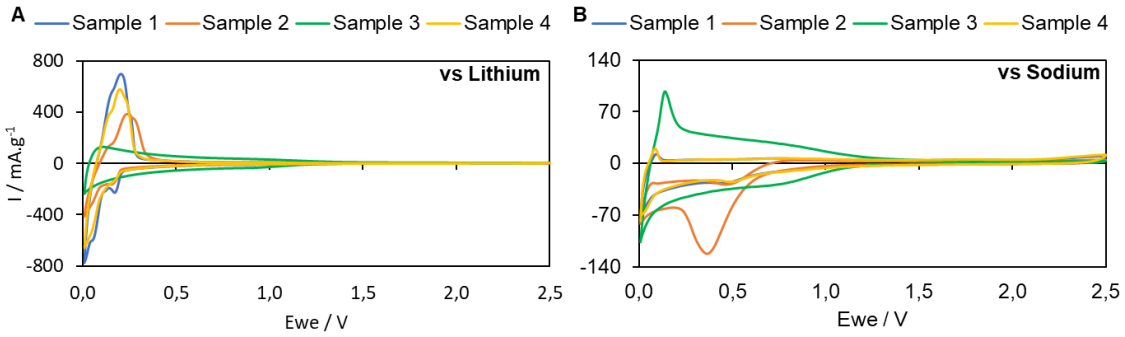

Figure 2. *Measured cyclic voltammetry of the prepared electrodes: A) vs. lithium; B) vs. sodium.*

TABLE I. *Initial discharge capacities of four different carbon samples*

.

Sample	Capacity in Li-ion / mAh.g^{-1}	Capacity in Na-ion / mAh.g^{-1}
Sample 1	356,43	43,26
Sample 2	317,63	-
Sample 3	237,54	147,47
Sample 4	300,43	49,42

Conclusion

The suitability of carbonaceous materials for Li-ion and Na-ion anode materials was verified by electrochemical measurements based on measured spectra from Raman spectroscopy. Samples 1, 2 and 4 possessing a large graphitic peak (G-band) indeed work very well in Li-ion, whereas in Na-ion they have very weak electrochemical activity leading to a small capacity of less than 50 mAh.g^{-1}. Moreover, sample 1 then reaches a capacity of 356.43 mAh.g^{-1}, which is very close to the theoretical capacity of graphite. This sample will therefore be the most ordered of all and its structure is close to that of ideal graphite. In contrast, in sample 3, which according to Raman spectroscopy reaches a high degree of disorder, significantly more electrochemical activity in the Na-ion system can be observed, together with a higher capacity of 147.47 mAh.g^{-1}. These results suggest that this is most likely the type of hard carbon that will be suitable for Na-ion battery anodes. In conclusion, we can say that with the use of Raman spectroscopy, it is easy and quick to determine whether a given carbonaceous material is suitable for a Li-ion or Na-ion battery system.

Acknowledgments

This work was supported by the specific graduate research of the Brno University of Technology No. FEKT-S-23-8286. CzechNanoLab project LM2023051 funded by MEYS CR is gratefully acknowledged for the financial support of the measurements at CEITEC Nano Research Infrastructure.

References

1. P. U. Nzereogu, A. D. Omah, F. I. Ezema, E. I. Iwuoha, and A. C. Nwanya, *Applied Surface Science Advances*, vol. 9, (2022).
2. M. H. Hossain, M. A. Chowdhury, N. Hossain, M. A. Islam, M. H. Mobarak, M. Hasan, and J. Khan, *Chemical Engineering Journal Advances*, vol. 17, (2024).
3. W. Luo, F. Shen, C. Bommier, H. Zhu, X. Ji, and L. Hu, *Accounts of Chemical Research*, vol. 49, no. 2, pp. 231-240, (2016).
4. H. Kang, Y. Liu, K. Cao, Y. Zhao, L. Jiao, Y. Wang, and H. Yuan, *Journal of Materials Chemistry A*, vol. 3, no. 35, pp. 17899-17913, (2015).
5. K. Li, Q. Liu, H. Cheng, M. Hu, and S. Zhang, Spectrochimica Acta Part A: Molecular and Biomolecular Spectroscopy, vol. 249, (2021).

Silicon/Graphite Composite as Lithiophilic Lithium Metal Anode

M. Tahertalari[a], SA Ahad[a], D. Capkova[a], H. Geaney[a] and D. Thompson[b]

[a] Department of Chemical Sciences, Faculty of Science and Engineering, University of Limerick, Limerick, Ireland

[b] Department of Physics, Faculty of Science and Engineering, University of Limerick, Limerick, Ireland

Lithium (Li) Metal Batteries (LMBs) are highly promising energy storage systems because of Li's exceptionally high specific capacity (3,860 mAh g^{-1}). However, their practical application is hindered by the low Coulombic efficiency (CE) of Li plating/stripping and safety concerns arising from uncontrolled Li dendrite formation and the presence of dead Li. Here, we proposed lithiophilic Silicon (Si)/graphite (Gr) composite anodes for uniform Li plating/stripping which shows dendrite inhibition and improved CE (>98%) as compared to pristine Li metal when tested against NMC811 cathode in LMBs.

Introduction

Development of energy storage systems such as batteries are of a high importance due to the increasing demand of clean and renewable energy. Lithium-ion batteries (LIBs) are the leading technology due to their energy density and cycle life compared to others (Lithium metal/ion, lead-acid and nickel-metal hybrid, etc). However, LIBs fail to meet the consistently growing need for storage devices with greater gravimetric and volumetric energy densities for long-range electric vehicles, as well as for large energy storage systems for power load-leveling.

Lithium metal anodes (LMAs) as the most promising anodes, with a theoretical capacity of 3860 mAh g^{-1} and the most negative electrochemical potential (−3.04 V vs. standard hydrogen electrode) among the other types of anodes (1). Moreover, due to the light weight of Li, it is considered as a very high energy density material especially when it is paired with Sulfur cathode (Li-S, 2600 Wh kg^{-1}), or when it is used in Li-air batteries (5210 Wh kg^{-1}) (2).

Despite having such advantages, LMAs face some challenges which hinder their practical performance. Safety issues caused by dendrite growth on the surface of the Li anode due to uneven deposition of Li^+ ions during Li plating induced by an unstable solid electrolyte interface (SEI) lead to short circuit of the battery, thermal runaway and even occurring catastrophic fires. Also, the uncontrolled growth of Li dendrites can puncture the inhomogeneous SEI and expose the fresh Li to the electrolyte causing low CE and a high overpotential (3,4).

To address these challenges, several methods have been developed to inhibit the formation of Li dendrites, including the construction of artificial SEI layers, both inorganic and organic (5), separator modification (6), additives of electrolyte (7), solid-state electrolyte (8), current collector modification/host structure (9), and so on. One of the practical approaches to alleviate dendrite is through using porous lithiophilic host structures such as silicon (Si) which has been previously demonstrated as an ideal model anode for Li plating and stripping due to several reasons: 1- Si forms a strong bond with Li and has an appropriate delithiation potential of ~0.3 V. The preferential adsorption of Li-ions onto Si atoms, rather than Li atoms, promotes uniform Li deposition and

reduces the nucleation over-potential for Li plating (9,10). 2- the Li loss during cycling can be accommodated by Si due to its high capacity (>3,000 mAh g^{-1}) leading to a long cycle life and repeated shallow dealloying of Li_xSi (10). Further, adding Gr to the Si anode brings even more benefit owing to the high electron conductivity of Gr (~ 10^3 S m^{-1}) (11) which can act as a conductive support network for Si.

In this work, the performance of Si/Gr composite and bare Gr is evaluated in half cells to achieve CEs by plating/stripping Li on the anode materials and then, the Si/Gr anodes were paired with sulfur and commercial NMC811 cathodes in full-cells.

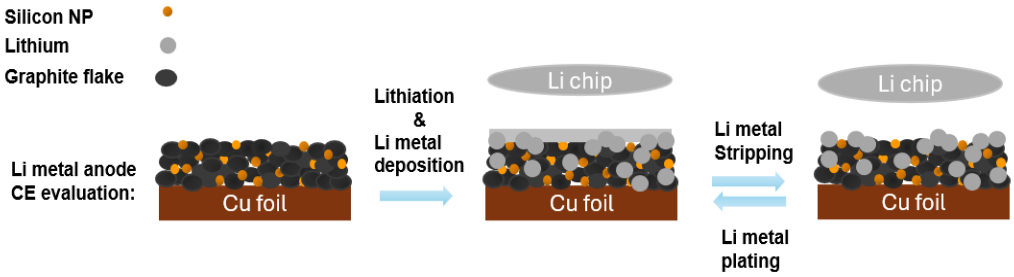

Figure 1. *Schematics of Si/Gr composite anodes and plating/stripping Li on them in a half-cell.*

Experimental

Different percentages of Si/Gr were mixed as active material (80%) of the slurry of the anode along with Carboxymethyl Cellulose (CMC) binder (10%) and Super C65 Conductive Carbon Black (10%). The casted slurry was dried and punched into 12 mm diameter electrodes. PPE Celgard was used as a separator and two different electrolytes according to the type of cathodes were used to assemble full-cells. 1M LiTFSI in DOL:DME (1:1) with 0.25M $LiNO_3$ were used for performing CE tests as well as sulfur full-cells. 1M $LiPF_6$ in EC/DEC with 10% FEC was used in the full-cells with NMC811. Sulfur electrodes were made using 60% sulfur, 10% PEO and 30% carbon Super P.

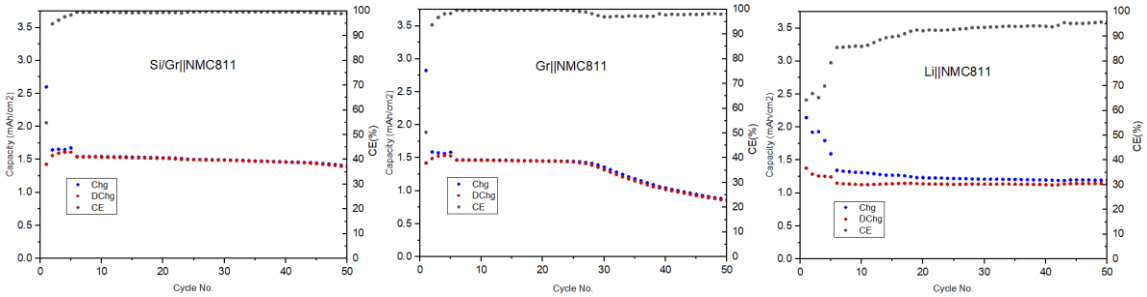

Figure 2. *Galvanostatic cycling of Si/Gr, Gr in a full-cell vs NMC811, as well as half-cell NMC (Li||NMC811) at C-rates of 0.1C for the 1st five cycles and then 0.2C for the remaining cycles.*

Conclusion

In Summary, it is shown that the Si/Gr composite has much better performance in a full-cell than bare Gr and NMC, and this can be attributed to the increased lithiophilicity of Si compared to Gr. The presence of Si eliminates Li dendrite formation and improves the CE and delivered capacity of the cell. The capacity of cells made using Gr showed a capacity fade after only 30 cycles.

Acknowledgments

This Project is sponsored by Department of Chemical Sciences, University of Limerick, No. 57624.

References

1. Li, J., et al., *Strategies to anode protection in lithium metal battery: A review.* InfoMat, 2021. **3**(12): p. 1333-1363.
2. Bruce, P.G., et al., *Li–O2 and Li–S batteries with high energy storage.* Nature materials, 2012. **11**(1): p. 19-29.
3. Sun, Y., et al., *A novel organic "Polyurea" thin film for ultralong‐life lithium‐metal anodes via molecular‐layer deposition.* Advanced Materials, 2019. **31**(4): p. 1806541.
4. Hou, Z., et al., *Lithiophilic Ag nanoparticle layer on Cu current collector toward stable Li metal anode.* ACS applied materials & interfaces, 2019. **11**(8): p. 8148-8154.
5. Kang, D., et al., *Rearrange SEI with artificial organic layer for stable lithium metal anode.* Energy Storage Materials, 2020. **24**: p. 618-625.
6. Natarajan, S., et al., *Regeneration of polyolefin separators from spent Li‐ion battery for second life.* Batteries & Supercaps, 2020. **3**(7): p. 581-586.
7. Shangguan, X., et al., *Additive‐assisted novel dual‐salt electrolyte addresses wide temperature operation of lithium‐metal batteries.* Small, 2019. **15**(16): p. 1900269.
8. Famprikis, T., et al., *Fundamentals of inorganic solid-state electrolytes for batteries.* Nature materials, 2019. **18**(12): p. 1278-1291.
9. Abdul Ahad, S., et al., *Cu Current Collector with Binder‐Free Lithiophilic Nanowire Coating for High Energy Density Lithium Metal Batteries.* Small, 2023. **19**(20): p. 2207902.
10. Chen, L., et al., *High-energy Li metal battery with lithiated host.* Joule, 2019. **3**(3): p. 732-744.
11. Marinho, B., et al., *Electrical conductivity of compacts of graphene, multi-wall carbon nanotubes, carbon black, and graphite powder.* Powder technology, 2012. **221**: p. 351-358.

Enhancing Supercapacitor Performance: Molybdenum Oxide Substrate for Molybdenum Sulfide Electrodes

P. Ondrejka[a], A. Petrík[a], M. Kemény[a], P. Novák[b], M. Sojková[c] and M. Mikolášek[a]

[a] Institute of Electronics and Photonics, Slovak University of Technology, Ilkovičova 3, 812 19 Bratislava, Slovakia

[b] Institute of Nuclear and Physical Engineering, Slovak University of Technology, Ilkovičova 3, 812 19 Bratislava, Slovakia

[c] Institute of Electrical Engineering SAS, Dúbravská cesta 9, 841 04, Bratislava, Slovakia

email: peter.ondrejka@stuba.sk

Supercapacitors are crucial for modern energy storage solutions due to their high power density and longevity. This work explores the use of molybdenum oxide (MoO_3) substrates for molybdenum disulfide (MoS_2) electrodes. MoO_3 offers low serial resistance, a conducive environment for MoS_2 crystal growth, and high surface area, enhancing the overall capacitance of supercapacitors. The results presented in this work indicate that the monoclinic phase of MoO_3, obtained at 500 °C, provides the best performance, with a specific capacitance of 1243.7 F/g and the lowest serial resistance.

Introduction

Supercapacitors have gained significant attention due to their ability to deliver high power densities and life cycles, making them essential for applications requiring quick bursts of energy. Despite these advantages, challenges such as limited energy density and the need for stable and efficient electrode materials remain. Molybdenum disulfide (MoS_2) is promising candidate for supercapacitor electrodes due to their excellent conductivity, mechanical stability, and high surface area (1). However, the choice of substrate material is critical to optimizing their performance. Molybdenum oxide (MoO_3) offers several advantages as a substrate: it has low serial resistance, which is crucial for efficient charge storage and transfer; it facilitates the growth of MoS_2 crystals due to the lower energy required for crystal formation compared to pure molybdenum; and it can be prepared with a high surface area, further enhancing the supercapacitor's overall capacitance (2). This work is focused on optimization of MoO_3 layers to serve as high-surface area substrates for MoS_2-based supercapacitor electrodes.

Experimental set-up

The sample preparation process involved several steps. Initially, the molybdenum foil was cleaned in isopropyl alcohol using an ultrasonic cleaner for 10 minutes. This was followed by a 10-minute cleaning in hydrochloric acid (HCl) and a rinse in water. After cleaning, the molybdenum foil was dried for 10 minutes. Subsequently, the foil was immersed in a 1M potassium hydroxide (KOH) solution for 1 minute. Finally, the molybdenum foil underwent an oxidation process for 1 hour at three different temperatures: 400 °C, 500 °C, and 600 °C. The prepared samples were

characterized using scanning electron microscopy (SEM), X-ray diffractometry (XRD), cyclic voltammetry (CV), galvanostatic charge/discharge (GCD), and electrochemical impedance spectroscopy (EIS). All experiments were conducted on prepared MoO_3 samples using a three-electrode setup. The potentiostat PalmSense 4 was used for all measurements and a voltage window ranged from -1.2 V to 0.5 V. Specific capacitance was calculated from CV and GCD measurements, while serial resistance was determined from EIS data.

Results and discussion

XRD analysis (Fig. 1a) shows prepared electrodes with different phases of MoO_3 by oxidizing the Mo foil at three different temperatures: 400 °C, 500 °C, and 600 °C. The sample prepared at 400 °C showed no sign of MoO_3 and consisted mainly of plain Mo. On the other hand, the sample prepared at 500 °C exhibited the monoclinic phase of MoO_3, while the sample prepared at 600 °C showed the orthorhombic phase. The studies indicated that the monoclinic phase could be more suitable for electrolyte ion intercalation (3), making it better for supercapacitor applications. This was confirmed by our electrochemical measurements (Fig. 2a,b).

SEM images (Fig. 1b,c,d) revealed that higher oxidation temperatures led to larger MoO_3 crystals. This trend suggests that samples prepared at higher temperatures have a higher surface area, which is beneficial for supercapacitor performance.

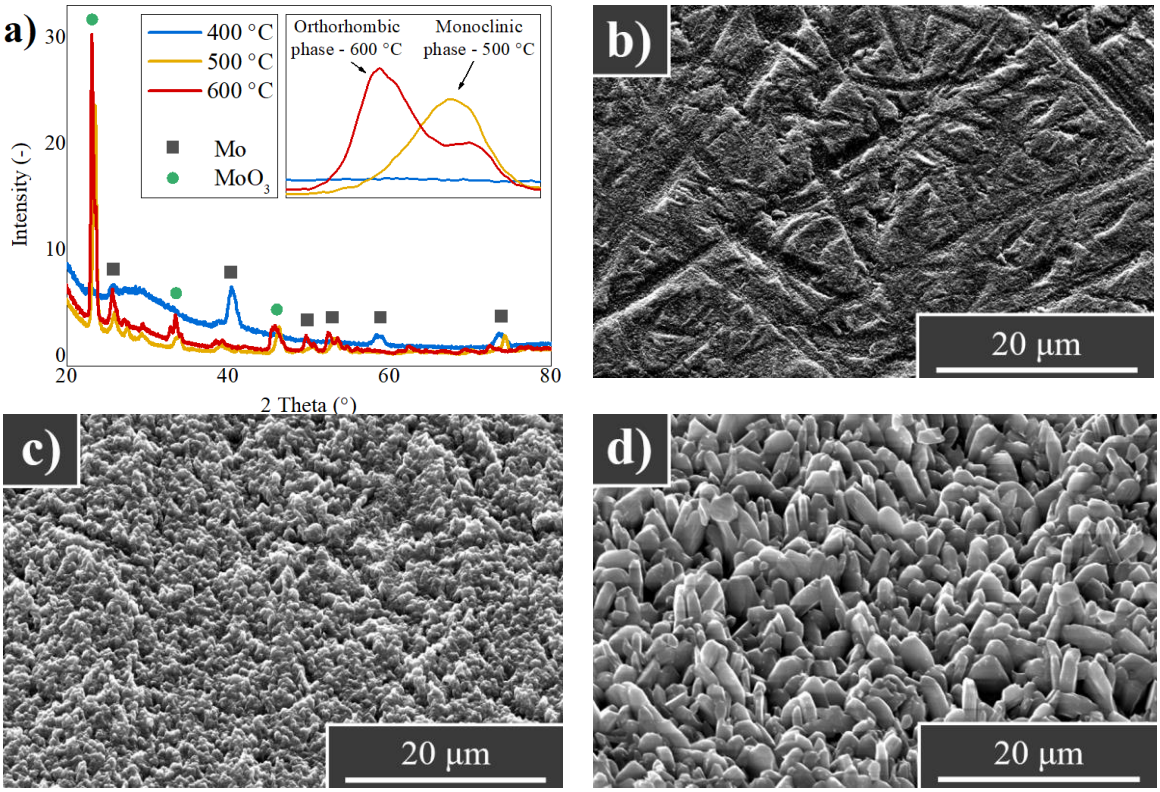

Figure 1. ***a)*** *XRD diffractogram of prepared samples at different oxidation temperatures,* ***b)*** *SEM image of MoO_3 sample prepared at 400 °C,* ***c)*** *SEM image of MoO_3 sample prepared at 500 °C, and* ***d)*** *SEM image of MoO_3 sample prepared at 600 °C.*

Electrochemical analyses, confirmed a pseudocapacitive charge storage mechanism of prepared samples via the presence of oxidation maxima (Fig. 2a). The specific capacitances of the

prepared samples correlated with the XRD results. The highest specific capacitance of 1243.7 F/g was observed for the sample with the monoclinic phase of MoO_3. Additionally, the sample with the highest specific capacitance exhibited the lowest serial resistance, highlighting its potential for use in supercapacitor electrodes (Fig. 2b).

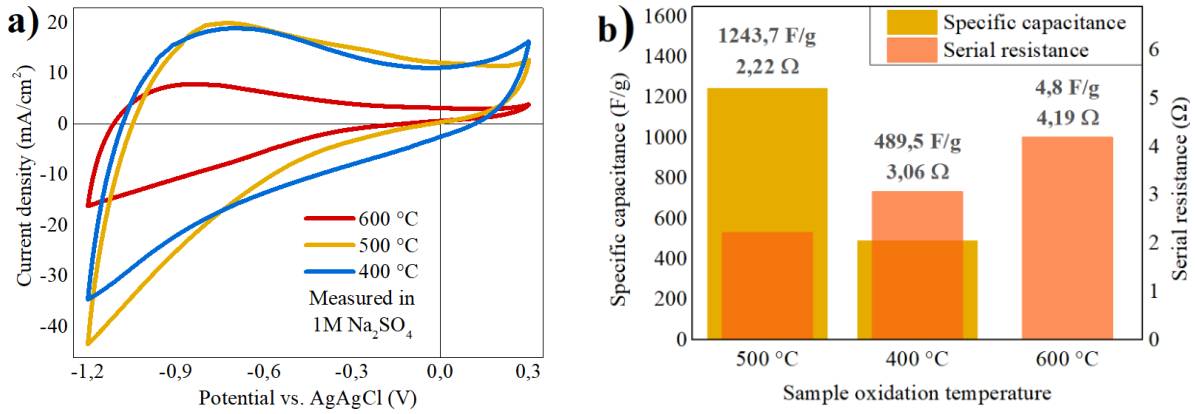

Figure 2. ***a)*** *Cyclic voltammogram measured in 1M Na_2SO_4 of samples prepared at different oxidation temperatures, and* ***b)*** *the specific capacitances measured at 1 A/g and serial resistances from EIS measurements of MoO_3-based samples prepared at different oxidation temperatures.*

TABLE I. *Specific capacitance and serial resistance values of prepared samples.*

Sample prepared at temperature	Specific capacitance (GCD)	Serial resistance
600 °C	4.8 F/g	4.19 Ω
400 °C	489.5 F/g	3.06 Ω
500 °C	1243.7 F/g	2.22 Ω

The possible utilization of MoO_3 substrates for hydrothermally prepared MoS_2 supercapacitor electrodes will be discussed in detail in the forthcoming publication.

Acknowledgments

This work was supported by Grants VEGA 1/0707/24 supported by the Ministry of Education, Science, Research and Sport of Slovakia and by the Slovak Research, Mat4Energy 23-03-03-B, and Development Agency under contracts APVV-20-0220 and APVV-21-0231.

References

1. K. Neha, et al. Journal of Electronic Materials 1-12. (2024).
2. S. Harish. The Japan Society of Vacuum and Surface Science, (2023).
3. A. Sarkar, et al. Journal of Physics: Condensed Matter, 30.15: 155001 (2018).

Development of the Reversible photoelectrochemical cell

S. V. Chivikov

V.I.Vernadskii Institute of General and Inorganic Chemistry of the NAS of Ukraine, 32/34 Academic Palladin Avenue, Kyiv, 03142, Ukraine.

Corresponding Author E-mail Address: s.v.chivikov@gmail.com

Improvement of a reversible photoelectrochemical system. The open circuit voltage of the cell has been doubled. In sunlight, the cell's open circuit voltage is more than 0.8V. The result was achieved by using a new electrolyte in the anode compartment. The cathode also needed to be replaced. Some cell elements have changed their functions. As with the original cell, the body parts were 3D printed.

Introduction

A reversible photoelectrochemical system has been described [1]. Such a system is capable of storing energy under the influence of solar radiation and releasing it in the absence of illumination, which is its obvious advantage. However, the characteristics showed low. The goal of further work is to improve the characteristics of this interesting system.

One of the main characteristics of a current source is the voltage.

As shown in work [2], the change in the photoanode potential under the influence of light is significantly higher if the electrolyte contains $K_3[Fe(CN)_6]$. This result was obtained for photoanodes based on ZnS, CdS, electrolyte was Na_2SO_4. Our tests for an anode based on CdSe and an alkaline electrolyte with the addition of $K_3[Fe(CN)_6]/K_4[Fe(CN)_6]$ showed similar results.

A problem arose with the choice of cathode for a reversible photoelectrochemical system. The standard potential of $K_3[Fe(CN)_6]/K_4[Fe(CN)_6]$ is 0.35V, so the metal hydride cathode cannot be used. Here and below, the potentials are given relative to a normal hydrogen electrode. The choice of cathode was quite a serious problem. My colleagues came to the conclusion that a suitable cathode does not exist!? They refused to use $K_3[Fe(CN)_6]/K_4[Fe(CN)_6]$ and accordingly refused the opportunity to increase the voltage of the reversible photoelectrochemical cell.

The change in the potential of a CdSe-based photoanode under the influence of solar illumination is about 0.8 V and a little more. Accordingly, the acceptable cathode potential for a reversible photoelectrochemical system is in the range of -0.2...-0.4V. Of course, it is possible to select an electrochemical system with a suitable potential. However, problems of stability, electrochemical activity and availability arise.

The polysulfide used in the initial version of the reversible photoelectrochemical cell [1] as the electrochemical system for anod has a potential not so far to that required for the cathode of the system with $K_3[Fe(CN)_6]/K_4[Fe(CN)_6]$. Polysulfides are a series of compounds - accordingly a series of potential values. Values for the potentials of various polysulfides are given in [3].

Results and Discussion

The design of the body of the photoelectrochemical cell at the first stage remained unchanged and was also printed on a 3D printer.

In general, the new cell is built from the same elements as the original version described in [1]. The components are obtained using the same technologies. The composition of the electrolyte in the anode compartment and the position and role of some components have been changed. The anode compartment contains a photo anode. The electrolyte of the anode compartment is 1M KOH + 0.25M $K_3[Fe(CN)_6]/K_4[Fe(CN)_6]$. The Cu_2S electrode in the new version of the cell, together with an alkaline polysulfide solution, is located in the cathode compartment and plays the role of a cathode. The nickel foil strip is the third electrode, which is located in the anode compartment.

The cell lost its metal hydride electrode and the ability to accumulate hydrogen.

After assembling the cell, the potential difference between the cathode and the third electrode was 0.95 V. The photo anode in sunlight showed a photopotential up to 0.82V, which excluded the possibility of charging and accumulation.

The cell was connected to a galvanostat by the cathode and the third electrode. Long-term cycling was carried out in the range of 0.8...0.4V. In the first cycles, an insignificant reversible capacitance was observed, which limited the initial cycling current to 60 μA. During the cycling process, the charge-discharge capacity increased from cycle to cycle. This made it possible to increase the current to 1mA or more. This result can be explained by the accumulation of polysulfide of the appropriate composition in the cathode compartment.

As a result. The cell was connected as a reversible photoelectrochemical system. Loaded with a discharge current of 3mA. The cell was discharged at voltages of 0.7...0.65 V in the absence of photoanode illumination. When the photoanode was illuminated, the voltage on the electrodes increased to 0.7 V and higher (at a discharge current of 3 mA).

Thus, the possibility of significantly increasing the operating voltage of a reversible photoelectrochemical cell was demonstrated.

Low current performance is determined by imperfect cathode design. What is usual for the first samples. At the initial stage of work, the original system [1] had similar current characteristics.

Conclusions

It has been shown that it is possible to increase the open-circuit voltage of a reversible photoelectrochemical system from 0.4V to 0.8V. For this purpose, an alkaline solution of $K_3[Fe(CN)_6]/K_4[Fe(CN)_6]$ was used as an electrolyte in the anode compartment. In the cathode compartment there is an alkaline solution of sodium polysulfide. The functionality of the system was ensured by electrochemical treatment to generate polysulfide with the required potential value. I would like to note that in terms of open-circuit voltage, this version of a reversible photoelectrochemical system is noticeably superior to widely used silicon elements.

It is not often possible to significantly increase the voltage of a chemical current source.

It should be noted that the result was obtained using extremely limited resources.

The result can be considered as a technology demonstrator; to evaluate the real capabilities of such a system, it is necessary to obtain an effective cathode.

References

1. V.Chivikov, I.A.Rusetskyi, S.S.Fomanyuk et al., Journal of Physics: Conference Series, 2382(1), (2022)
2. I.V. Demidenko, Elektronnaya Obrabotka Materialov, 78-85, 58(3) (2022)
3. D.D. Wagman, W.H. Evans, I. Halow et al. Selected values of chemical thermodynamic properties. Tables for the first thirty-four elements in the standard order of arrangement. NDS Technical Note p. 264, Institute for Basic Standards, Washington (1968)

The Effect of Backsheet Repairs on Insulation Resistance in Photovoltaic Modules

T. Finsterle[a], J. Kasper[a], P. Hrzina[a], L. Černá[a]

[a] Department of Electrotechnology, Faculty of Electrical Engineering, Czech Technical University in Prague, Technicka 2, 166 27 Prague, Czech Republic.

The degradation of the backsheet layer of photovoltaic modules is a highly relevant topic today. It was not initially anticipated that the plastics and encapsulation materials used could degrade. Recent findings indicate that this degradation significantly reduces the lifespan of photovoltaic modules manufactured around 2010. Additionally, the degradation of the backsheet layer dramatically decreases the insulation resistance of individual modules and the entire chain, often leading to the disconnection of the entire string for safety reasons, causing production losses. Repairs of photovoltaic modules directly in the field are highly sought after, and assessing the increase in insulation resistance after such repairs is critical and will be the subject of the following study.

Introduction

The reliability of photovoltaic (PV) panels strongly depends on the quality of their encapsulation, especially during the lamination process. Encapsulation thus plays a crucial role in protecting PV cells from various environmental stressors such as moisture, oxygen, and mechanical damage. Ethylene-vinyl acetate (EVA) is commonly used as an encapsulation material due to its excellent electrical insulation properties and ability to maintain mechanical integrity [1], [2]

However, the efforts of manufacturers to continually reduce the production costs of photovoltaic modules, along with the requirements for the most recyclable plastics used in module production, have led to a decrease in both the quality and quantity of encapsulation materials used. [2], [3], [4]. The back sheets, which protect the module's components from environmental stress, have also declined in quality. They have transitioned from high-grade polyvinyl fluoride (PVF) to less durable options like polyvinylidene fluoride (PVDF), polyethylene terephthalate (PET), and polyamide (PA) [3]. The back sheet primarily acts as a moisture barrier and environmental shield, essential for maintaining PV module performance in harsh conditions [3]. Degradation of these materials can lead to problems such as water vapor diffusion, causing corrosion of metallic components, hydrolytic degradation of the encapsulant, and delamination between layers [4], [5]

Cracking of the back sheet, which results from decreased tensile strength, allows moisture ingress and is considered the most catastrophic failure mode because it significantly impacts performance and reliability. This hydrolysis reduces tensile strength, which is crucial for the mechanical integrity and crack resistance of the back sheet [6].

Methods

Diagnose the functionality of repairs to the backsheet of photovoltaic modules and the impact of these repairs on the change in the insulation resistance of the modules is the subject of the study.

Since the issue of cracked backsheets is relatively new, methods and materials for repairs (such as epoxy, polyurethane, acrylic, nitrile rubber, and silicone materials) are still under development and research. Currently, there are two types of repairs on the market:

a) coating with polysiloxane gel, usually done on-site at the power plant;
b) coating with laminate foil, done after removing the respective module and repaired in a repair shop.

The samples used, specifically four Candian Solar photovoltaic modules, were repaired with gel; two modules were repaired only in the cracked joints and one was repaired over its entire surface. The last fourth module remained unrepaired as a reference.

The insulation resistance of the modules was calculated based on the leakage currents that could be obtained thanks to automated measurement of voltage drop on an additional resistor (Rm) 330 kΩ. The calculation of insulation resistance (R1) was performed according to the equation [1]. Each PV module was stressed with a DC voltage of about 600 V. The entire experiment was set up according to the diagram in Figure. 1.

$$I_1 = \frac{U_1}{R_m}$$

$$U_x = U_1 + I_1 R_{test} = U_1 + \frac{U_1}{R_m} R_{test}$$

$$R_1 = \frac{U_x}{I_1} - R_m$$

Equation 1

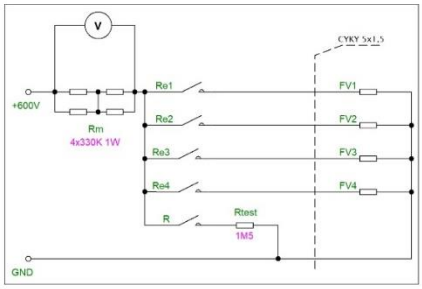

Figure. 1

Results and discussion

The switching of measurements between individual modules or the reference resistance (R_{test}) of 1.5 MΩ was facilitated using a control board equipped with 5 relays. The measurement of the entire setup occurred cyclically every 15 minutes. This periodic measurement allowed for relatively continuous monitoring of the insulation resistance, enabling further evaluation of the influence of environmental factors such as humidity and outdoor temperature on the insulation resistance of individual modules and any effects of repairs made using insulating gel. Details and the status of the repair are indicated in tab. 1.

TABLE I.

Serial number	Mark of module	Mark in Figure 1	Insulation resistance	Repair status
610190450330	1	FV1	R1	uncorrected
610190451868	2	FV2	R2	along the seams
610190450398	3	FV3	R3	Full corrected area
610190451860	4	FV4	R4	along the seams

The main axis of the graph present the insulation resistance trajectories of the modules and the humidity trend are plotted. On the secondary axis, the graph shows the ambient temperature and dew point temperature in degrees Celsius. The graph reveals four significant drops in resistance. When the temperature curve intersects with the dew point temperature, condensation on the module occurs, followed by a decrease in insulation resistance. The subsequent drying phase is visible as the humidity decreases, the temperature rises, and the insulation resistance increases. During the second and third major resistance drops of R1 (unrepaired module), the values reach tens to single megohms. Extreme

drops occur due to rainfall and condensation when water enters the module, potentially soaking the encapsulating EVA layer.

The decrease in insulation resistance is mainly due to the water-absorbing properties of ethylene vinyl acetate (EVA). Typically used as an encapsulating material, EVA has adequate mechanical, optical, and chemical properties suitable for PV module production but is hydrophilic. The backsheet, usually made of Tedlar, protects the encapsulating EVA material and the entire PV module from moisture penetration. Degradation of this cover layer and its subsequent cracking expose the absorbent EVA film, potentially creating a conductive path between the photovoltaic cells and the frame, leading to current leakage.

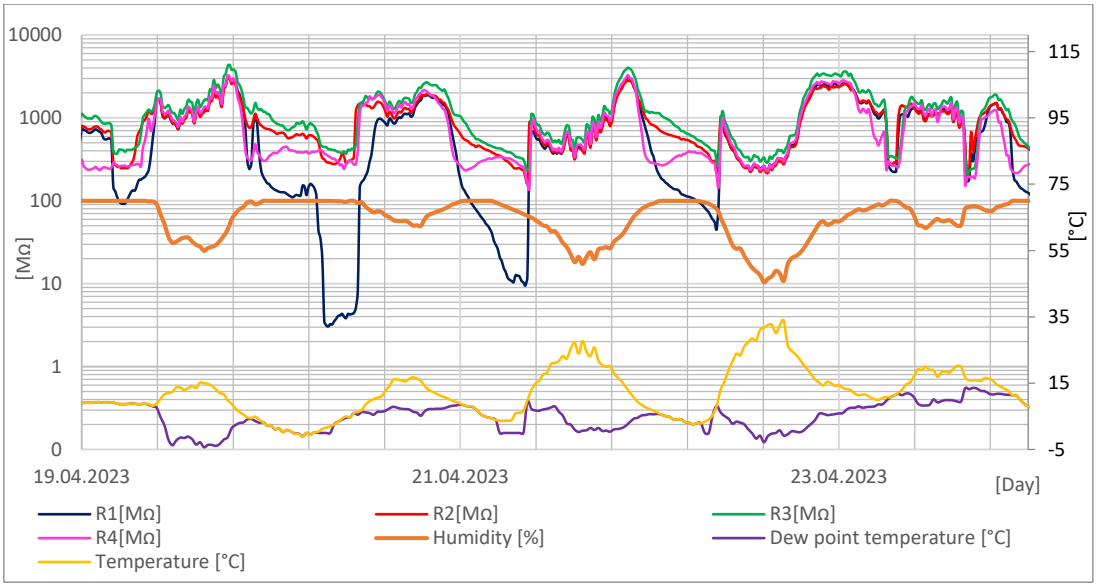

From the measured data, it is evident that the repair with silicone gel prevented a sharp decrease in insulation resistance upon contact with water. The threshold insulation resistance is 40 MΩ per module area, with anything below this value considered a module failure. Modules that underwent our measurements had a threshold value of 31.3 MΩ. The unrepaired module reached this minimum value several times, as shown in Graph 1, whereas the repaired modules never dropped to 31.3 MΩ. The best insulation resistance values were measured on module number 3, which was repaired across its entire surface.

Acknowledgments

This work was supported by the project "The Energy Conversion and Storage", funded as project No. CZ.02.01.01/00/22_008/0004617 by Programme Johannes Amos Comenius, call Excellent Research.

References

1. S. Jiang, K. Wang, H. Zhang, Y. Ding, a Q. Yu, „Encapsulation of PV Modules Using Ethylene Vinyl Acetate Copolymer as the Encapsulant", Macromol. React. Eng., roč. 9, č. 5, s. 522–529, říj. 2015, doi: 10.1002/mren.201400065.
2. D. Wu et al., „Influence of Lamination Conditions of EVA Encapsulation on Photovoltaic Module Durability", Materials, roč. 16, č. 21, s. 6945, říj. 2023, doi: 10.3390/ma16216945.

3. V. Poulek, I. Tyukhov, a V. Beranek, „On site renovation of degraded PV panels – Cost and environmental effective technology", Sol. Energy, roč. 263, s. 111956, říj. 2023, doi: 10.1016/j.solener.2023.111956.
4. S. Chakraborty, A. K. Haldkar, a N. Manoj Kumar, „Analysis of the hail impacts on the performance of commercially available photovoltaic modules of varying front glass thickness", Renew. Energy, roč. 203, s. 345–356, úno. 2023, doi: 10.1016/j.renene.2022.12.061.
5. A. Fairbrother, N. Phillips, a X. Gu, „Degradation Processes and Mechanisms of Backsheets", in Durability and Reliability of Polymers and Other Materials in Photovoltaic Modules, Elsevier, 2019, s. 153–174. doi: 10.1016/B978-0-12-811545-9.00007-0.
6. N. Tz. Dintcheva, E. Morici, a C. Colletti, „Encapsulant Materials and Their Adoption in Photovoltaic Modules: A Brief Review", Sustainability, roč. 15, č. 12, s. 9453, čer. 2023, doi: 10.3390/su15129453.

Comparison of the use of a virtual battery in a photovoltaic system

J. Vanek[a], and J. Pekarek[a]

[a] Department of electrotechnology, Brno University of Technology, Brno, Czech Republic

In this paper, we compare different photovoltaic systems with battery storage of electricity for a defined family house in the Czech Republic in the Opava area and a variant of this power plant with direct sale to the grid or with the use of a distributor service called virtual battery. The work also includes an economic analysis and a calculation of the return on investment, considering the available energy products from energy suppliers in the Czech Republic

Analyzed photovoltaic system

The house is located in a densely populated street where approximately the same tall buildings are present on both sides, which could overshadow any potential installation. Other considerations include a chimney on the west side of the roof and a large walnut tree towering to the northwest.

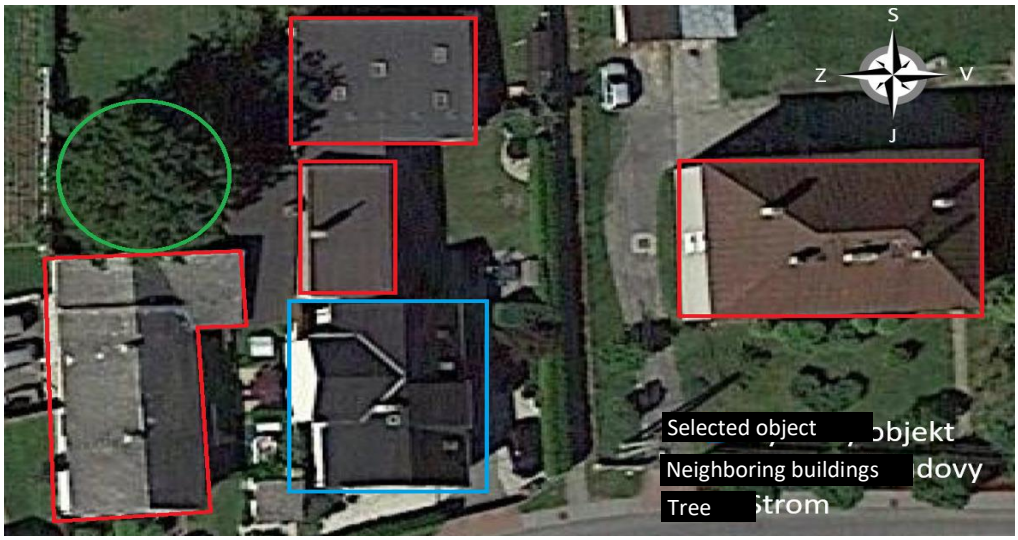

Figure 1. *Map of the surroundings of the selected object*

Figure 2 below shows the energy consumption of the selected building in each month. This is the load profile of a household with 4 adults where a heat pump is used for heating, which has a significant impact on this profile. The household had a total energy consumption of 7.6 MWh in 2023, of which approximately 3.3 MWh was consumed by the heat pump. It is the heat pump that is a substantial load in periods when there is less sunlight and therefore PV modules do not produce much. During this period, even storage in possible batteries will probably not be sufficient and the distribution grid will have to be used to measure the electricity supply. On the other hand, we can compensate for this shortfall in the summer months if we establish a contract for the purchase of surplus energy for a suitable amount of money.

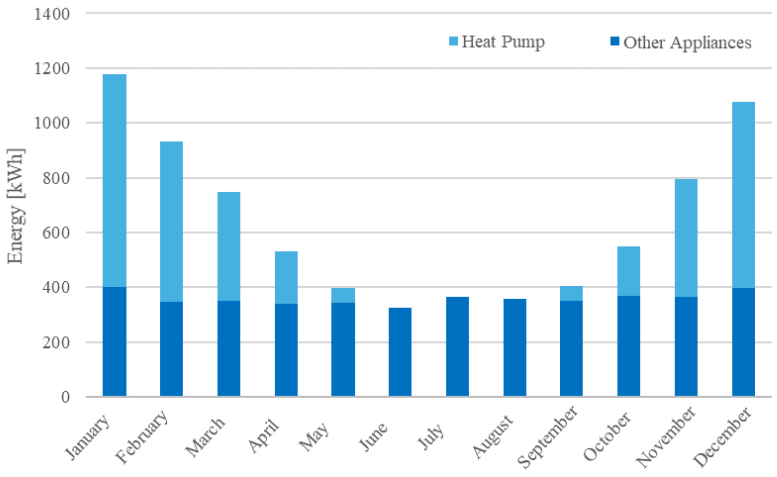

Figure 2. *Household load profile throughout the year*

Result of simulation

Table 1. *Financial analysis of supplier products for 8.55 kWp and 7.20 kWp installations*

Photovoltaic power plant power	8.55 kWp	7.20 kWp
Energy consumption	7667 MWh	7667 MWh
Supply from the grid	3.588 MWh	3.921 MWh
Supply to the grid	3.877 MWh	2.724 MWh
Annual price per product		
"Elektřina Fix na 3 roky bez FVE"	49 693.89 Kč	
"Elektřina Fix na 3 roky bez výkupního tarifu"	27 296.95 Kč	29 125.39 Kč
"Elektřina Fix na 3 roky s výkupním tarifem 2 Kč/MWh"	19 542.95 Kč	23 677.39 Kč
"Elektřina pro soláry"	15 917.23 Kč	21 155.49 Kč
Price per kWh		
"Elektřina Fix na 3 roky bez FVE"	6.48 Kč	
"Elektřina Fix na 3 roky bez výkupního tarifu"	7.61 Kč	7.43 Kč
"Elektřina Fix na 3 roky s výkupním tarifem 2 Kč/MWh"	5.45 Kč	6.04 Kč
"Elektřina pro soláry"	4.44 Kč	5.40 Kč
Saving finances		
"Elektřina pro soláry" versus "Fix na tři roky bez výkupu"	11.379,72 Kč	7.969,90 Kč
"Elektřina pro soláry" versus "Fix na tři roky s výkupem"	3.625,72 Kč	2.521,90 Kč
"Elektřina pro soláry" versus option without PVS	33.776,66 Kč	28.538,40 Kč
"Elektřina pro soláry" PVS 8,55 kWp "versus PVS 7,2 kWp with feedin	7.760,16 Kč	
"Elektřina pro soláry" PVS 8,55 kWp" versus PVS 7,2 kWp no feedin	5.238,26 Kč	

Return on investment

The total financial cost of the investment after deducting the subsidy is around CZK 276,563 for the 8.55 kWp installation and CZK 244,585 for the 7.20 kWp installation. From the previous chapter, we have seen how much financial savings we can expect compared to the case without the PV plant. If we determine the payback by simply dividing the cost by this saving, we could say that an 8.55 kWp PV plant pays for itself in 8.2 years.

Acknowledgments

This work was supported by the specific graduate research of the Brno University of Technology No. FEKT-S-23-8286.

References

1. PHOTOVOLTAIC GEOGRAPHICAL INFORMATION SYSTEM. JRC Photovoltaic Geographical Information System (PVGIS) - European Commission, Online. © European Union, 1995-2024. 1.3.2022, https://re.jrc.ec.europa.eu/pvg_tools/en/tools.html [cit. 2024-04-25].
2. NOVÁ ZELENÁ ÚSPORÁM. Závazné pokyny pro žadatele a příjemce podpory – Rodinné domy (Standard). Online. © Státní fond životního prostředí ČR. Dostupné z: https://novazelenausporam.cz/dokument/3381 [cit. 2024-05-18].
3. VICTRON ENERGY. MultiPlus-II GX Inverter/Charger. Online, katalogový list. Dostupné z: https://eshop.neosolar.cz/documents/4747/CS/Datasheet-MultiPlus-II-GX-inverter-charger-EN-.pdf [cit. 2024-05-10].
4. SKUPINA ČEZ. Ceníky | Podpora | Skupina ČEZ. Online. Copyright 2024 ČEZ, a. s. Dostupné z: https://www.cez.cz/cs/podpora/ceniky.html [cit. 2024-05-10].
5. SKUPINA ČEZ. Ceník elektřiny pro domácnosti – Elektřina pro soláry. Online. ČEZ Prodej a.s., 13.2.2024. Dostupné z: https://www.cez.cz/webpublic/file/edee/ceniky/moo_ele_cez_pro_solary_080324_2024.pdf [cit. 2024-04-20].
6. SKUPINA ČEZ. Ceník elektřiny pro domácnosti – Elektřina Fix na 3 roky. Online. ČEZ Prodej a.s., 1.5.2024. Dostupné z: https://www.cez.cz/webpublic/file/edee/ceniky/moo_ele_cez_fix_na_3_roky_010524_2024.pdf [cit. 2024-05-10].

Advanced Exploration of the Electrode-electrolyte Interface using Elimination Voltammetry with Linear Scan

X. Li, L. Trnkova

Department of Chemistry, Faculty of Science, Masaryk University, Kamenice 5, 625 00 Brno, Czech Republic

This contribution discusses the importance and possible applications of elimination voltammetry with liner scan (EVLS), which is based on linear or cyclic voltammetry experiments. Its software approach in the form of elimination functions is designed to eliminate some current components and preserve others. The elimination procedure reveals new possibilities for employing voltammetric data to obtain a detailed characterization of the electrode/electrolyte interface and thus for a deeper understanding of electrode processes.

Cyclic voltammetry (CV) is one of the most widely used electrochemical methods for studying electroactive substances. It is a versatile technique that allows investigation of the mechanisms of redox and transport properties of the electrochemical system (1). The cathodic and anodic polarization of the electrode provides information not only about the reduction and oxidation steps of the studied depolarizer but also about its behavior in the electric double layer. In other words, although voltammograms show the overall electrode process and indirectly give some evidence of the effects of different experimental parameters, deeper insight into the electrode process in the dependence of electric double-layer can provide the elimination voltammetry with linear scan (EVLS). By software processing electrochemical data collected by linear sweep or cyclic voltammetry *via* its functions, EVLS can eliminate some particular current components and conserve others (2-4). The EVLS functions, which simultaneously eliminate two current components, require voltammograms recorded at three scan rates, one of which is chosen as the reference scan rate. For the following three most frequently used EVLS functions E4, E5, and E6, the scan rate ratio is equal to two, e. g., I is the reference scan rate, $I_{1/2}$ and I_2 are one-half and double the reference scan rate, respectively:

$$\text{E4 } f(I) = -11.6570\, I_{1/2} + 17.4850\, I - 5.8284\, I_2 \quad (1)$$

which eliminates simultaneously charging and kinetic currents (I_c and I_k) with conserving the diffusion current (I_d),

$$\text{E5 } f(I) = 6.8284\, I_{1/2} - 8.2426\, I + 2.4142\, I_2 \quad (2)$$

which eliminates simultaneously charging and diffusion currents (I_c and I_d) with conserving the kinetic current (I_k), and

$$\text{E6 } f(I) = 4.8284\, I_{1/2} - 8.2426\, I + 3.4142\, I_2 \quad (3)$$

which eliminates simultaneously the kinetic and diffusion currents (I_k and I_d) with conserving the charging current (I_c).

The theory of EVLS was based on a reversible process where the capacity current is linearly dependent on a scan rate, the kinetic current is independent of a scan rate, and the diffusion current corresponds to the square root dependence of a scan rate. EVLS approach was initially used only for the mercury drop electrode and provided excellent results due to the renewable, equally defined surface. Now this method is used for solid electrodes, especially graphite ones. However, the above-presented EVLS functions were used for the polymer pencil graphite electrode (pPeGE), which exhibits great electroanalytical sensitivity in its lateral surface. It can be a stable and highly available sensor with excellent electrical properties such as high electrical conductivity, an electron transfer rate (higher than glassy carbon) and a low background current. An electrochemical redox probe $[Fe(CN)_6]^{3-/4-}$ was chosen to investigate the electrode/electrolyte interface.

For a reversible diffusion-controlled electrode process, the EVLS functions E5 and E6 eliminating the diffusion component of the current should provide a zero line of the capacitive and kinetic current components. However, the application of this elimination procedure showed that this is not the case and EVLS E5 shows a specific signal with a current depression that varies depending on the experimental conditions. As an example, an elimination voltammogram registered for different concentrations of the redox probe $[Fe(CN)_6]^{3-/4-}$ on pPeGE is shown in Fig.1. With increasing concentration of the complex, the current depressions increase and the cyclic recording gives them the shape of a drop. The figure shows a clear difference between the capacity and kinetics. The kinetic current does not change with the change in the concentration of the complex and is close to the theoretically assumed zero.

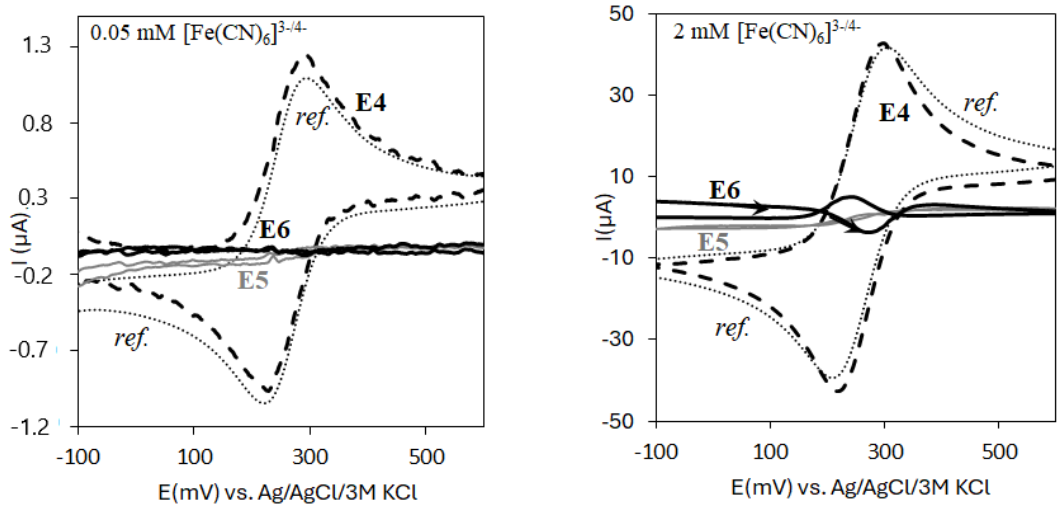

Figure 1. *A comparison of the recordings: the cyclic voltammograms and the calculated elimination functions (E4 ----, E5 , and E6) of different concentrations of redox standard: (A) 0.05 mM and (B) 2mM [Fe (CN)6]3-/4- in 0.1 M KCl on a polymer pencil graphite electrode (pPeGE).*

Above all, the last of the two functions E6 (Eq. 3), allowing us to gain an insight into the electrode/electrolyte interface, yielded a complex picture of the interphases and the influence of experimental conditions on the electron transfer mechanism, including not only the morphology of the graphite electrode surface but also the range of the scan rates at which the redox is investigated, the concentrations of both the analyte and the supporting electrolyte, the polarization potential range, and the presence of oxygen in the examined solutions (5, 6). This is the first time EVLS has been used to eliminate the corresponding reversible current, attempting to explore the "secret" of the

electrochemical process monitored by cyclic voltammetry and to understand it from a different point of view.

Acknowledgments

The financial support provided by Masaryk University (project: Development of methods and instrumentation for the analysis of biologically important substances (MUNI/A/1421/2022 and MUNI/A/1594/2023).

References

1. R.G. Compton, C.E. Banks, *Understanding Voltammetry*, 3rd Edition, World Scientific (2018).
2. L. Trnkova, *J. Electroanal. Chem.*, **582**, (1-2), 258 (2005).
3. L. Trnkova, *J. Electroanal. Chem.*, **905**, 115961 (2022).
4. O. Dracka, *J. Electroanal. Chem.*, **402** (1-2), 19 (1996).
5. X.C. Li, I. Triskova, L. Trnkova, *Electrochim. Acta*, **442,** 141921 (2023).
6. X.C. Li, J. Cechal, L. Spanhel, S. Toscani, J. Martinik, R. Oborilova, L. Trnkova, Electrochim. Acta **475,** 143615 (2024).

Advanced approaches for state-of-charge (SOC) and state-of-health (SOH) estimation of Li-ion batteries

Miroslav Mikolášek*, Lukáš Gardian, Martin Brázda, Boris Bajla, Martin Kemény, and Matej Novak

[a)] Institute of Electronics and Photonics, Slovak University of Technology, Ilkovičova 3, 841 04 Bratislava, Slovakia

*Corresponding author: miroslav.mikolasek@stuba.sk

The estimation of the state of health (SOH) and state of charge (SOC) of Li-ion batteries is crucial to ensure reliable and safe operation and optimization of battery performance and lifespan. New approaches with the ability to increase the amount of information gained from the battery are required to increase the estimation accuracy of such states. This paper presents an application of differential thermal voltammetry (DTV) and acoustic emission measurements (AE) as a perspective approach for state estimation of Li-ion batteries. Analyzed are various application conditions to evaluate the sensibility and applicability of these techniques for li ion battery state estimation.

Introduction

The capacity and lifetime of Li-ion batteries are strongly determined by the condition under which the battery operates (1). The accurate estimation of battery states, such as state of health (SOH) and state of charge (SOC) are important challenges for the management of battery systems, increasing their lifetime and safety. These states are strongly related to the condition under which the battery operates and are affected by the degradation mechanism, which occurs in the battery (1). Battery states are not possible to directly measure with high accuracy, therefore there is a strong effort to develop new sensing approaches, algorithms, and mathematical models for their estimation (2, 3). Commonly used techniques such as incremental capacity analysis (ICA) or charging/discharging have limited ability to gain insight on degradation and SOH evolution and are very time-consuming (4) New techniques with the ability to asset battery states are needed to gain accurate information about battery states.

This paper aims to introduce differential thermal voltammetry (DTV) and acoustic emission (AE) measurements and analyze their perspectives for the estimation of SOC and SOH states. Acoustic emission technology has shown promise in providing insights into battery condition assessment and fault diagnosis, offering a non-destructive means of monitoring the SOC and SOH of batteries in real time (5, 6). Differential thermal voltammetry (DTV) is a non-destructive method, which involves monitoring the voltage and temperature of batteries during operation to assess their state of health (SOH) and track degradation (7).

Experimental set-up

All experiments were carried out on cylindric Li-ion battery NCR18650B ($LiNiCoAlO_2$ cathode and a graphite anode) from Panasonic, which is popular for electromobility applications.

The capacity of the battery is 3350 mAh, the recommended charge rate is 0.5C (1.625 A), maximum allowed C-rate is 0.7C (2.38 A). The Maximum and minimum voltages of the battery are 4.2 V and 2.5 V, respectively. All electrical characterizations were carried out by Gamry Interface 5000P potentiostat/galvanostat and cycler Neware BTS4000.

Acoustic emission measurements were done using SIUI SyncScan UT2 and probe SIUI T5-6L-M. A Li-ion Polymer pouch cell Melasta SLPB6945135HV was used for acoustic emission measurements during 1C charging and discharging. Measurement set-up was configured to pulse-echo reflection mode. All cycling and acoustic characterizations were done in the laboratory at a controlled temperature.

Results and discussion

Acoustic emission measurements were performed on pouch cell Melasta SLPB6945135HV by using an SIUI T5-6L-M probe with a frequency of 5 MHz. Fig. 1a shows A-scans measured on the battery at different SOC during discharge. A clear trend of increased peak amplitude upon the SOC is observed from the scan. The higher change observed for peaks in the higher deep is due to the reflection of such signal from the deeper part of the battery, thus assessing the information from a higher number of layers. The change of the peak F and G amplitude vs. SOC is plotted in Fig. 1b, showing the linear trend. Detailed analysis and study of the applicability of AE for SOC and SOH state estimation will be provided during the presentation.

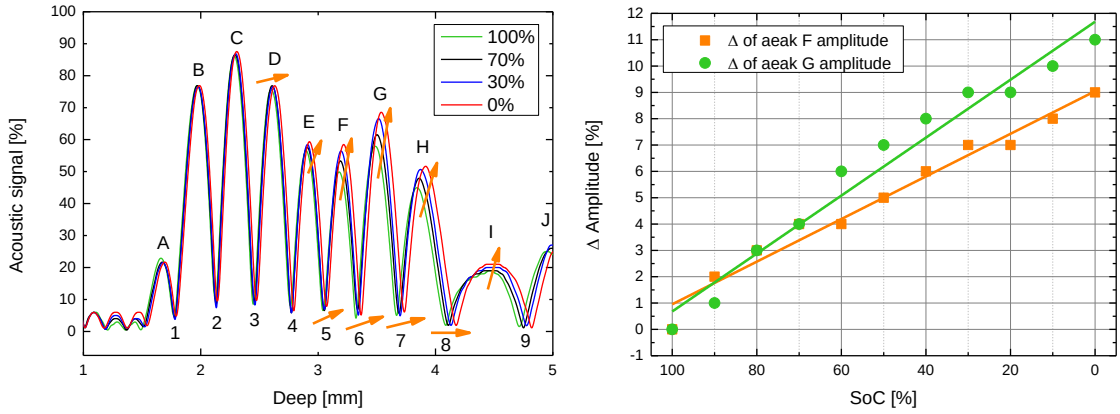

a) b)

Figure 1. *a) A-scan obtained from acoustic emission as a function of SOC, b) change of F and G peak amplitude vs. SOC of the battery.*

Differential thermal voltammetry (DTV) is based on the tracking of thermal entropy processes in the battery, which are associated with different degradation processes. To analyze the possible utilization of DTV for SOH estimation, the NCR18650B was charged and discharged with different currents ranging from the interval of 0.03 to 1.5 C-rate. The temperature scans were used for the construction of DTV curves plotted as a function of voltage. Constructed DTV curves revealed one prominent peak, associated with thermal entropy in the battery. Fig.2a shows the shift of the dominant DTV peaks upon cycling degradation with a 1C rate current, indicating the ability to use such relationship for SOH estimation. Fig.2b shows the analysis of DTV peak position as a function of capacity fades for 1 and 0.7 current rates and for charging and discharging. The linear trend of DTV peak voltages upon the capacity fade shows a good application of DTV for SOH estimations.

Further DTV results and outcomes and comparison of this approach for SOH estimation with incremental capacity analysis technique (ICA) will be provided in the final paper.

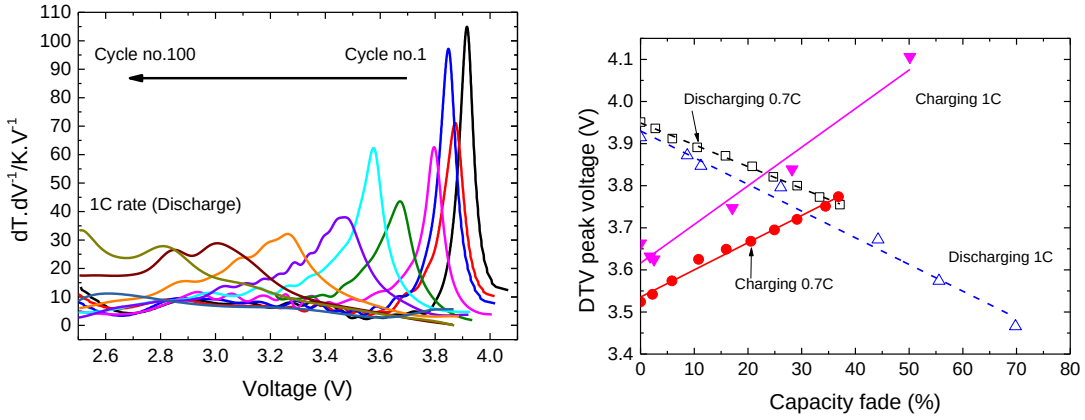

a) b)

Figure 2. *a) DTV curves at 1C-rate discharge for different degradation cycles, b) dominant DTV peaks position voltages and their approximation as a function of capacity fade for charging (CH) and discharging (D) with 0.7C and current 1C current rates.*

Acknowledgments

This research was funded by the Ministry of Education, Science, Research, and Sport of Slovakia under the grant VEGA 1/0707/24; and by the Slovak Research and Development Agency under grants APVV-20-0111, APVV-22-0132, APVV-20-0220 and APVV-21-0231.

References

1. Birkl, R., et al., Journal of Power Sources, 341, p.373, (2017).
2. Hu, Xiaosong, et al. Renewable and Sustainable Energy Reviews, 114, (2019).
3. Roman, Darius, et al. Nature Machine Intelligence 3.5, p. 447, (2021).
4. Kemeny M., Ondrejka P., Mikolasek M., Batteries 9, no. 1, 33. (2023).
5. Komagata, S., et al., Ecs Transactions, 25(33), 163-167, (2010).
6. Zhou, N., Cui, X., Han, C., & Zhou, Y., Energies, 15(5), 1775, (2022).
7. Wu, B., et al., Journal of Power Sources, 273, 495-501, (2015).

R&D Development Path of Inobat´s Cell Chemistry

B. Rajagopalan, G. Thorat, L. Pavlovec, N. Fernando, K. G. Kalligowdan, S. Khankeshizadeh, N. Levy, and J. Reiter

Inobat Auto, R&D and production centre, Voderady 429, 919 42, Voderady, Slovakia

Inobat – a new advanced Li-Ion cell chemistry manufacturer will be presented with the focus on the NMC-based cell chemistry development within the IPCEI project.

InoBat Auto focuses on in-house research and development of advanced cell chemistries, aiming to manufacture and supply world-class lithium-ion batteries to e-mobility off takers. InoBat Auto is working under one-roof, and it includes research and development on materials and their combinations and finally applies the results in a large format pouch cell (from 30Ah to 90Ah) in a pilot line (SOP Q1/2024).

Fig 1 presents the Gen1-Gen5 cells with liquid electrolyte, mostly based on NMC cathode chemistry and advanced Si-based anode chemistry. Material screening and development of customized chemistries allows to focus on different cell designs: Design-to-Energy cell (recent NMC811/HiSi 31 Ah prototype with 328 Wh/kg), Design-to-Power (recent 31 Ah prototype 5C continuous rate from 100 to 0% SOC), Design-to-lifetime (cell chemistry for NMC622-Gr focusing 3500 full cycles).

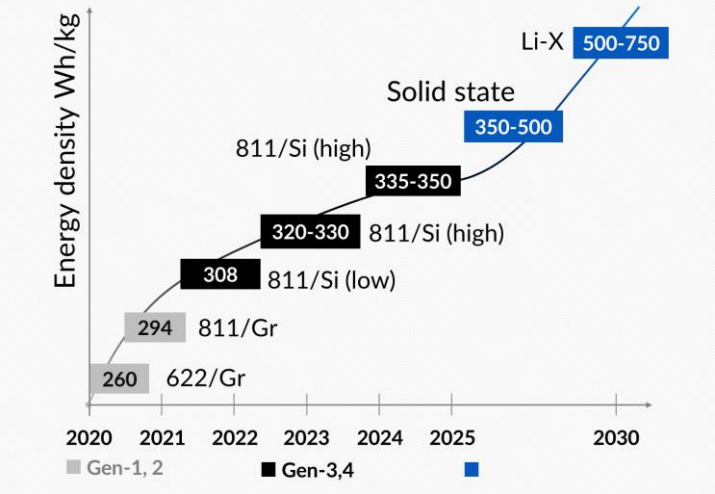

Figure 1. *Cell chemistry developments in Inobat ’s research and development program.*

Pilot production line (50 MWh) is giving the opportunity to manufacture cells and scale up the results from Inobat´s internal development and from the R&D projects with research institutes, universities, SMEs and material suppliers. In the consequent step, Volta 2 Gigafactory will be able to cover production of the final product with SOP 2026 and the production capacity between 1 and 4 GWh/y.

Figure 2. *Inobat Volta 1 R&D and production center (Slovakia) - inobat.eu.*

Acknowledgments

The project was supported under the EU sponsored program Important Projects for Common European Interest (IPCEI).

Comparison of machine learning techniques for estimating battery health

M. Sedlařík[a], T. Kazda[a], D. Capkova[b], P. Vyroubal[a]

[a] Department of Electrical and Electronic Technology, Faculty of Electrical Engineering and Communication, Brno University of Technology, Brno, Technická 10, 616 00, Czech Republic

[b] Department of Chemical Sciences, Bernal Institute, University of Limerick, V94 T9PX Limerick, Ireland

The increasing number of lithium-ion (Li-ion) batteries across a wide range of industries emphasizes their reliability, which is primarily achieved through accurate estimation of State-of-Health (SOH). Numerous methods exist for determining SOH, and this study focuses on estimating battery life parameters using machine learning (ML), which appears to be a fast and promising approach for this application. Experimental measurements were performed using Constant Voltage Constant Current (CCCV) tests, from which discharge cycle parameters were extracted for SOH estimation. The suitability of these parameters was verified using Pearson correlation analysis, demonstrating their appropriateness for estimation as well as their redundancy, which adversely affects overfitting. Two types of ML methods are compared, each with its own advantages and disadvantages: Support Vector Regression (SVR) and Gaussian Process regression (GPR).

Introduction

In recent years, the demand for Li-ion batteries has grown significantly as they are increasingly used across a wide range of technological sectors for electrical energy storage, especially in transportation. Li-ion batteries undergo gradual degradation due to calendar or cyclic aging, which leads to a decrease in capacity and an increase in resistance, resulting in a performance reduction. Accurate specification of the battery capacity loss, expressed by a parameter SOH, is essential for ensuring safe and reliable operation and determining when maintenance is required.

A variety of electrochemical, empirical, and mathematical models exist for predicting battery health. Electrochemical models describe the battery's behavior and provide a detailed description of the complex processes that occur during charging, discharging, and particle transport. In contrast, empirical models, particularly those based on data only, generate output based on the quality and quantity of the input data. Another category is semi-empirical models, where the battery is represented by an equivalent electrical circuit (ECM), with the dual polarization model being the most commonly used. Although these models are grounded in experimental measurements, they effectively describe the behavior of the battery. Hentunen et al [1] discuss a method for identifying parameters of ECM model. In recent years, data-driven models, especially those utilizing ML techniques [2,3], have emerged as a highly promising method for SOH estimation. These techniques can detect various anomalies in experimentally measured data, which could be difficult or impossible to analyze using other methods. Data-driven models with a probabilistic approach, such as the GPR method, are also used for SOH prediction [4].

Experimental

This study compares the deterministic method SVR and the probabilistic method GPR, each of which approaches the task in a different way. The aim of the study is to determine which method best estimates the SOH parameter based on defined input data, such as voltage, current, and battery temperature, from which direct input parameters for the predictive models are extracted. SVR is an adaptation of a Support Vector Machine (SVM) for regression task, designed to handle small sample sizes and non-linear data. SVR constructs hyperplanes in a high-dimensional space to predict output values accurately, ensuring deviations within a predefined margin while maintaining model complexity. [3] GPR is a Bayesian, non-parametric regression method that models the distribution over functions fitting the data. It uses a mean and covariance function (kernel) to make probabilistic predictions, providing both point estimates and confidence intervals, making it effective for small datasets and uncertainty quantification. [4] Each model also has a certain computational complexity that must be considered in the final comparison.

The research is performed on Samsung INR18650-35E batteries, which have a nominal capacity of 3.4 Ah, with lithium-nickel-manganese-cobalt oxides (NMC) as the cathode material and graphite as the anode material. These batteries were tested using the CCCV method at ambient temperature, with 600 cycles performed. The batteries were cycled at a constant current of 0.5 C, with the transition to the constant voltage (CV) phase occurring at 4.2 V and the discharge cut-off voltage set at 2.65 V. The specification of Samsung INR18650-35E are described in Table 1.

TABLE I. *Parameters of Samsung INR18650-35E battery.*

Parameter	Value
Type	Cylindric
Nominal Capacity	3.4 Ah
Nominal Voltage	3.6 V
Maximum Voltage	4.2 V
Minimum Voltage	2.5 V
Maximum Current	8 A

Feature Selection

Although this study involves laboratory cycling, only parameters that can be influenced by battery charging were selected. This ensures some practical applicability, as batteries are typically randomly discharged and then recharged from a certain level of discharge in real-world scenarios. The parameters were chosen to align with the SOH trend, ensuring their mutual correlation, which is verified by Pearson Correlation Analysis (see Figure 1).

The chosen parameters include the time when the voltage reaches 4.15 V during the charging cycles $t_{V\,(ch)}$, which is shorter with increasing cycle number [3], and the time when the current drops to 0.5 A during CV charging $t_{I\,(ch)}$, as these parameters reflect the SOH trend. Additionally, the average temperature $T_{avg\ (ch)}$, which affects battery degradation mechanisms, and the average charging voltage $V_{avg\,(ch)}$, which negatively correlates with the output, were selected.

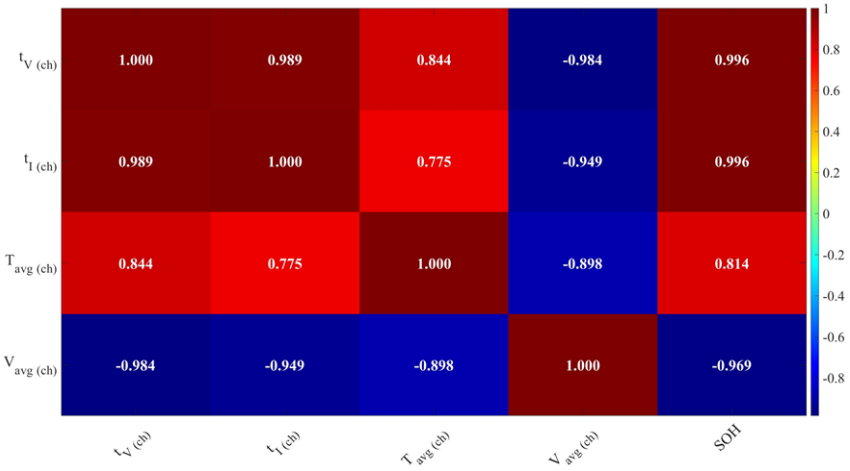

Figure 1. *Pearson Correlation Analysis between input features and SOH.*

Conclusion

The prediction of SOH in this research was conducted on a dataset comprising half training data and the rest testing data. Due to the strong mutual correlation of features $t_{V\,(ch)}$ and $t_{I\,(ch)}$, the $t_{I\,(ch)}$ input was neglected, which saves computational time. The SVR method achieved a total Root Mean Square Error (RMSE) of 0.25%, whereas the GPR method achieved 0.35%. With a decreasing number of training data, the RMSE for GPR increases exponentially compared to SVR, but with a larger amount of data, GPR is more accurate, which also confirms the fact that GPR is more reliable for larger datasets. The computational complexity for SVR was recorded at 0.25 seconds, while for GPR it is almost twice as large at 0.49 seconds.

Acknowledgments

This work was supported by the BUT specific research program (project No. FEKT-S-23-8286).

References

1. A. Hentunen, T. Lehmuspelto, and J. Suomela, “Time-Domain Parameter Extraction Method for Thévenin-Equivalent Circuit Battery Models”, *IEEE Transactions on Energy Conversion*, vol. 29, no. 3, pp. 558-566, 2014.
2. D. Yang et al., “A Neural Network Based State-of-Health Estimation of Lithium-ion Battery in Electric Vehicles”, *Energy Procedia*, vol. 105, pp. 2059-2064, 2017.
3. X. Shu et al., “A uniform estimation framework for state of health of lithium-ion batteries considering feature extraction and parameters optimization”, *Energy*, vol. 204, 2020.
4. R. R. Richardson, M. A. Osborne, and D. A. Howey, “Gaussian process regression for forecasting battery state of health”, *Journal of Power Sources*, vol. 357, pp. 209-219, 2017.

Elimination Voltammetry with Linear Scan: Theory and Applications

L. Trnkova, X. Li

Department of Chemistry, Faculty of Science, Masaryk University, Kamenice 5, 625 00 Brno, Czech Republic

This paper presents the theory and applications of elimination voltammetry with liner scan (EVLS) as a new tool in the research of electrochemical processes. The elimination procedure is implemented *via* EVLS functions that eliminate some selected current components and preserve others. By an appropriate choice of these functions or their combinations, electrochemists and electrical engineers can reveal processes hidden in linear sweep or cyclic voltammetric responses. In addition to studying the mechanisms of electrode processes, EVLS is a useful software tool for studying the electrode/electrolyte interface connected with the electrical double layer.

Voltammetric methods have been developed in both instrumentation and theory for many decades. The rapid development of computer technology was and is decisive for both approaches. Digitization successfully intervenes in the area of faster and more accurate data acquisition and processing (1). Such digital data processing is represented by elimination voltammetry with linear scan (EVLS), which can eliminate some current components and preserve others (2-4). The original theory of EVLS and the derivation of different types of elimination functions were related to reversible electrode processes, where the capacitive current I_c is directly proportional to the scan rate, the diffusion current I_d has a dependence corresponding to the square root of the scan rate, and the kinetic current I_k is independent of it. Assuming the validity of two conditions, when the total voltammetric current corresponds to the sum of the partially eliminated currents and when each partial current can be expressed as the product of the polarization speed function and the potential function, it is possible to simultaneously eliminate two partial currents by using three total voltammetric records obtained at three different scan rates. In general, *n*-voltammetric records must be obtained to eliminate *n-1* currents.

An ingenious and essential pillar of EVLS is the normalization of currents, where one speed of polarization is chosen as a reference and the other two scan rates are related to it in a certain ratio. For these purposes, different ratios of polarization speeds can be chosen, but the optimal, least error-laden ratio is the ratio corresponding to the whole number two (integer 2). The elimination function for the three measured voltammetric currents takes the form: $f(I) = aI_{1/2} + bI + cI_2$, where the I represents the chosen reference current, $I_{1/2}$ and I_2 currents with half and double the scan rates, coefficients a, b, c elimination coefficients that can be calculated using a procedure published several times in our earlier works.

As previously stated, EVLS functions that eliminate two current components require the acquisition of three total voltammetric records. For integer 2, Table I of three different EVLS functions with the respective coefficients a, b, c is presented. While the E5 function retains the kinetic component of the current and shows the importance of a possible preceding chemical reaction, the E6 function, preserving the capacitive current component, provides new information about changes in the electrical interface electrode/electrolyte.

TABLE I. *EVLS Functions E4, E5, and E6 in the form:* $\boldsymbol{f(I) = aI_{1/2} + bI + cI_2}$

Functions	*a*	*b*	*c*
E4 (I_d conservation)	-11.6570	17.4850	- 5.8284
E5 (I_k conservation)	6.8284	- 8.2426	2.4142
E6 (I_c conservation)	4.8284	- 8.2426	3.4142

The original theoretical basis of elimination voltammetry is based on a reversible process, where the scan rate exponent for diffusion current, kinetic current and capacitive current corresponds to the values 1/2, 1, and 0, respectively. The EVLS theory was verified experimentally on electrochemical processes on a mercury electrode, which guaranteed good reproducible results due to its well-defined and easily recoverable surface. Gradually, EVLS was also applied to solid electrodes, especially graphite electrodes. One of these graphite electrodes is the polymer pencil graphite electrode (pPeGE), which exhibits a surprisingly high rate of charge transfer (higher than other graphite electrodes), excellent wettability in aqueous solutions, outstanding conductivity and a low value of current background (capacitive currents). Moreover, pencil leads are very simple available. An electrochemical redox probe, e.g., $[Fe(CN)_6]^{3-/4-}$ can investigate the electrode/electrolyte interface. For a simple reversible diffusion-controlled electrode process, the elimination functions E5 and E6 eliminating the diffusion component of the current should provide the zero line of the capacitive and kinetic components of the current.

The assumption of zero I_k and I_c lines in functions E5 and E6 gave the idea of using EVLS for testing electrode systems. Especially, the E6 function was found to monitor changes in the electrode/electrolyte interface. An example could be an uncompensated electrical resistance, a change in geometry in the three-electrode set, a bad response of the reference electrode, an effect on a different value of the scan rate, and a change in the electrical double layer due to the presence of other chemical species or their concentrations. An example can be the presence of oxygen during a redox process $[Fe(CN)_6]^{3-/4-}$ (Figure 1), where current depressions in the shape of a drop are higher in the absence of oxygen. The presence of oxygen in the electrical double layer indicates its favorable effect on the electron transfer of the monitored complex. The qualitative result of the EVLS procedure with the supporting effect of oxygen was confirmed by quantitatively higher values of the heterogeneous rate constants.

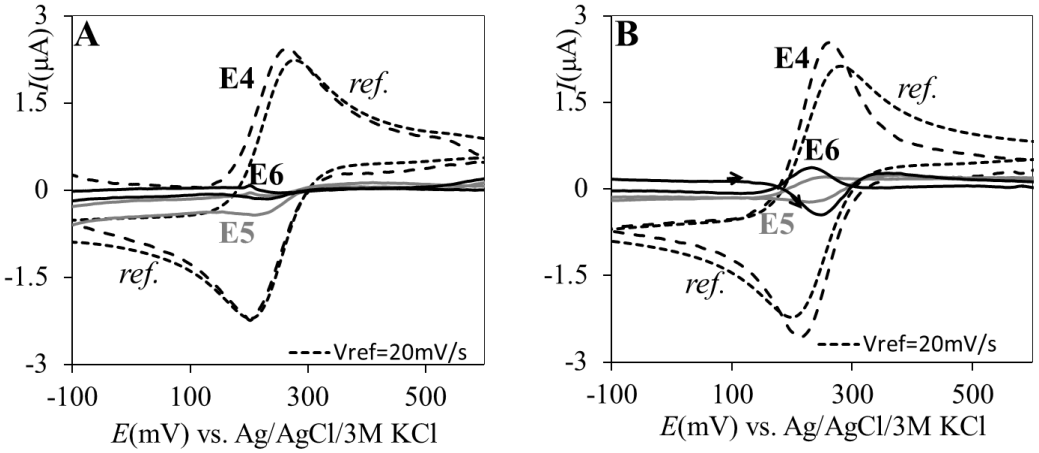

Figure 1. *Cyclic voltammograms and the calculated elimination functions (E4 ----, E5 ——, and E6 ——) 1mM* $[Fe(CN)_6]^{3-/4-}$ *on a polymer pencil graphite electrode (pPeGE) in 0.1 M KCl with (A) and without oxygen (B). The reference scan rate was 20 mV/s.*

Our experience shows that the EVLS function E6 allows insight into the electrode/electrolyte interface and provides a more comprehensive picture of the electrical double layer (5, 6). Its testing, informative and revealing roles manifest themselves in the form of different current depressions, which in cyclic voltammetry create a drop shape (Drop Shape Depression - DSD) change depending on:

a) electrode material (surface morphology and its chemistry, including fouling),

b) electrochemical parameters (scan rate, cycle, potential range, starting potential, concentration of components), and

c) possible participation of species of chemical or physical origin in the electrode processes (e.g. oxygen, nanoparticles, surfactants, etc.).

In conclusion, it can be stated that EVLS with the test probe can detect nuances, which cannot be detected *via* any voltammetric procedure.

Acknowledgments

The financial support provided by Masaryk University (project: Development of methods and instrumentation for the analysis of biologically important substances (MUNI/A/1421/2022 and MUNI/A/1594/2023).

References

1. R.G. Compton, C.E. Banks, *Understanding Voltammetry*, 3rd Edition, World Scientific (2018).
2. L. Trnkova, *J. Electroanal. Chem.*, **582**, (1-2), 258 (2005).
3. L. Trnkova, *J. Electroanal. Chem.*, **905**, 115961 (2022).
4. O. Dracka, *J. Electroanal. Chem.*, **402** (1-2), 19 (1996).
5. X.C. Li, I. Triskova, L. Trnkova, *Electrochim. Acta*, **442,** 141921 (2023).
6. X.C. Li, J. Cechal, L. Spanhel, S. Toscani, J. Martinik, R. Oborilova, L. Trnkova, Electrochim. Acta **475,** 143615 (2024).

Influence of Scan Rate on Potentodynamic Polarisation Measurement of Sintered Materials

S. Bátorová[a], M. Zatloukal[a] and G. Fafilek[b]

[a] Department of Electrical and Electronic Technology, Brno University of Technology, Brno 612 00, Czech Republic

[b] Vienna University of Technology, Vienna 1040, Austria

This paper studies the influence of scan rate on the results of potentiostatic polarization measurement of sintered materials. For best measurement precision, the optimal scan rate of the measurement has to be determined.

Introduction

Corrosion is a common phenomenon present in everyday life. Usually, it is associated with the negative effects of material deterioration. In the case of this paper, corrosion is studied in the context of wanted and controlled disintegration of biodegradable bone implants inside the human body. It is a part of a study of corrosion of various materials placed in conditions similar to the inside of the human body. For a better understanding of the nature of this kind of corrosion, a proper scan rate of the measurement technique needs to be chosen.

Theoretical analysis

When a metal corrodes, two reactions occur that change the composition of the material: the oxidation and reduction reactions. Oxidation is associated with the loss of electrons of the atoms inside the material, while reduction represents the gain of electrons. These two reactions are then responsible for a change in composition at the material's surface, called a passivation layer. It consists of a layer of compounds, which can protect the material against further corrosion (1).

During corrosion (in aqueous solutions), current density is measured in order to determine the rate of corrosion. In an ideal scenario, the current density comes solely from the corrosive reaction. In reality, there is another factor influencing current density. The interface between the solution and the material acts as a capacitor during the measurement, adding to the resulting current density. In order for the measured data to be accurate, this unwanted influence needs to be minimized. This is usually done by reducing the scan rate to a point where this disturbance is negligible. However, reducing the scan rate too much results in other issues, in particular the change in the material's structure (2,3). At the same time, local changes in the aqueous solution may also occur, resulting in a decrease in measurement accuracy at lower scan rates (4). A proper balance must, therefore, be found.

According to ASTM (American Society for Testing and Materials) Standard G61, the recommended scan rate is 0.6 V/h, or 0.1667 mV/s (5). Still, the most commonly found scan rates in academic literature are in the broad range of 10-0.1 mV/s (2). For example, for pure iron and magnesium, scan rates of 0.333 mV/s and 1 mV/s (respectively) were used in previous works (6,7).

It must be noted that the ideal scan rate varies for different materials and the aqueous solutions they are in. The different reactions present between these cases are too distinct to all be measured with the same rate. The ideal scan rate has to be determined on a case-by-case basis (2,4).

Measurement

Sample composition

The sample used in this study was an iron-magnesium alloy with polystyrene with a following composition: 9 g Fe + 1 g Mg + 2 g PS. After sintering, the polystyrene evaporated, leaving behind empty pockets that increase the porosity of the sample. The sample was submerged in 9 g/l NaCl solution on 13th of October and kept at a temperature of 37 °C.

Measurement procedure

The range of scan rates in this measurement was picked to be 100-0.1 mV/s. There were four measurements in total, performed all on the same sample. The measuring set up consisted of three electrodes: saturated calomel electrode as the referential electrode, platinum electrode as the counter electrode and a paraffin-impregnated graphite electrode (PIGE) as the measuring electrode. The resulting characteristics of the measurement are shown in Figure 1 below.

Measurement results

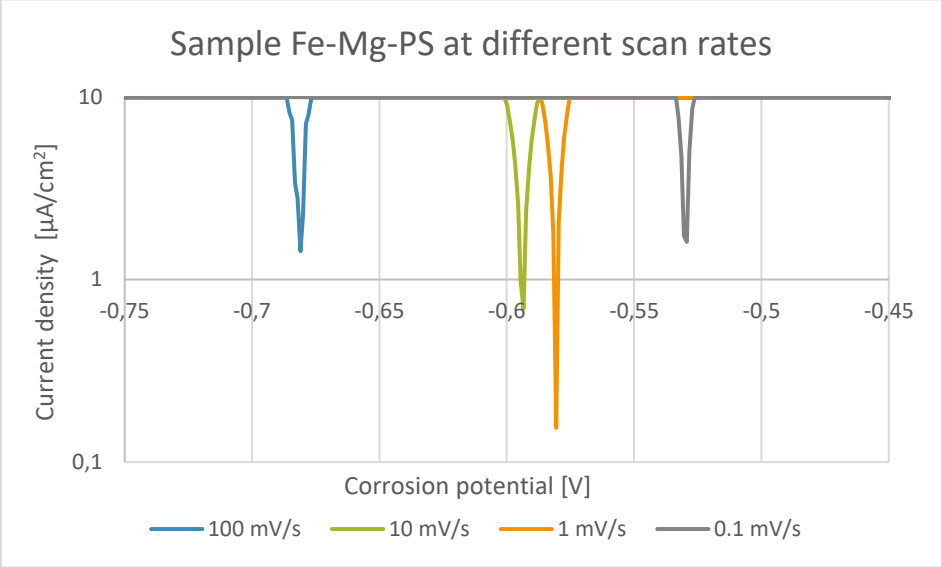

Figure 1. *Influence of scanning rate on the dependence of corrosion current density on corrosion potential*

From the graph is apparent that the values of corrosion potential kept getting higher with lower scan rates. At the same time, the values of current density were the highest at the ranges of the measurement, with the lowest current density value being at scan rate 1 mV/s. The results of the measurement are in Table 1.

TABLE I. *Results of the measurement.*

Scan rate [mV/s]	Corrosion potential, E_{corr} [V]	Current density, i_{corr} [µA/cm^2]
100	-0.68	4.92
10	-0.59	3.18
1	-0.58	2.81
0.1	-0.53	4.29

Conclusion

A theoretical analysis of the topic was performed, based on which the premise of the experiment took place. The scan rate range was chosen as 100-0.1 mV/s, based on its prevalence in other measurements in scientific literature. The experiment found that the values of corrosion potential increase with slower scan rates. This increase can be attributed to longer anodic and cathodic reactions. The values of current density also varied throughout the measurement, with the highest values appearing at rates 100 and 0.1 mV/s.

The most precise values are clearly in the range of 10-1 mV/s. For future experiments, a more detailed measurement of values from this range should be performed.

Acknowledgments

This work was supported by an internal grant "FEKT-S-23-8286 Materiály a technologie pro elektrotechniku V".

References

1. N. Perez, *Electrochemistry and Corrosion Science*. Boston, NY: Kluwer Academic Publishers (2004). ISBN 1-4020-7860-9
2. X. L Zhang, Zh. H. Jiang, Zh. P. Yao, Y. Song and Zh. D. Wu, Effects of scan rate on the potentiodynamic polarization curve obtained to determine the Tafel slopes and corrosion current density, *Corrosion Science*, **51**(3) (2009). doi: 10.1016/j.corsci.2008.12.005
3. S. Esmailzadeh, M. Aliofkhazraei and H. Sarlak, Interpretation of Cyclic Potentiodynamic Polarization Test Results for Study of Corrosion Behavior of Metals: A Review, *Protection of Metals and Physical Chemistry of Surfaces*, **54**(5) (2018). doi: 10.1134/S207020511805026X
4. D. A. Fischer, I. T. Vargas, G. E. Pizzaro, F. Armijo and M. Walczak, The effect of scan rate on the precision of determining corrosion current by Tafel extrapolation: A numerical study on the example of pure Cu in chloride containing medium, *Electrochimica Acta,* **313** (2019). doi: 10.1016/j.electacta.2019.04.064
5. ASTM International, *ASTM G61-86 (Reapproved 2024).*
6. R. Liu, Y. Cui, L. Liu and F. Wang, Study on the mechanism of hydrostatic pressure promoting electrochemical corrosion of pure iron in 3.5% NaCl solution, *Acta Materialia,* **203** (2021). doi: 10.1016/j.actamat.2020.11.009
7. L. Yang, X. Zhou, M. Curioni, S. Pawar, H. Liu, Z. Fan, G. Scamans and G. Thompson, Corrosion Behavior of Pure Magnesium with Low Iron Content in 3.5 wt% NaCl Solution, *Journal of The Electrochemical Society*, **162**(7), C362 (2015). doi: 10.1149/2.1041507jes

Distribution of Relaxation Times (DRT) for Determination of Internal Temperature of EV Battery Modules

M. Kemény[a], P. Ondrejka[a], D. Šišmišová[b], M. Mikolášek[a]

[a] Institute of Electronics and Photonics, Slovak University of Technology in Bratislava, Ilkovicova 3, 841 04 Bratislava, Slovakia

[b] ZTS – Výskum a Vývoj, a.s., Lieskovec 598/75, 018 41 Dubnica nad Váhom, Slovakia

This work analyses the suitability of the distribution of relaxation times (DRT) technique for determining the internal temperature of the electric vehicle (EV) battery module to enhance the safety of battery modules in EVs as well as in 2nd life applications. Temperature-dependent DRT features were recognized, and their ability to accurately determine the internal temperature of the module was evaluated. The analysis was done for temperatures ranging from 0 °C to 50 °C with a ten-degree step and for states of charge (SOC) ranging from 10% to 90% with a ten-percent step. This work suggests that DRT peaks corresponding to the highest and to the lowest of frequencies are promising features for determining the internal temperature of the EV battery modules.

Introduction

The greatest safety risk arising from using current batteries in on-board and 2nd life applications is the possibility of thermal runaways, leading to fire or explosion (1). Moreover, the usage of EV batteries outside of their recommended temperature window may lower their longevity (2). Therefore, it is of vital importance to monitor the internal temperature of battery modules (3). These temperatures are commonly assessed by the surface temperature measurements of the battery casing (4), however, this approach may easily lead to inaccurate temperature estimation arising from the thermal behavior of the cell/module casing. Therefore, it is desirable to develop on-board approaches for determining the internal temperature of the cells used in EV battery packs (5). DRT obtained via mathematical conversion of electrochemical impedance spectroscopy (EIS) data is a technique that enables the analysis of changes in electrochemical properties of the studied system while being highly sensitive to temperature changes, making it a promising candidate for determination of the internal temperature of the studied cell. This work provides an analysis of the temperature dependency of individual DRT features, while their suitability for assessing the internal temperature of EV modules is evaluated.

Experimental

In order to study the temperature dependency of DRT curves in EV battery modules, a 24 kWh Nissan Leaf module (2S2P) was used, while one parallel sub-module (2S1P) was used for EIS measurements. EIS measurements were executed for temperatures ranging from 50 °C to 0 °C and for SOC ranging from 90% to 10%. The temperature of the module was controlled in a climate chamber. To enable even heating/cooling of the module, a relaxation of 5 hours was allowed after all temperature changes.

Results and discussion

EIS measurements of 24 kWh Nissan Leaf sub-module (2S1P) were carried out at various temperatures and SOC and were processed by DRT analysis. The distinction of individual DRT peaks is shown in Figure 1a. The peak corresponding to the highest frequencies, Peak A, can be ascribed to the inductive properties of current collectors, Peak B to the properties of double-layers, Peak C follows the charge-transfer processes, and the peak for the lowest frequencies, Peak D, describes the diffusion of lithium ions. The DRT curves were calculated by standard Tikhonov regularization using $\lambda = 10^{-3}$ for all measured EIS data. The DRT curves for all studied temperatures at SOC 50% are shown in Figure 1b. From this plot, it is clear that all DRT peaks are increasing in their magnitudes with decreasing temperatures, while there are also observable shifts in time constants at which these peaks are manifested, mainly for Peak A. Figure 1c and Figure 1d display DRT curves for all studied SOC levels at 50 °C and 20 °C, respectively. At 20 °C, the magnitude of Peak B increases with decreasing SOC. At 50 °C however, Peak B for SOC above 40% disappears, pointing out that this feature is not suitable for the determination of the internal temperature of the studied EV battery module.

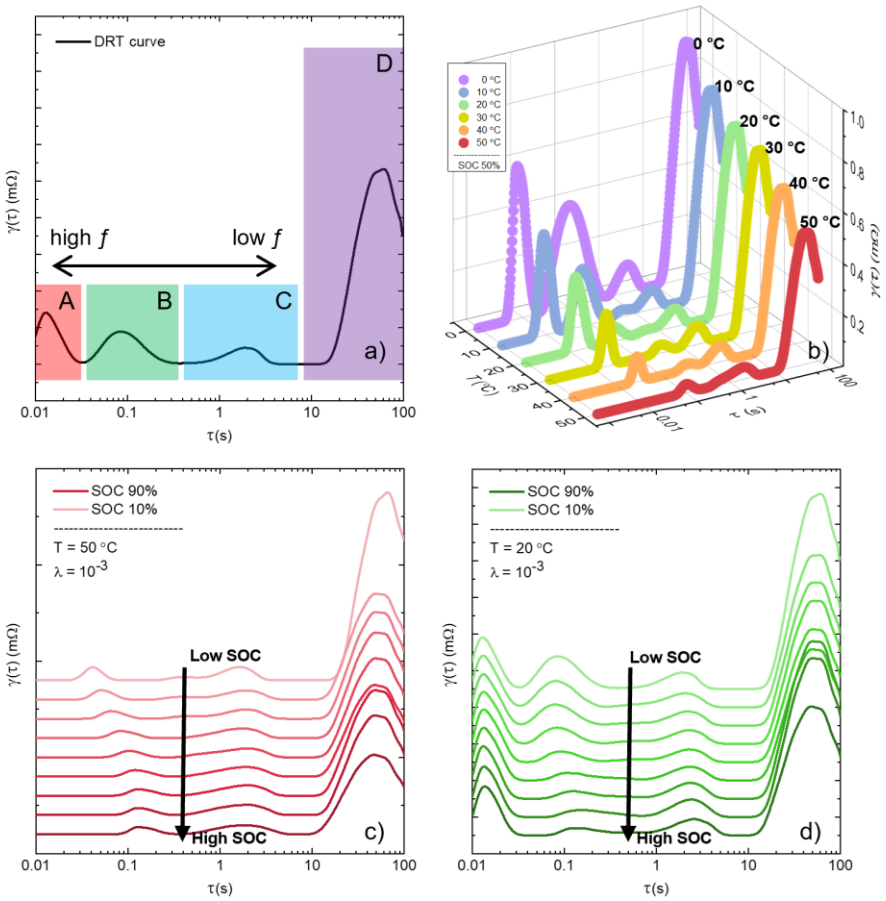

Figure 1. *a) Visual division of a DRT curve into four peaks; b) DRT curves for various temperatures at SOC 50%; and DRT curves for various SOC at c) 50 °C and d) 20 °C.*

The changes of magnitudes of all remaining DRT peaks for all temperatures at all SOC were fitted by logarithmic functions to study the ability of DRT peaks to determine the internal temperature. Absolute deviations ($|T_{DEV}|$) between the magnitudes of DRT peaks and between the fitted logarithmic functions were calculated, as plotted in Figure 2. Peak A at SOC above 50% shows a great ability to determine the temperature with $|T_{DEV,\ Peak\ A,\ MAX}| \leq 6$ °C, while for the lower

SOC, the deviation rises to 10 °C, making it insufficient to determine the temperature in the SOC ≤ 50% region (Figure 2a). Peak C suffers from insufficient accuracy across the range of studied SOC and temperatures, making it unsuitable for the purposes of temperature determination (Figure 2b). Peak D shows $|T_{\mathrm{DEV,\ Peak\ D}}| \leq 6$ °C across the entire range of SOC, suggesting its ability to determine the internal temperature of the module (Figure 2c). When comparing the ability of Peak A and Peak D to determine the internal temperature, Peak D outperforms Peak A with its ability to determine the temperature with desired accuracy for the entire SOC region, while Peak A enables such accuracy only for SOC above 50%.

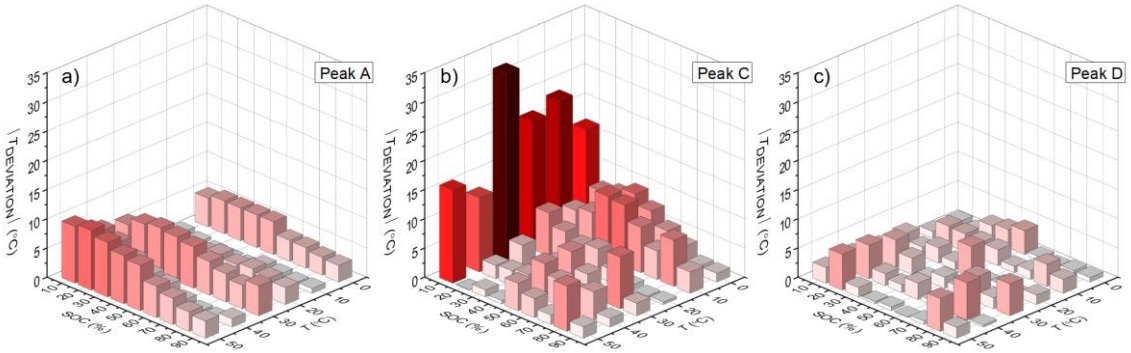

Figure 2. *Absolute deviations between the measured maxima values of individual DRT peaks at various SOC and T and the predicted values by the fitted logarithmic functions, where a) represents Peak A, b) Peak C, and c) Peak D deviations.*

Conclusion

This work provides insight into the abilities of DRT to determine the internal temperature of EV battery modules for EV on-board applications as well as for 2nd life applications. The EV module was analyzed via DRT at temperatures ranging from 0 °C to 50 °C at various SOC. Four individual DRT peaks were recognized. Analysis revealed that the tracking of peak A for SOC above 50% and peak D for the entire range of SOC led to satisfactory results for internal temperature estimation application.

Acknowledgments

This work was supported by the grants VEGA 1/0707/24, APVV-22-0132 and APVV-20-0111. Moreover, this work was supported within the Operational Programme Integrated Infrastructure for the project: Regeneration of used batteries from electric vehicles, ITMS2014+: 313012BUN5, which is part of the Important Project of Common European Interest (IPCEI), called European Battery Innovation in the Operational Program Integrated Infrastructure, call code: OPII-MH/DP/2021/9.5-34, co-financed from the resources of the European Regional Development Fund.

References

1. B. Xu, et al. Renewable and Sustainable Energy Reviews 150: 111437 (2021).
2. J. Edge, et al. Physical Chemistry Chemical Physics, 23.14: 8200-8221 (2021).
3. X. Zhang, et al. Energy Material Advances, 4: 0008 (2023).
4. T. Heenat, et al. Nature, 617.7961: 507-512 (2023).
5. M. Nascimento, et al. Journal of Power Sources, 410: 1-9 (2019).

A Current Pulse Response as an Alternative to EIS Measurements for Accurate Internal Temperature Estimation of Lithium-Ion Battery Cells

M. Novák[a], M. Kemény[a], and M. Mikolášek[a]

[a] Institute of Electronics and Photonics, Slovak University of Technology in Bratislava, Ilkovičova 3, 841 04 Bratislava, Slovakia

Electrochemical Impedance Spectroscopy (EIS) has become an essential tool for battery characterization. However, traditional EIS measurements suffer from limitations in real-world applications. This work proposes a novel approach to address these limitations by supplementing EIS measurements with pulse measurements. The results revealed a strong correlation of impedance obtained from EIS and pulse excitations. Moreover, a possible utilization of such data for internal temperature estimation is discussed.

Introduction

Electrochemical Impedance Spectroscopy (EIS) is one of the dominant techniques for lithium-ion battery (LIB) characterization, capable of providing valuable insights into internal processes and parameters (1) that influence health and safety of LIBs. However, traditional EIS measurements can have limitations in real-world applications. This study provides DTR analysis of EIS measurements for internal temperature estimation and proposes a novel approach to supplement EIS measurements with pulse measurements. Pulse measurements offer a faster approach of the LIB's electrochemical processes characterization by applying current pulses during LIB charging and discharging. This study focuses on the extraction of the real part of the impedance (Z_R) from the pulse responses and analysis of the possible utilization of Z_R for temperature estimation. Z_R of LIBs is a parameter that varies significantly with the LIB's state of charge (SOC), current load, and temperature (2). Low temperatures can have a critical impact on the performance of LIBs, leading to an increase in internal resistance, decrease in capacity (3) and development of lithium plating. Z_R has been identified as the best EIS indicator for estimating cell temperature (4). This approach aims to bridge the gap between the traditional EIS measurements conducted in ideal laboratory conditions and between the dynamic nature of real-world conditions of LIB operation.

Experimental

In this study, NMC811 Li-ion cells by Molicel (INR-21700-P45B LIB) are analyzed using a battery cycler (Neware BTS4000 series 5V6A) and potentiostat-galvanostat (Gamry Interface 5000P). The measurements were conducted in a climate chamber at temperatures ranging from 20 °C to 50 °C in two parallel approaches. In the first approach, galvanostatic EIS measurements are conducted for the entire range of SOC with 10% step, while the level of SOC was changed via 0.8 A constant current pulses (both charge and discharge). Prior to all EIS measurements relaxation period of 30 minutes was allowed, while OCV was measured. The second approach is based on charging and discharging via 5 A current pulses, while for each 5% change in SOC, the current is lowered to 4.5 A for 60

seconds, and the voltage changes are monitored. The experiment was repeated via 0.8 A pulses, while in this scenario, to monitor the voltage changes, the current was being lowered to 0 A for 60 seconds. Moreover, various magnitudes of the current pulses (varying from 1 A to 5 A) are studied to gain insight into the longest usable measurement interval.

Results and discussion

The EIS measurements at SOC 50% at various temperatures represented as Nyquist plots are displayed in Fig. 1a. From the temperature development of these plots, it is clear that all impedance features are decreasing with increasing temperature. DRT was calculated using standard Tikhonov regularization ($\lambda = 10^{-3}$). These DRT curves consist of four recognizable peaks (Fig. 1b). Such peaks can be ascribed to four individual electrochemical and dynamic processes. Individual DRT features are sensitive to temperature changes, and hence have potential to be used to assess the internal temperature of the studied system (5). To analyze the ability of these peaks to determine the internal temperature of studied NMC 811 LIB cells, the magnitudes of individual DRT peaks were fitted by logarithmic functions, as displayed in Fig. 1c. This analysis suggests that DRT, primarily the feature ascribed to Peak C, is a promising method when it comes to on-board determination of internal temperature the studied cells.

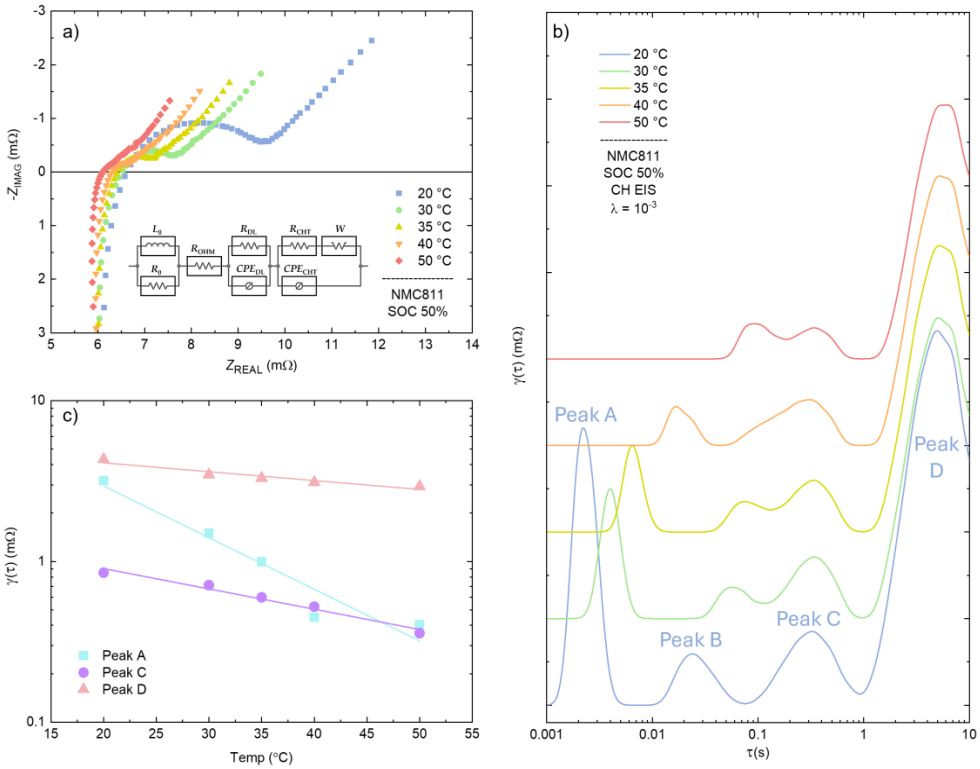

Figure 1. *a) Nyquist plots for NMC811 at SOC 50% at various temperatures; b) DRT curves calculated using standard Tikhonov regularization; c) Magnitudes of DRT peaks recognizable across all studied temperatures.*

Moreover, when analysis EIS data via data-fitting, it is necessary to describe the system by a suitable equivalent circuit model (ECM), however, it is quite challenging to

construct the ECM solely based on visual analysis of EIS data, since LIBs are complex systems consisting of many electrochemical and dynamical processes. Hence, to construct correct ECM requires a great understanding of the system and additional analysis. For such additional analysis,

DRT can be used. This technique deconvolutes EIS data from frequency domain into time domain and enables to distinguish between individual electrochemical and dynamical processes with greater clarity.

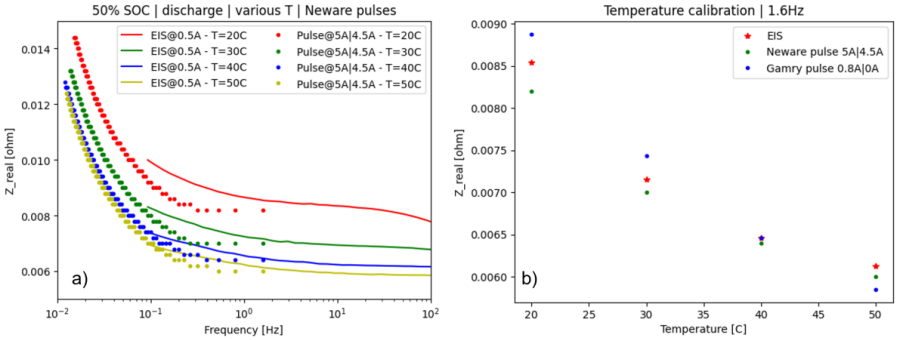

Figure 2. *a) Comparison of Z_R parameters calculated from 60s pulses and EIS measurement. b) Inverse correlation between the Z_R parameters and between the temperature of studied NMC811 LIB cell.*

The values of Z_R calculated from the voltage arising from the current pulse change from 5 A to 4.5 A and from 0.8 A to 0 A, as well es Z_R obtained from EIS, can be seen in Fig. 2a. The results revealed a strong correlation between the EIS measurement and the pulse measurements. The relationship between the internal temperature and the internal resistance of LIB is inversely correlated (Fig. 2b). These results strongly indicate that the analysis via pulse measurements during real-world applications is a suitable method to effectively supplement in-lab EIS measurements, hence it is a promising approach for ensuring the effective use of LIBs within the safety conditions.

Acknowledgments

This research was funded by the Ministry of Education, Science, Research, and Sport of Slovakia under the grant VEGA 1/0707/24; and by the Slovak Research and Development Agency under grants APVV-20-0111, APVV-22-0132, and STU internal grant ESG 23-03-15-A. This work was supported by an Industry Cooperation funded by Infineon Technologies Austria AG in the course of IPCEI Microelectronics.

References

1. D. Guo, et al. *Energies*, 13, 915, (2020).
2. D. Stroe, et al. *Tenth International Conference on EVER*, (2015).
3. J. Jun, et al., *Energy Proceedings*, (2024).
4. I. Lalinde, et al. *IEEE 32nd ISIE*, (2023).
5. M. Jung, et al. *Journal of Power Sources*, 611, (2024).

Development of Machine Learning Methods for State of Charge Estimation of Li-ion Batteries: A Comparative Study

Mitchell Rae[a], Michela Ottaviani[b,c], Dominika Capkova[c,d], Tomáš Kazda[d], Luigi Jacopo Santa Maria[c], Kevin M. Ryan[c], Stefano Passerinie, Mehakpreet Singh[a,*]

[a]Mathematics Applications Consortium for Science and Industry (MACSI), Department of Mathematics and Statistics, University of Limerick, Limerick V94 T9PX, Ireland

[b]Department of Applied Sciences, Technological University of the Shannon, Moylish Campus, Limerick V94EC5T, Ireland

[c]Department of Chemical Sciences and Bernal Institute, University of Limerick, Limerick V94 T9PX, Ireland

[d]Department of Electrical and Electronic Technology, Faculty of Electrical Engineering and Communication, Brno University of Technology, Brno, Czech Republic

[e]Helmholtz Institute Ulm (HIU) für Elektrochemische Energiespeicherung, Helmholtzstraße 11, 89081 Ulm,Germany

Abstract

In today's technologically advanced world, the rapidly growth of applications for Li-ion batteries (LIBs) is creating a fierce demand for improved battery production, monitoring, and testing technologies. The global push to reach sustainability goals as proposed by The Paris Agreement - UNFCCC has driven a significant acceleration in the implementation of electric vehicles. By 2022, the number of electric cars alone on the road exceeded 26 million, marking a 60% increase compared to 2021 and surpassing more than five times the stock recorded in 2018 (Trends in electric light-duty vehicles – Global EV Outlook 2023 – Analysis - IEA). This advancement must be supported by effective technologies that can secure the safety and reliability of the LIBs in use. Furthermore, significant advancements in the mathematical modelling of LIBs and their properties during all life phases is crucial to the success of climate change and sustainability efforts.

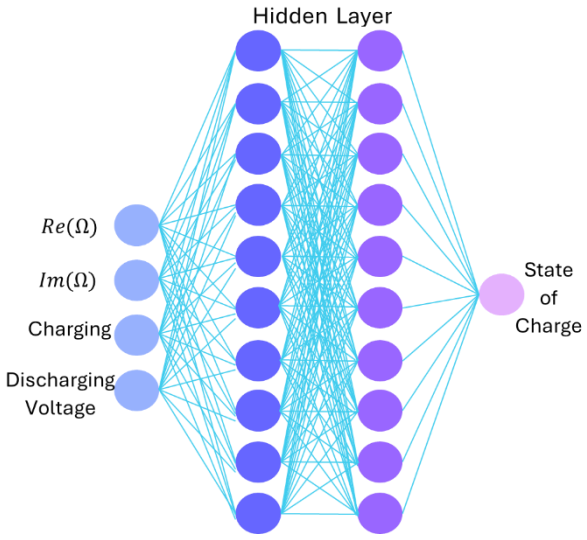

This research delves into the application of artificial neural networks (ANNs) for predicting the state of charge (SOC) of Li-ion batteries (LIBs). ANNs are a mathematical tool that attempt to mimic the natural information processing of the brain. ANNs consist of an input layer for the explanatory variables which feed into the hidden layer. The hidden layer is considered a black box process in which the input variables are manipulated through activation functions and learning algorithms such that they reach the output layer with the correct value. The training process is completed by comparing the initial outputs with a training dataset, errors between the predicted and expected outputs are propagated through the network such that the subsequent outputs approach the expected values. Repetition of this process is called *training*. Once complete, the ANN, if successful, will accurately predict the output of a new dataset which we call *testing*.

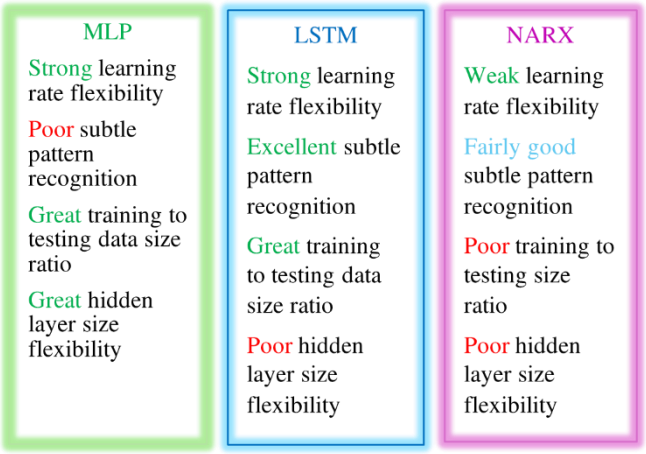

The study scrutinizes three prevalent ANN architectures: the nonlinear autoregressive (NARX) model, the multilayer Perceptron (MLP) model, and the long short-term memory (LSTM) model. The examination targets the architectural differences and the role they play in performance, flexibility, and adaptability of each model regarding its aptitude to make accurate predictions with changes to the initial set up and the adjustable ANN parameters. The performance is assessed based on computational cost (in seconds and in number of computations), overall predictive accuracy, and its flexibility of parameters including the learning rate, hidden layer size, number of iterations, and the proportion of training and testing datasets. The statistical values used for this analysis include adjusted R^2 and relative error between the exact and predicted measurements. Furthermore, the portion of data used for testing and validation is in no way used in the training, this is to maintain the integrity of the evaluation methods.

This research utilized experimental data from Samsung INR18650-35E cells featuring NMC chemistry. The cell was charged at 0.1 C and discharged at 0.5 C over 100 cycles. Two cycles at 0.1 C for both charging and discharging were conducted before cycling, and after 50 and 100 cycles. The first cycle served as a pre-conditioning step to erase the cell's 'cumulative history', while the second cycle measured the actual charge and discharge capacity prior to the EIS measurement at various SOCs. Greater correlation between ANN prediction accuracy was observed for EIS measurements taken at 0% SOC, therefore, only this data was used in ANN modelling.

The MLP and LSTM were found to outperform the NARX in most areas. Specifically, the LSTM exhibited superior pattern recognition when the learning rate was decreased, while the MLP demonstrated greater parameter flexibility. Further comparisons of strengths and weaknesses are drawn between the models to outline their key characteristics. To this extent, the reader of this research gains two things: 1) the knowledge of which of these three leading ANN designs is the most successful in SOC prediction of LIBs and the adaptability of each model; and 2) the method of how

to judge and assess the general performance of an ANN and how to efficiently select an appropriate ANN model for their data.

In this way, the research fills a significant gap in the literature by addressing the challenges of selecting an appropriate ANN model for a given task. Furthermore, the use of coarse data for the training process in this study demonstrates the plausibility of reducing experimental cost and labour during the production of commercialised cells. The importance of machine learning in battery research is highlighted, particularly its potential to reduce waste, experimental labour, material waste, and costs. The use of ANNs in monitoring battery states contributes to the safe use of batteries and promotes sustainability. This research provides valuable insights into the role of machine learning in advancing the development of Li-ion batteries for electric vehicles.

Advanced in-situ SEM Analysis of Electrode Structural Changes in Li-ion Coin Cell During Cycling

D. Trochta[a, b], O. Klvač[a, b], T. Kazda[a], L. Novák[b]

[a] Department of Electrotechnology, Brno University of technology, Brno 616 00, Czech Republic

[b] Thermo Fisher Scientific Brno, Vlastimila Pecha 12, Brno 627 00, Czech Republic

This paper provides a concise overview of in-situ experiments conducted within a scanning electron microscope to study lithium-ion batteries. These experiments allow for real-time observation of changes in the electrode structure, which can be correlated with electrochemical measurements. By employing this characterization method, we can gain deeper insights into the internal processes occurring within batteries during charging and discharging cycles. Consequently, this knowledge can be leveraged to optimize the key properties and performance of lithium-ion batteries.

Introduction

Although lithium-ion (Li-ion) batteries are widely used and applicable across various fields, challenges related to their performance, safety, and lifespan persist. Consequently, ongoing research focuses not only on developing new types of materials but also on devising efficient methods to investigate Li-ion batteries. These methods aim to provide valuable insights into their performance, ultimately leading to enhancements in their overall functionality and reliability. [1; 2]

These methods include in-situ scanning electron microscopy (SEM) cycling, which offers valuable data on electrode changes during cycling. The primary advantage of SEM is the high-resolution imaging it provides. Additionally, these images, along with the observed electrode changes and internal processes, can be interpreted in the context of electrochemical measurements in real time, enhancing the overall understanding of the battery's behavior [3; 2; 4]. In this paper, we present our in-situ experiments with Li-ion batteries and the obtained results.

Experimental

For our experiments, we employed a classical coin-cell 2032 battery design, which we modified to enable direct observation and operation within a SEM. The modifications included creating an observation window in the battery case prior to assembly. Additionally, several significant changes were necessary for the experiment itself. The electrode under investigation, positioned directly beneath the observation window, was coated on a grid-current collector to facilitate direct observation of the electrode material. Lastly, we replaced the conventional organic solvent-based electrolyte with an ionic liquid-based electrolyte to prevent evaporation of the electrolyte in the vacuum environment.

As anodes, we used commercial lithium titanate (LTO) electrodes from Custom Cells. Before use, the electrodes were dried in a vacuum oven at 110 °C for 24 hours. The electrodes (cathodes)

under investigation required in-house fabrication to be coated on a grid-current collector. For this purpose, lithium nickel manganese cobalt oxide (NMC) 4:2:2 was used, with Super P and a polyvinylidene fluorid (PVDF) binder in a final ratio of 8:1:1. N-Methyl-2-pyrrolidone **(**NMP) served as the solvent for the binder. The electrode slurry was stirred for one day using a magnetic stirrer at 550 rpm. The mixture was then applied to an aluminium grid current collector using a 200 µm coating bar. After drying in an oven at 60 °C, 16 mm discs were die-cut and subsequently pressed with a 1000 kg/cm2. The electrodes were further dried in a vacuum oven at 110 °C for 24 hours before being transferred to a glove box with an argon atmosphere. The coin cells were then assembled in the box. A 16 mm diameter glass fiber separator from Whatmann was placed between the electrodes and filled with 80 µl of ionic liquid-based electrolyte, specifically 0.5M LiTFSI in 1-Butyl-3-methylimidazolium bis(trifluoromethylsulfonyl)imide (BMIIm).

For the experiment, we utilized a Quattro electron microscope from Thermo Fisher Scientific, which also provided a specially designed stage and holder (Figure 1) to accommodate and electrically connect the coin cells. Electrical contacts were routed through a vacuum feedthrough to an SP-150 potentiostat from Biologic, which managed the electrochemical measurements. Synchronization and data processing from both the electron microscope and the potentiostat were handled using a custom Python script.

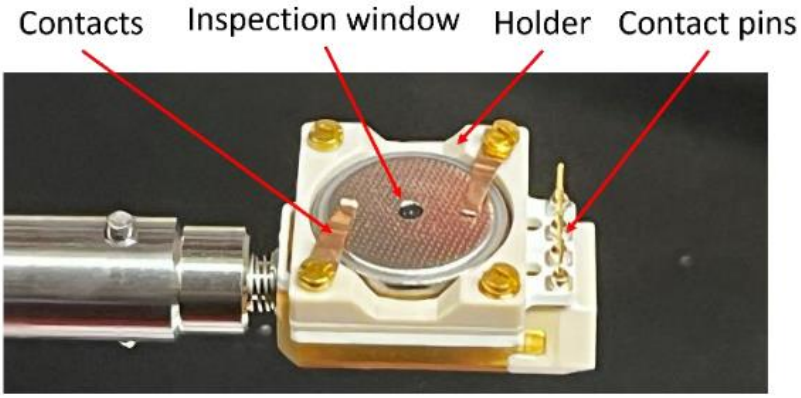

Figure 1: *Coin cell placement in the holder*

Results

The typical output of our experiments consists of videos that display SEM images and electrochemical data side by side, facilitating easy interpretation. Figure 2 illustrates an example of galvanostatic cycling (GCPL) at a current of 0.5 C. In addition to GCPL, the script is also capable of processing cycling voltammetry (CV) data in the same manner, ensuring comprehensive analysis and visualization of the experimental results.

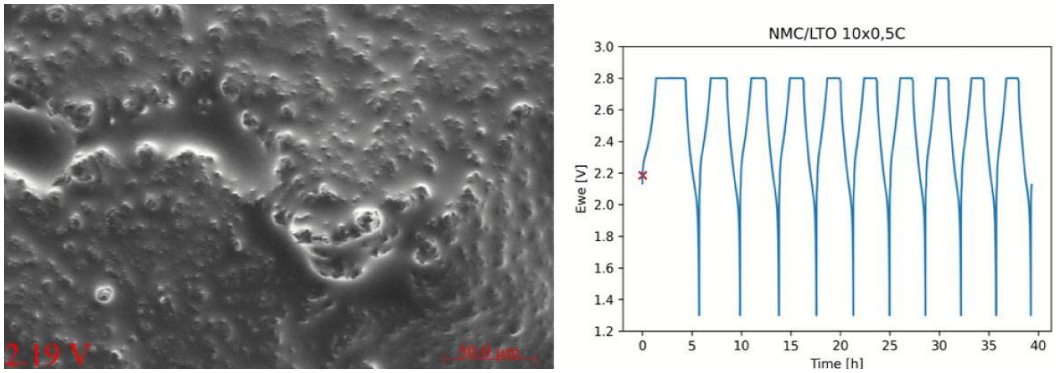

Figure 2: *Example of a typical GCPL measurement output*

During cycling, mainly volumetric changes due to thermal expansion and the processes of lithiation and delithiation can be observed. However, other associated phenomena that occur during cycling can also be investigated. This is the case, for example, of the cracking of the electrode material shown in Figure 3. Cracks are probably caused by uneven charging or discharging because the examined area is far from the current collector.

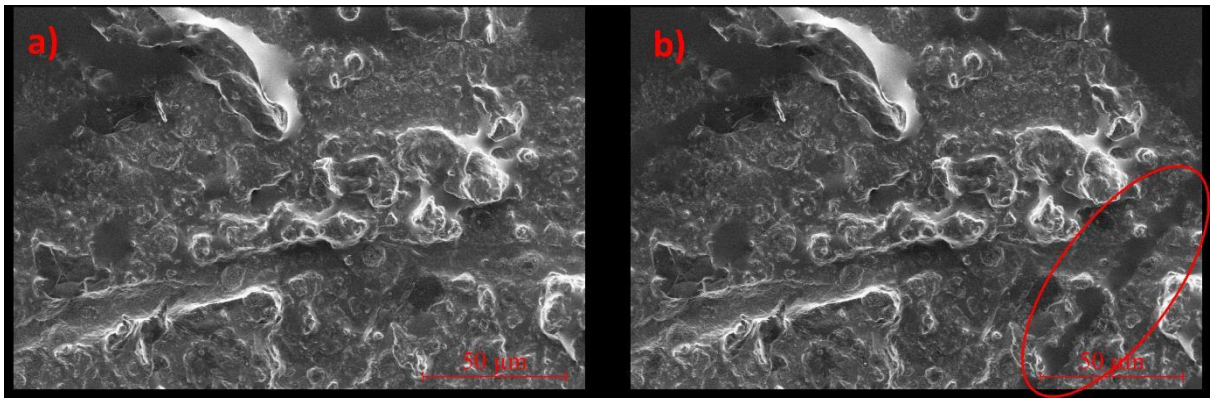

Figure 3: *a) before the start of the experiment; b) after the cycling with the crack*

Conclusions

Overall, several in-situ battery cycling experiments were conducted using SEM, revealing that volume changes during cycling and other associated phenomena can be observed and interpreted within the context of electrochemical measurements. Once optimized, this method proves to be relatively straightforward and can be applied to investigate a variety of other battery materials, providing valuable insights into their behavior during cycling. However, a limitation of this setup is that only one electrode can be observed from a top view at a time, preventing the acquisition of comprehensive information about the entire system's complex behavior.

Acknowledgments

This work was supported by the specific graduate research of the Brno University of Technology No. FEKT-S-23-8286 and created in cooperation with Thermo Fisher Scientific Brno.

References

1. A. D. A. Bin Abu Sofian, I. S. Imaduddin, S. R. Majid, T. A. Kurniawan, K. W. Chew, C. - H. Lay, and P. L. Show, *Journal of Cleaner Production*, vol. 435, (2024).
2. J. Wu, M. Fenech, R. F. Webster, R. D. Tilley, and N. Sharma, *Sustainable Energy & Fuels*, vol. 3, no. 7, pp. 1623-1646, (2019).
3. S. Zhou, K. Liu, Y. Ying, L. Chen, G. Meng, Q. Zheng, S. -G. Sun, and H. -G. Liao, *Current Opinion in Electrochemistry*, vol. 41, (2023).
4. D. Chen, S. Indris, M. Schulz, B. Gamer, and R. Mönig, *Journal of Power Sources*, vol. 196, no. 15, pp. 6382-6387, (2011).

HPPC Data Preparation for Reduced Order Model of Li-Ion Battery

P. Vyroubal[a], T. Kazda[a]

[a] Department of Electrical and Electronic Technology, Brno University of Technology, Technická 10, 616 00 Brno, Czech Republic

This paper deals with the preparation of HPPC (Hybrid Power Pulse Characterization) data for the ECM model of Lithium ion battery. This is a semi-empirical model that is used to describe the battery behavior and can be very well used in the field of digital twins, as it eliminates the problem of solving partial differential equations. The applicability of this model is then primarily not in the material development of LIBs, but rather in the application domain, where we are very quickly able to obtain a description of how the battery behaves in a given application.

Introduction

In today's world, there is a growing focus on renewable energy sources and the efficient use of electric vehicles (EVs), which places increased demands on accurate and reliable battery modeling. Lithium-ion batteries play a crucial role in this context due to their high energy density and long lifespan. To optimize their performance and ensure safety, it is essential to develop accurate mathematical models that can predict their behavior under various operating conditions [1].

One of the key tools for obtaining relevant data for battery modeling is Hybrid Pulse Power Characterization (HPPC). HPPC tests allow for the determination of dynamic properties of batteries, such as resistance and capacity, at different state of charge (SoC) levels. These tests are critical for creating a Reduced Order Model (ROM), which simplifies the complex electrochemical processes within the battery into a form suitable for real-time implementation in embedded systems [2].

The aim of this article is to describe the methodology for acquiring and processing HPPC data for the creation of a ROM battery model. First, we will focus on a detailed description of HPPC tests, their execution, and specifics. Next, we will discuss the analysis of the obtained data and its transformation into a form suitable for ROM modeling. Finally, we will present a specific implementation of the ROM model and demonstrate its validation based on experimental data [3].

Reduced Order Model (ROM)

Reduced Order Models (ROM) represent an effective tool for simulating battery behavior in real-time, which is crucial for Battery Management Systems (BMS) in electric vehicles (EVs) and other energy storage systems. ROM models simplify the complex electrochemical processes within the battery into a form that is computationally less demanding but still sufficiently accurate for performance prediction.

Hybrid Pulse Power Characterization (HPPC) tests are a standard method for obtaining the data needed to create ROM models. These tests involve applying a series of charge and discharge pulses to the battery and measuring the voltage response. The resulting data provides key information on the battery's dynamic properties, such as internal resistance and capacity at various state of charge (SoC) levels.

The process of developing a ROM model begins with the collection of data from HPPC tests, which is then analyzed and processed to extract relevant parameters. These parameters are subsequently integrated into a mathematical model that simplifies the battery's behavior into a few state variables. The resulting ROM model can quickly and efficiently predict battery behavior under different operating conditions, which is crucial for optimizing battery performance and longevity in real applications.

The validation phase involves comparing the outputs of the ROM model with experimental data to ensure its accuracy and reliability. This step is essential to verify that the model can faithfully reproduce the actual behavior of the battery.

The advantage of using ROM models lies in their ability to provide fast and accurate predictions, which is necessary for effective real-time battery management. This enables BMS systems to better monitor and optimize battery performance, leading to increased lifespan and reliability in applications such as electric vehicles and energy storage systems.

Hybrid Power Pulse Characterization (HPPC)

Figure 1 shows an example of HPPC experimental data measured on a 18650 Li-Ion battery with a capacity of 2600 mAh.

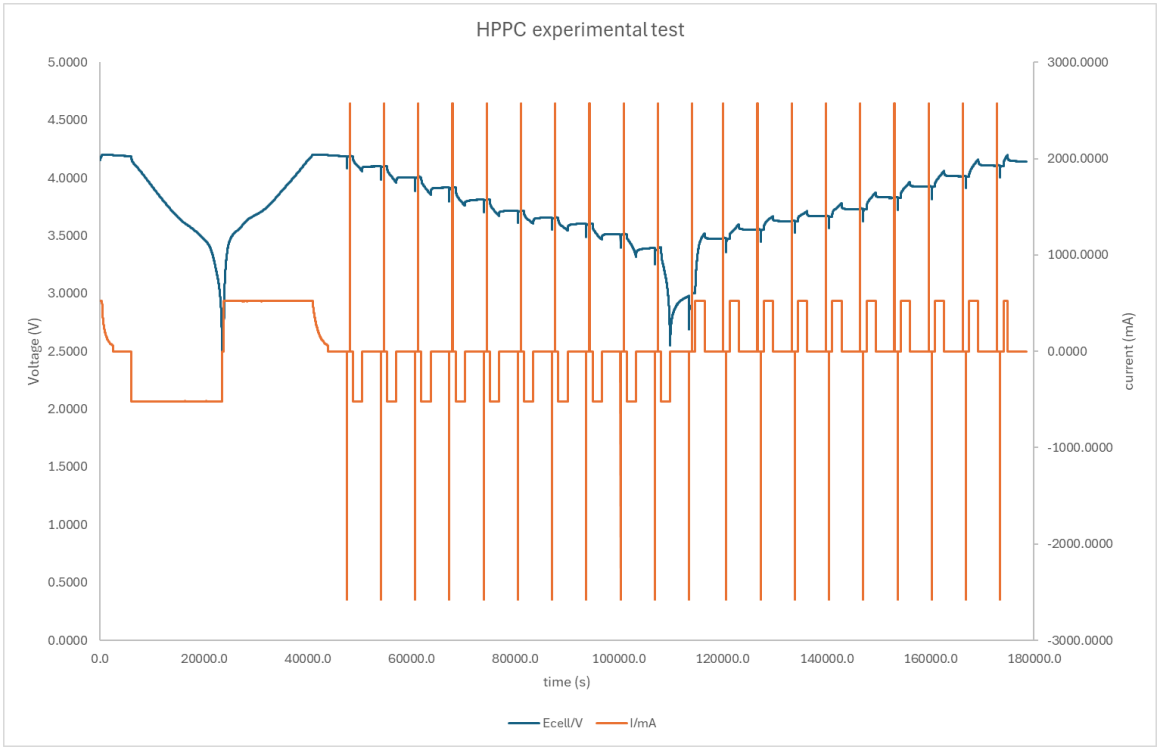

Figure 1. *HPPC data for 23 °C 18650 Li-Ion battery.*

Hybrid Pulse Power Characterization (HPPC) is a standardized testing method used to evaluate the dynamic performance of batteries. The HPPC test involves applying a sequence of charge and discharge pulses to the battery and recording the voltage response. This test is typically conducted at various state of charge (SoC) levels to obtain a comprehensive overview of the battery's behavior.

During the HPPC test, the battery is initially fully charged to 100% SoC. It is then subjected to a series of discharge pulses, with each pulse followed by a rest period during which voltage is

measured. This cycle is repeated at gradually decreasing SoC levels, often in steps of 10%. After reaching a low SoC level (e.g., 10%), the battery is fully charged again, and the entire process is repeated for charge pulses.

The data obtained from the HPPC test allows for analysis of key parameters such as internal resistance and capacity of the battery, which are essential for developing accurate battery models, including Reduced Order Models (ROM). This data is also critical for optimizing battery performance and longevity in real-world applications such as electric vehicles and energy storage systems.

Conclusion

Hybrid Pulse Power Characterization (HPPC) is a crucial method for obtaining dynamic battery properties essential for developing accurate mathematical models like Reduced Order Models (ROM). This test evaluates internal resistance, capacity, and other parameters at various state of charge (SoC) levels, critical for optimizing battery performance and lifespan in electric vehicles and energy storage systems.

Proper interpretation and processing of HPPC test data are crucial for accurately simulating battery behavior in ROM models. Integrating these data enables real-time battery management, enhancing safety, reliability, and performance across applications.

The significance of HPPC tests is growing alongside the rise of electric vehicles and renewable energy sources, where precise battery state prediction and control play an increasingly vital role in the sustainable energy sector. Continued advancements in this area are expected to further enhance battery utilization and efficiency in modern energy systems.

Acknowledgments

This work was supported by the specific graduate research of the Brno University of Technology No. FEKT-S-23-8286.

References

1. Zhang, Y., & Wang, C. Y. (2009). Battery Systems Engineering. John Wiley & Sons.
2. He, H., Xiong, R., Guo, H., & Li, S. (2012). Comparison study on the battery models used for the energy management of batteries in electric vehicles. Energy Conversion and Management, 64, 113-121.
3. Plett, G. L. (2004). Extended Kalman filtering for battery management systems of LiPB-based HEV battery packs: Part 1. Background. Journal of Power Sources, 134(2), 252-261.

Corrosion of Fe-Mg Material in 0.9 % NaCl Solution

Petra Slotová[a], Marie Sedlaříková[a], Pavel Čudek[a]

[a] Department of Electrical and Electronic Technology, FEEC, Brno University of Technology, Brno, Czech Republic

This paper addresses the topic of biodegradable bone implants. Currently, titanium alloys, known for their ability to reinforce bone structure, are utilized for fracture fixation. Nevertheless, post-healing, their extraction from the body becomes necessary. Biodegradable implants serve the same purpose but undergo gradual degradation upon exposure to bodily fluids. Consequently, the need for additional surgical procedures for their removal is obviated.

Introduction

This paper deals with biodegradable sintered materials based on iron and their corrosion. Nowadays, titanium-based materials are mainly used for this purpose, as they have excellent mechanical strength and other properties. However, after partial healing of the fracture they must be surgically removed. Biodegradable materials based on inorganic substances such as iron, magnesium or zinc could help prevent further surgical intervention. The bone support will be gradually absorbed by the corrosion processes and safely removed from the patient's body [1], [2].

Corrosion is a spontaneous, gradual transformation of metals or non-metallic organic and inorganic materials. It arises as a result of a chemical or electrochemical reaction of the basic material with the external environment. It consists of an anodic and a cathodic reaction, which are interconnected, and one cannot occur without the other unless an external current is passed through the corroding metal. The anodic reaction represents the oxidation of the metal [3].

Preparation of samples

The production of the biodegradable bone implant samples was carried out in the following steps. First of all, it was necessary to prepare the material for sintering. The mixture was made by mixing metal powder (9 g Fe) with magnesium (1 g Mg) and polystyrene (0.5 g PS). The next step was the sintering of the material. The sintering was carried out in two stages. First, the sample was exposed to temperatures of 450 °C for one hour, at which time the polystyrene was baked out of the sample. During the next two hours it was exposed to up to 1 000 °C and gradually cooled. After this the solid material was ready for insertion into the corrosive environment. The entire sintering was carried out in an inert atmosphere in the presence of argon [2].

After sintering, the sample was submerged into a 30 ml solution of 9 g/l NaCl. The sample soaked in the solution was then placed in a 37 °C environment to simulate human body temperature [2].

Energy dispersive X-ray analysis

Energy dispersive X-ray analysis is an analysis that is used to determine the distribution of elements in a sample and their percentages. It was performed on the sample three times: before it being embedded in solutions, then 3 and 8 months after embedding. The area from which the elemental analysis was performed may have played an important role in determining the elemental composition [3].

EDAX analyses of Sample

In Fig. 1, the structures of the sample are captured using backscattered electrons at different times after immersion in the solution. Table 2 summarizes the detected amount of each element after each analysis. Before immersion in the solution, iron is the most abundant element in the sample, which is consistent with expectations. Other elements found were carbon, magnesium, and oxygen. The carbon here represents the residue left over after the polystyrene was burnt away. After immersion in the solution, the composition percentage changed. The amount of carbon and magnesium decreases. The amount of oxygen increases after soaking, which is due to the decomposition of water. The amount of iron first decreases and then increases, which is due to the proportionate decrease of other elements. The composition percentage is in Table 1.

TABLE I. *Spectroscopy results of a sample with 0.5 g of polystyrene.*

	Before wetting		**After 3 months**		**After 8 months**	
Element	Norm. C/wt.%	Atom. C/at.%	Norm. C/wt.%	Atom. C/at.%	Norm. C/wt.%	Atom. C/at.%
Iron	60.27	34.53	56.92	29.74	69.05	39.21
Carbon	4.98	13.27	6.43	15.63	3.14	8.28
Magnesium	25.33	33.35	19.61	23.54	3.87	5.05
Oxygen	9.42	18.85	17.04	31.08	23.94	47.45

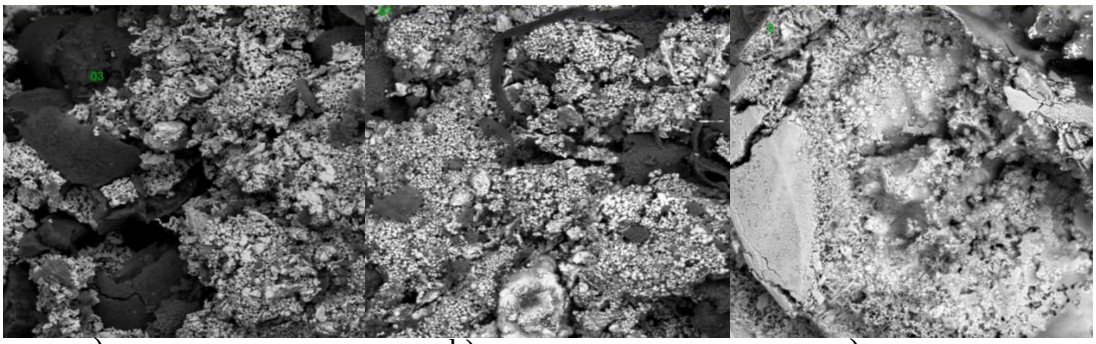

a) b) c)

Figure 1. *BSE images of a sample with 0.5 g of polystyrene a) before wetting, b) after 3 months, c) after 8 months*

Conclusion

This work is primarily focused on long-term monitoring of sample degradation in physiological solution. EDAX analysis was used to monitor the change in the percentage of each element in the sample.

Based on the results, it can be said that magnesium is indeed released and excreted into solution. As far as carbon is concerned, same behavior can be observed as well, since both elements (Mg and C) bind to oxygen and form oxides. On the other hand, the amount of oxygen increases, which is due to the decomposition of water. In the case of iron, it is not yet clear. According to the numbers, it looks like its amount first decreases and then increases, which is not actually the case. There is indeed a degradation of iron, just slower than for the other elements. Thus, as the numbers decrease rapidly for other elements, they must increase again somewhere else (the total must still be 100 %).

In conclusion of this paper, iron-based materials containing magnesium and polystyrene do indeed degrade over time and it makes sense to continue to monitor them over a longer time horizon.

Acknowledgments

The completion of this paper was made possible by the grant FEKT-S-23-8286 -" Materials and technologies for electrical engineering V" financially supported by the Internal science fund of Brno University of Technology.

References

1. Sun, Jie, Annika Hammerle, Gunter Fafilek, et al. *Electrochemical investigation for understanding the bactericidal effect of Cu_2Se and Ag_2Se for biomedical applications.* Journal of Applied Electrochemistry. 2021, (52), 15.
2. Hrubovcakova M., Kupkova M., Dzupon M. *Fe and Fe-P Foam for Biodegrada- ble Bone Replacement Material: Morphology, Corrosion Behaviour, and Mecha- nical properties.* Institute of Materials Research of SAS, Kosice, Slovakia. September 29, 2016.
3. Scimeca, M., Bischetti, S., Lamsira, H. K., Bonfiglio R., Bonanno, E. *Energy Dispersive X-ray (EDX) microanalysis: A poweful tool in biomedical research and diagnosis.* European Journal of Histochemistry. 2018, 62.

Development and Parameterization of a Realtime Thermal Model as an Extra Safety Layer for Battery Management Systems

M. Ceylan[a]

[a] Department of Electronics Engineering, Gebze Technical University, Kocaeli, Turkey

Temperature is a vital aspect for safe and efficient operation of battery packs, and it must be carefully monitored by a battery management system (BMS) during operation. Thermal models (TM) are valuable tools for estimating temperature and providing information for predictive control. There are very advanced 1D to 3D thermal models available that can simulate the heterogeneous temperature distribution of a cell or an entire pack of many cells, however they are mostly used for extensive analysis during the initial pack design stage or thermal safety simulations, and are not fast enough to be practically implemented in BMS applications that typically employ low power embedded microcontrollers. In this work, a safety oriented, simplified 0D thermal model with very low computational cost was developed and validated. Parameterization of specific heat capacity and heat transfer coefficent, without the need for expensive calorimeters, is also presented.

References

1. Bernardi D., Pawlikowski E., Newman J., "A General Energy Balance for Battery Systems", *Journal of the Electrochemical Society*, **132**, 1 (1985).
2. von Böch P., Wetzel T., "Heat Transfer, Basics and Practice", *Springer* (2012).
3. He F., Li X., Ma L., "Combined experimental and numerical study of thermal management of battery module consisting of multiple Li-ion cells", *International Journal of Heat and Mass Transfer*, 7, 622-629 (2014).
4. Li W., Wang X., Cen P.Y., Chen Q., De Cachinho Cordeiro I.M., Kong L., Lin P., Li, A., "A Comparative Numerical Study of Lithium-Ion Batteries with Air-Cooling Systems towards Thermal Safety", *Fire*, 7, 2 (2024).

Simulation of Properties of Composite Electrodes Using Monte Carlo 3D Equivalent Electronic Circuit Network

D. Budáč[a], V. Miloš[b], M. Carda[a], M. Paidar[a], K. Bouzek[a]

[a] Department of Inorganic Technology, University of Chemistry and Technology, Prague, Czech Republic

[b] Mathematical Institute, Charles University, Prague, Czech Republic

Porous composite materials are used in a large variety of energy applications concerning both fuel cells and batteries. The use of composites results in superior properties due to the synergistic effect of the constituents. Electrodes based on such materials consist of ion conductor, electron conductor and void phase constituents. Due to their complex behavior, the tailoring of the properties of electrodes based on porous composites is often time consuming and expensive. We propose a 3D equivalent electronic circuit network model for simulation of the electrochemical properties of porous composite electrodes. The model was validated against experimental data. Model demonstrates reliability in prediction of electrochemical properties of composite materials of up to 55% porosity. Conversely, the model enables determination of microstructural properties of composite materials with porosity higher than 55%, providing information qualitatively comparable to tomographic analytical methods. The model offers fast performance and reliable results based on easily obtainable input parameters and thus will increase the effectivity of material optimization process.

Introduction

Solid oxide cells (SOCs) are highly efficient energy conversion devices with significant potential in the hydrogen economy concept as both water electrolysers and fuel cells. Their high efficiency is directly related to significantly enhanced kinetics due to high operation temperature (up to 900 °C). However, the elevated operational temperature imposes stringent stability requirements on the materials used, predominantly limiting choices to ceramics and cermets. SOCs consist of three key components: electrolyte and two electrodes. The electrolyte requires high ionic conductivity, negligible electronic conductivity, and gas tightness, while the electrodes need high electro-catalytic activity, high electrical conductivity, and gas permeability. This work deals with the properties of the electrodes as their features are critical for the SOC performance.

At the oxygen electrode, oxygen evolution or reduction reactions occur depending on the SOC's operation mode. Perovskite-based materials, particularly lanthanum strontium manganite (LSM), are attractive for the oxygen electrode due to their high electro-catalytic activity and electron conductivity. However, negligible ionic conductivity of LSM limits the electrochemical reactions to active sites, the triple-phase boundaries (TPB), i.e. interfaces of the electrode, electrolyte, and gaseous phase. Introducing an ion conductive phase into the LSM electrode increases the TPB length, enhancing the overall electro-catalytic performance. Composite electrodes, commonly LSM paired with yttria-stabilized zirconia (YSZ) in a 50:50 weight ratio, are used to address this limitation. Even though YSZ is required for the increase in active sites, its significantly higher electrical resistance hinders the charge transport properties of the composite electrode. To obtain the

optimal electrode it is important to optimize the trade off between electrocatalytic activity, conductivity and gas permeability of the electrode material. Conventionally, time-consuming and expensive experimental studies (e.g., FIB-SEM tomography [1]) are conducted to optimize the material properties. This work proposes a fast, efficient and easy to use tool for examination and optimization of porous composite materials based on a simplified Monte Carlo model.

Model

We propose a 3D Monte Carlo equivalent electronic circuit network model able to predict the electrochemical properties of composite porous electrodes [2]. The key feature of the model is that it is based on only easily accessible input parameters, represented by phase composition (LSM fraction, YSZ fraction, void phase fraction), single-phase material properties (electrical conductivity of each phase) and degree of void phase coalescence (κ_p). This model differentiates between multiple material phases: electron conductor, ion conductors, and void phase. Based on input material composition an in-silica specimen is generated, consisting of randomly distributed material phases in cubic lattice. Subsequently, the in-silica specimen is transformed to a 3D equivalent circuit network based on the single-phase properties and defined interface phenomena. The equivalent circuit networks are solved to provide a prediction of material impedance behavior. This approach enables for the prediction of electrochemical properties of porous composite materials up to 55 % porosity (please see the 'results' section for explanation), i.e. κ_p=0. For higher porosity, i.e. κ_p>0, the model enables to gather information about the material microstructure. This is enabled based on material composition, single phase properties and effective conductivity of the material.

Experiments

To validate the EEC network model, multiple porous samples with varying LSM:YSZ compositions were prepared. LSM:YSZ powder mixtures of compositions between 1:0 and 0:1 were homogenized and subsequently fired at 1150 °C to produce the validation dataset. Electrochemical impedance spectroscopy (EIS) was used to evaluate the electrochemical properties of these samples at temperatures ranging from 400 to 800 °C.

Results

Following input parameters were used for the model validation: phase composition of the experimental samples, temperature-dependent conductivity of YSZ based on our previous work [3] and LSM conductivity determined based on one of the experimental samples.

Assuming κ_p=0, the mathematical model was run for prediction of the effective conductivity values of the experimental samples. The model showed good agreement with experimental data up to porosity of 55%. Above this threshold, the model's accuracy diminished, with significant errors observed between 55% and 68% porosity. The model failed to generate in-silica specimen at 75% porosity due to present void phase coalescence.

Above porosity of 55%, the model was unable to predict the material conductivity due to the requirement on the κ_p value. Conversely, based on the experimental conductivity of the highly porous materials, κ_p could be fitted. The fitted κ_p values enable to visualize experimental samples reconstruction providing information similar to information often obtained by tomographic methods. However, in our case, this information did not require expensive tomography equipment but rather a conductivity measurement and an average computer setup

Conclusions

A novel 3D Monte Carlo equivalent circuit network model was proposed. The model is suitable for prediction of the electrochemical properties of composite porous electrodes with only easily accessible input parameters. The model enables accurate prediction of electrochemical properties of porous composites of porosity up to 55%. Conversely, the model enables to gather information on material microstructure based on simple conductivity measurement.

Acknowledgement

This work was supported by the project "The Energy Conversion and Storage", funded as project No. CZ.02.01.01/00/22_008/0004617 by Programme Johannes Amos Commenius, call Excellent Research and by the Technology Agency of the Czech Republic under project no. TK04030143.

References

[1] S. Jang et al. ECS Trans., 111(6), 2023

[2] D. Budáč et al., Electrochim. Acta, 457, 2023

[3] M. Carda et al., Energies, 15(7), 2022

pragolab

Pragolab

Špičkové služby a přístroje z oboru analytické chemie, mikroskopie, materiálografie a fyzikálního měření pro český a slovenský trh. Již více než 30 let.

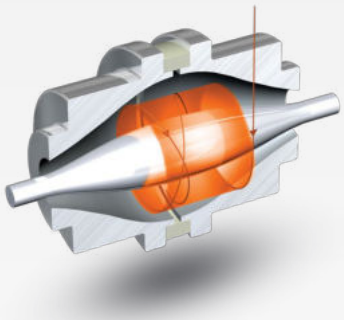

ORGANICKÁ ANALÝZA A SEPARAČNÍ TECHNIKY

MIKROSKOPIE A PŘÍPRAVA VZORKŮ PRO METALOGRAFII

FYZIKÁLNÍ A MATERIÁLOVÉ ANALÝZY

plynová chromatografie **ICP-OES** příprava vzorku **elementární analýza** elektrochemie **testery akumulátorů** EIS **SEA** analýza povrchů **separační techniky** DVS **reologie** atomová spektroskopie **GC** temperace **kapalinová chromatografie** UV-VIS **spektrometrie** GC-MS **lyofilizátory** konfokál **B.E.T.** lims **mikroskopie** materiálografie **metalografie** technická čistota **optická mikroskopie** elektronová mikroskopie **koncentrátory** CHNSO **analýza** AAS **analýza částic** HPLC **hmotnostní spektrometrie** centrifugy **extruze** ICP-MS **servis** AIR monitoring **XPS** widefield **textura** spotřební materiál **NMR** DLS **automatické dávkování** iGC **TOC analýza** RVC **stopped-flow** cirkulární dichroismus **XRF** XRD

www.pragolab.cz

Title:	Advanced Batteries Accumulators and Fuel Cells – 25th ABAF
Edited:	Marie Sedlaříková Vítězslav Novák Tomáš Kazda Petr Bača
Publishing Office:	Marie Sedlaříková Vítězslav Novák Tomáš Kazda Petr Bača
Deadline:	July 21st 2024
Publisher:	Brno University of Technology Faculty of Electrical Engineering and Communication Department of Electrical and Electronic Technology
Year:	2024

The autors are fully responsible for the content and language of their contribution

ISBN 978-80-214-6257-1